DESIGN OF A HIGH GRAVITY DISTILLATION UNIT FOR ON-FARM ETHANOL DEWATERING

By

YASH TAMHANKAR

B.E. in Chemical Engineering

University of Pune

Pune, Maharashtra

2006

Submitted to the Faculty of the
Graduate College of the
Oklahoma State University
in partial fulfillment of
the requirements for
the Degree of
MASTER OF SCIENCE
December, 2010

DESIGN OF HIGH GRAVITY DISTILLATION FOR ON FARM ETHANOL DEWATERING

Thesis Approved:

Dr. James R. Whiteley

Thesis Adviser

Dr. Jan Wagner

Dr. Danielle Bellmer

Dr. Mark E. Payton

Dean of the Graduate College

ACKNOWLEDGMENTS

First, I would like to thank my adviser Dr. James Whiteley for his immense understanding, patience and above all his insight into vapor and liquid flows in distillation columns. His logical approach, reasoning and thought provoking questions have been instrumental in completion of this work. I would also like to thank Dr. Martin High and Dr. Sundar Madihally for their support and Dr. Gasem for having faith in me. I am extremely grateful to Dr. Unde, Dr. Gadgil, Dr. Ravetkar and Mr. Anil Muskawad for spiking my interest in distillation design and operation.

I would like to thank my sister Manasi Tamhankar for all her advice, understanding and support. I would also like to acknowledge my parents, Ketaki Tamhankar (Kekutai) and Sharadchandra Tamhankar (Sharad) for their support, love and concern. I am grateful to Ajit Chiplunkar (Ajit dada) and Sujata Chiplunkar (Sujata tai) for their financial backing.

Special thanks are due to Anuradha Mukherjee (Anu), my lab mate and good friend, for all her technical input, immense help with documentation, and above all her support. Thanks for being there! I am grateful to Eileen Nelson for proof-reading this document. I would like to acknowledge Mindy Bumgarner for all her help.

I wish to thank my other lab members, Jey, Anand, Anil and Raj for all their input and help. I also would like to acknowledge Nikhil Kundargi for all his efforts in finding literature. I would like to express my gratitude to Pramod Raul & Saugata Mahapatra (Bobby) for their timely advice.

Finally, I would like to thank Prarthana, Gargi, & Sahith for making my stay in Stillwater extremely enjoyable.

TABLE OF CONTENTS

Chapter Page

LIST OF TABLES

Table Page

LIST OF FIGURES

Figure Page

NOMENCLATURE

Variables

a_c = acceleration at the eye of the rotor, m/s^2

a_{dyn} = dynamic area of liquid in packing, m^2/m^3

a_e = effective interfacial area, m^2/m^3

a_m = acceleration at mean radius, m/s^2

a_p = specific surface area of the packing, m^2/m^3

a_{st} = static area of liquid in packing, m^2/m^3

ATU = area of transfer unit, m^2

a_w = wetted surface area of the packing, m^2/m^3

b = width, m

C = concentration of component, $kmols/m^3$

D = diffusion coefficient of component, m^2/s

d_a = diameter of packing element, m

d_h = hydraulic diameter of channel, m

d_p = specific diameter of packing, m

g = gravitational acceleration, m/s^2

G = mass flowrate of vapor, kg/s

G' = superficial mass flowrate of vapor, kg/m^2-s

h = axial height of the rotor or length of wetted wall column, m

h_t = total holdup, m^3 of liquid / m^3 of packing

h_s = static holdup, m^3 of liquid / m^3 of packing

h_o = operating or dynamic holdup, m^3 of liquid / m^3 of packing

HETP = height equivalent of a theoretical plate, m

HTU = height of a transfer unit, m

K = overall mass transfer coefficient, m/s

k = local mass transfer coefficient, m/s

$K.a_e$ = overall volumetric mass transfer coefficient, s^{-1}

$k.a_e$ = local volumetric mass transfer coefficient, s^{-1}

L = mass flowrate of liquid, kg/s

L' = superficial mass flowrate of liquid, kg/m^2-s

m = slope of equilibrium curve

M_w = molecular weight

N = mass transfer flux of component, kmols/m^2-s

NTU = number of transfer units

P_c = power consumption, kW

P = pressure, Pa

P_T = total pressure, Pa

Q = volumetric flowrate, m^3/s

Q_w = liquid flowrate per unit width of packed bed, m^2/s

R = resistance to mass transfer of component, s/m

r = radius of rotor, m

s = fractional rate of replacement of individual species

t_E = exposure time of component, s

U_G' = superficial flooding velocity, m/s

U_G = superficial operating velocity, m/s

u = velocity, m/s

V = volume of packing, m^3

$\overline{V}$ = slip velocity, m/s

x = mole fraction of liquid

X = Sherwood chart abscissa

ΔX = surface renewal parameter or the distance traveled by liquid film, m

y = mole fraction of vapor

Y = Sherwood chart ordinate

Z_0 = constant, kW

Z_1 = constant, kW

Greek

δ = effective film thickness, m

Γ = liquid mass flowrate per wetted perimeter, kg/m-s

μ = viscosity, kg/m-s

ρ = density, kg/m^3

Δ = incremental drop or increase

ε = porosity of the packing

σ = surface tension, N/m

ω = rotational velocity, rad/s

ν = kinematic viscosity, m^2/s

Subscripts

A = component A

abs = absorption

avg = average

c = critical

g, G = gas phase

i = interface, inner

l, L = liquid phase

max = maximum

o = outer

r = radial

vap = vaporization

w = water

1 = at inlet

2 = at outlet

θ = tangential

Superscripts

* = equilibrium value

CHAPTER I

INTRODUCTION

High gravity distillation is a prime example of process intensification. Process intensification is the strategy of reducing the size and weight of processing equipment while maintaining capacity (Cross and Ramshaw 1986). In a high gravity distillation unit or a Higee, the components are separated based on differences in their boiling points in a rotating packed bed device instead of a conventional vertical column arrangement. The origin of Higee can be traced to the patent filed by Imperial Chemical Industries (Ramshaw 1981). The escalating capital cost of chemical equipment at that time was the prime reason for developing such a device (Singh 1989). The aim was to build smaller, lighter and less costly processing equipment.

Higee uses centrifugal force to create artificial gravity. Mean accelerations greater than 200 times earth's acceleration (9.81 m/s^2) can be generated by increasing the rotational velocity of the device (Ramshaw 1981). The increased acceleration results in higher flooding velocities, thinner liquid films and smaller bubble sizes. The higher flooding velocities help in accommodating greater liquid and gas rates. Thinner liquid films and smaller bubble sizes result in lower resistance to mass transfer, thereby increasing the mass transfer flux. Height equivalent to a theoretical plate (HETP) reductions from 1- 3 feet for conventional columns to 1-3 inches in Higee units have been reported (Kelleher 1993).

Small size or footprint and low weight are the primary advantages of Higee (Fowler 1989 a). These result in

1. Material savings in shell
2. Reduction in foundation and support costs
3. Possibility of setting up skid mounted units for offshore operations and retrofits
4. Setting up of mobile units which can be transported from one site to the next
5. Housing of Higee units inside buildings which can ensure year round performance in frigid and temperate climates.

Apart from these, the residence time of the fluids inside Higee is very low. This makes Higee ideal for processing heat sensitive systems.

Higee is a rotating packed bed. Additional power must be put in to rotate the device (Fowler 1989 b). Operational costs for Higee are expected to be greater than conventional columns of the same capacity. Packing in Higee rotor is susceptible to choking by solids in the fluid streams. Pressure drop of vapor across the Higee rotor is large because of rotation of the device (Fowler 1989 b). This makes Higee unfit for vacuum services (Kelleher 1993).

The Department of Biosystems and Agricultural Engineering at Oklahoma State University (OSU) has been investigating a farm scale model for ethanol production from sweet sorghum for the past several years based on the Sorganol™ process envisioned by entrepreneur Lee McClume (sorganol.com 2010). Sweet sorghum is an ideal alternative feedstock for ethanol production (Mukherjee 2009).

In the farm-scale ethanol model, cultivation of sweet sorghum, cutting and pressing of the crop to extract sugar rich juice, and the subsequent fermentation and dewatering steps to produce azeotropic or fuel grade ethanol, all take place on the farm. The farm-scale ethanol model is depicted in Figure 1.1.

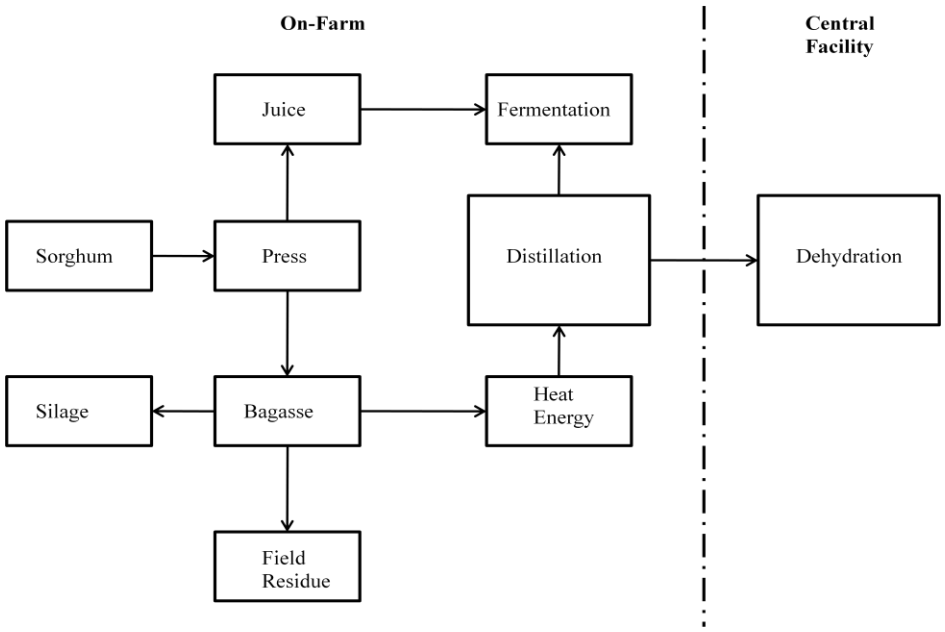

Figure 1.1 - Farm Scale Ethanol Model
[Reference: Bellmer, D., R. Huhnke (2008). Feasibility of in-field ethanol production from sweet sorghum. Sweet Sorghum Ethanol Conference, February 2008.]

The primary advantages of this model are as follows:

1. The cost of transporting high volumes of water rich unfermented or fermented juice to a centralized dewatering facility is avoided (Mukherjee 2009).
2. Since all activities are performed on a farm, any byproducts generated can be directly utilized on the farm (Mukherjee 2009).
3. The farm scale model provides farmers an additional source of income (Mukherjee 2009).

Mukherjee (2009) analyzed the sweet sorghum juice to estimate the solid content of the juice in order to predict the fouling tendency. It was found that the total solid content was less than 2 wt %. The solid content in fermented juice from corn has been reported to be as high as 10 % of the total volume (Öhgren, Rudolf et al. 2006). Thus, the sweet sorghum fermented juice is much cleaner and will result in less fouling compared to fermented juice from corn.

Mukherjee (2009) also evaluated the use of various technologies for dewatering ethanol on a farm scale. Distillation to produce azeotropic, or 190 proof, ethanol, followed by molecular sieve dehydration to produce fuel grade ethanol were found to be most suitable. Based on these findings, a detailed design of distillation unit to dewater ethanol on farm was done. Currently, this design is being used to build a farm scale test facility (Mukherjee 2010). The designed system is to handle 250 gallons per hour of fermented juice with 6.5 % ethanol in two 12 –inch diameter columns. The expected azeotropic ethanol is to be produced at 10-15 gallons per hour. Highlights of this design are as follows:

1. Two column system (rectification and stripping sections are separate) with trayed stripping column and packed rectification column. This limits fouling issues to only the stripping, or beer, column.
2. Use of anti-fouling specialized trays for the stripping column.
3. Overhead air cooled condenser to reduce requirement of cooling water.
4. Steam to be used as the stripping agent.
5. Reboiler run on combustion gases (to be incorporated in the future).
6. State of the art instrumentation and control.

Limitations of the present system design are summarized below:

1. Each of the two 12 inch diameter columns are greater than 30 ft in height (tangent line – tangent line). Thus, heavy support structures and foundation are needed. The large height limits the possibility of housing the columns inside buildings.
2. The bulky column structure prevents setting up of cheap mobile processing units which can be transported from one site to the next. As a result, every farmer or farm needs an independent two column dewatering unit.

3. The installed capital cost of the two columns was estimated to be around $ 50,000 (Mukherjee 2009). However, the expected cost of building and installing these two columns has been found to exceed this mark (Whiteley 2010).
4. A large amount of instrumentation is required for the column structure. The total cost of instruments accounted for 40% of the total capital cost.
5. The return on investment analysis shows the current farm scale model to be economically unfavorable.

Thus, there is a need to reduce the size and weight of the columns and their associated structure to distill the fermented juice. Any means to achieve this could potentially tip the economics in favor of the farm scale ethanol model, thereby making it more viable.

The small volume of fermented juice required to be processed, the heat sensitive nature of fermented juice, and the need to reduce the weight and size of distillation columns and their associated structure, makes Higee well suited for distilling fermented juice on farm. The small size and low weight of Higee units could open up the possibility of setting up mobile units which could be transported from one farm to the next. Multiple farmers could then come together to own mobile units. However, the presence of solids in the fermented juice ($\geq$ 2 wt %) could possibly choke the packing in Higee units. Additionally, the power required for rotating the Higee unit needs to be defined. Thus, there is a need to evaluate the use of Higee for on farm ethanol dewatering.

Evaluation of Higee for on-farm ethanol can be achieved through the steps outlined in Figure 1.2. The first step is to perform a forward design of Higee unit capable of distilling 250 gallons per hour of fermented juice with 6.5 vol % ethanol to produce 190 proof, or azeotropic, ethanol. This is the primary focus of the present study. The objectives of this study are listed below:

1. Size Higee rotors for both the rectification column and the stripping column,

2. Evaluate the power required for rotating the units,
3. Estimate the pressure drop across the two rotors, and
4. Establish a control strategy for the Higee units.

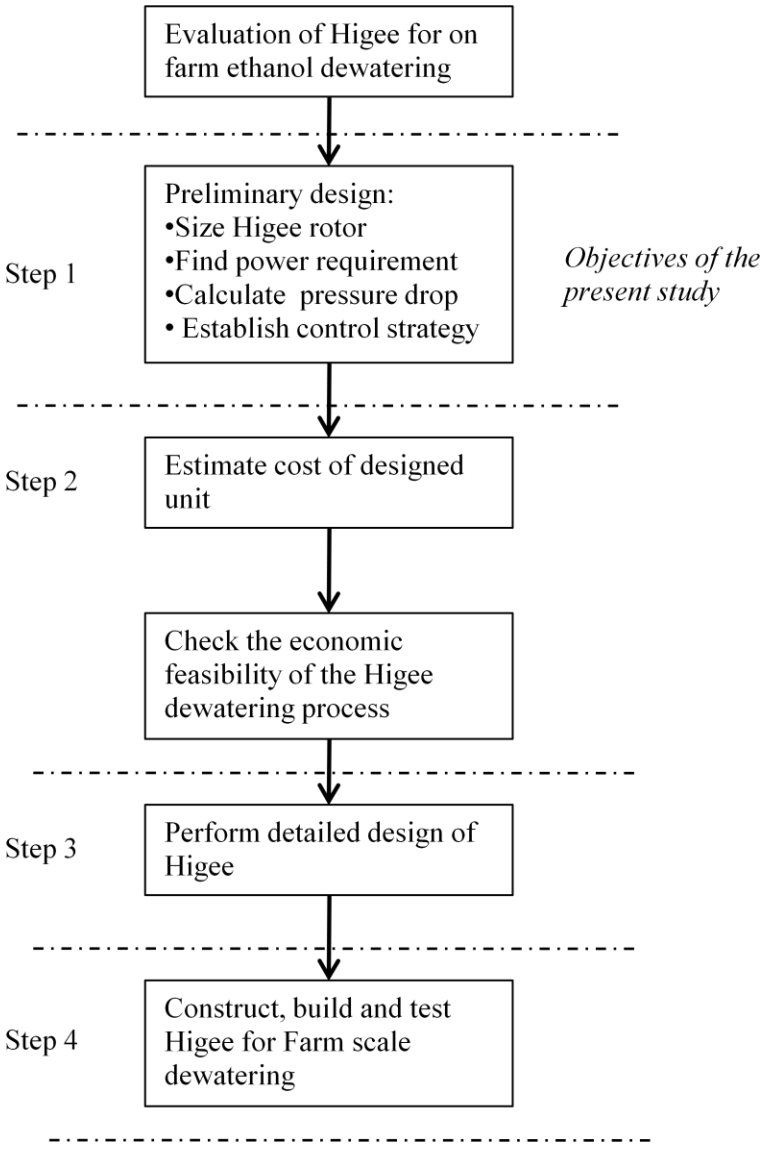

Figure 1.2 – Roadmap for Evaluating Higee for On Farm Ethanol Dewatering

In this thesis, Chapter II outlines the development of Higee and its typical construction and operation. Work done by previous researchers on Higee is summarized in Chapter III. The design and corresponding results are presented in Chapter IV. Highlights of present work, limitations of present work, insight and direction for future work are pointed out in Chapter V.

CHAPTER II

HIGEE – BASICS

II.1- Development of Higee

Process intensification refers to the strategy of reducing chemical equipment size while still meeting the production objectives (Cross and Ramshaw 1986). Reduced size of equipment helps eliminate support structures, foundations, and long pipe runs, thereby reducing overall cost of the plant. Rotating Packed Beds (RPB) are a prime example of process intensification.

The origins of rotating packed bed type contactor for mass transfer operations can be traced to the patent filed by C. Ramshaw and R. Mallinson from Imperial Chemical Industries (ICI) (Ramshaw 1981). The driving forces behind the development of such a device at that time were the escalating costs of chemical plant equipment and the request made by United States National Aeronautics and Space Administration (NASA) to carry out experiments in outer space (Singh 1989). The emphasis was to build more efficient, smaller, lighter, and less costly processing equipment. ICI built and demonstrated a torus shaped, rotating packed bed for distillation and absorption service. This new device was capable of generating mean accelerations greater than 200 times the terrestrial acceleration of gravity (9.81 m/s^2) using centrifugal force. The new device was hence named “Higee” for the high gravity it could generate.

II.2 – Construction

Figure 2.1 shows the typical construction of Higee. The doughnut shaped rotor containing the packing is enclosed in a stationary casing. Specific surface areas greater than 2500 m^2/m^3 and

void fractions greater than 0.9 are typically used for the packing (Fowler 1989 a). Liquid is introduced at the center or eye of the rotor by use of a stationary liquid distributor. The packing is rotated using a motor shaft assembly. Vapor is introduced tangentially through the casing and forced through the rotating packing by applying a pressure gradient. A static seal at the bottom of the casing prevents liquid and vapor escape. A dynamic seal ensures that the vapor does not bypass the rotor packing.

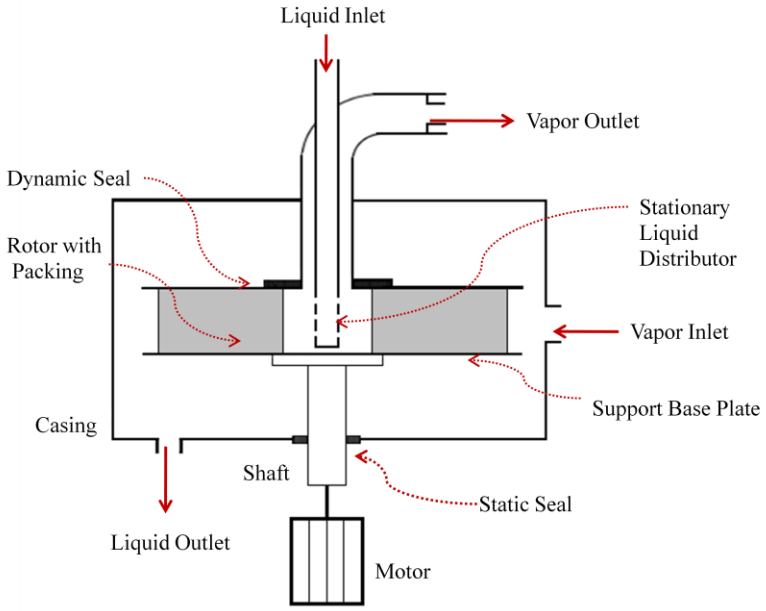

Figure 2.1 – Schematic of Higee Unit

II.3- Operation

Liquid is introduced at the center of the rotor (eye) by means of a distributor into the inner periphery of the rotor in the form of jets or spray of droplets. The liquid exiting the distributor should have sufficient velocity or the liquid may get entrained by the vapor (Singh 1989; Kelleher 1993). Because of the centrifugal head, the liquid is accelerated radially outward through the void spaces in the packing (rotor). Vapor enters the casing tangentially and is forced through the rotor, where it comes in contact with the liquid, and exits through the eye. The exiting liquid impinges on the casing, collects and flows through the outlet nozzle.

High centrifugal acceleration results in smaller liquid films and bubble sizes. This reduces the resistance to mass transfer, resulting in higher mass transfer flux (Kelleher 1993). Height equivalent to a theoretical plate (HETP) reductions from 1- 3 feet for conventional columns to 1-3 inches in Higee units have been reported (Kelleher 1993). The increased acceleration also facilitates higher flooding velocities being accommodated for the same liquid and vapor rates. Thus, the hydraulic capacity of the equipment is enhanced resulting in small size of the equipment.

II.4 Advantages and Disadvantages of Higee

II.4.1- Advantages

1. The primary advantages of Higee are its small size and low weight. Fowler (1989 b) found that compared to an equivalent column for CO_2 removal, a Higee unit would be 36 ft less in height and weighed nearly 60,000 lbs less. The small size of Higee makes it beneficial for high pressure services where material savings for the shell can be significant, and in services where expensive alloys for construction are required (Fowler 1989 a). The low weight of Higee results in savings for foundation and supports, which is of great value in off shore applications and retrofits. Higee units can be mounted on skids (Singh 1989).
2. The small size and low weight of Higee units may allow them to be transported from one processing plant to another (Fowler 1989 a; Kelleher 1993). This makes Higee units suitable for onsite processing. The units could also be housed inside buildings making them operable year round in temperate and frigid climates.
3. Higee units are insensitive to motion (Fowler 1989 a). Along with their small size and low weight, this makes Higee units attractive for ship mounted applications.

4. The short residence time of liquids inside Higee makes it ideal for processing of heat sensitive materials (Fowler 1989 a). Mean liquid residence times are on the order of 1-2 seconds (Keyvani 1989).
5. Higee units are likely to achieve steady state more rapidly compared to conventional columns resulting in smaller volumes of off-spec products (Fowler 1989 a).

II.4.2 – Disadvantages

1. Higee is a rotating device and thus requires additional power (Fowler 1989 b; Kelleher 1993). The operating cost of Higee would be greater than that of comparable conventional columns. Rotation of the packing makes Higee susceptible to seal failures.
2. The conventional mechanical arrangement of the Higee rotor does not provide for feed introduction at some intermediate radial distance from the inner periphery or the eye. Hence, for continuous distillation, two Higee units are required, one for the rectification section and one for the stripping section, respectively (Wang *et al.* 2008).
3. Rotation of packing results in greater pressure drop across the Higee rotor (Fowler 1989 b).
4. Liquid distribution at the inner periphery, or the eye, greatly affects the performance of Higee (Trent 1999). For large liquid loads, uniform liquid distribution is essential to prevent offsetting the rotor from its plane of rotation.
5. Presence of solids in the liquid stream can potentially choke the rotating packing.
6. Lack of information regarding scale up, mechanical design, control philosophy, cost, and reliability limits the use of Higee.

In short, Higee seems to be well suited for small-scale, on-site processing of heat sensitive fluids. The small size and weight permits setting up of mobile skid mounted units.

CHAPTER III

REVIEW – HIGEE PERFORMANCE AND DESIGN

III.1- Performance

Performance of Higee can be characterized in terms of packing efficiency, hydraulic capacity, pressure drop, and power required for rotation. Packing efficiency can be measured in terms of the mass transfer taking place. The hydraulic capacity is limited by flooding. Thus, the hydraulic capacity is quantified in terms of flooding.

As explained earlier, Higee is a rotating packed bed, which employs centrifugal acceleration instead of earth's terrestrial acceleration. In order to review the development of performance parameters for Higee, analogy with conventional packed columns has been drawn wherever necessary.

III.1.1- Mass Transfer

The majority of the work pertaining to mass transfer in Higee has been limited to absorption processes. Most absorption systems are liquid side controlling (Kelleher 1993), wherein the resistance to transport of a component through the gas phase is negligible. The mass transfer theory in the following section is limited to liquid side controlling systems.

III.1.1.i - Theory

Mass transfer can be defined as the net movement of a component from one location to another driven by the difference in concentration of that component at those locations (Seader 2006). In

separation processes like distillation and absorption, this transfer of component takes place between two phases across the gas-liquid interface.

Consider absorption of pure component A from the gas phase to the bulk liquid across the thin stagnant liquid film of thickness δ as shown in Figure 3.1. The entire resistance to mass transfer is limited to the stagnant film. The concentration of component A at the gas-liquid interface is assumed to be in equilibrium with the gas phase. As component A is pure, there is no resistance to mass transfer in the gas phase. Across the thin liquid film, component A diffuses (molecular diffusion) because of the driving force $C_{Ai} - C_{Al}$.

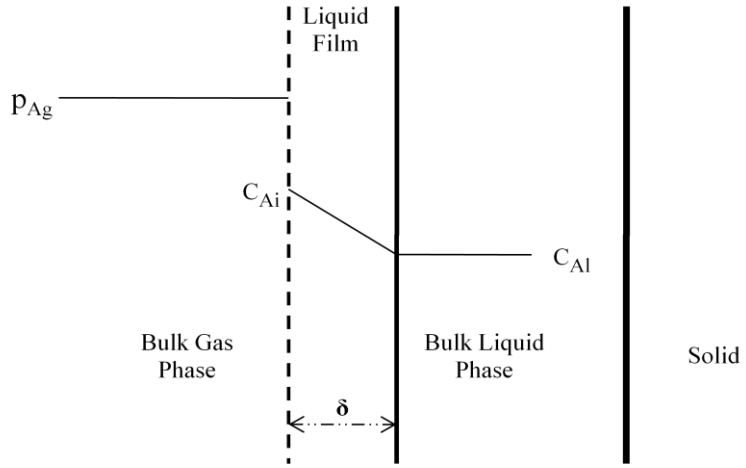

Figure 3.1 – Mass Transfer between Two Phases
[Reference: Seader, J. D., E.J. Henley (2006). Separation Process Principles, John Wiley and Sons, Inc.]

Ignoring the bulk movement of component A, the steady state mass transfer flux across the liquid film is given by Equation 3.1 below.

$$N_A = \frac{C_{Ai} - C_{Al}}{R_A} \qquad (Eq\ 3.1)$$

where,

N_A = mass flux of component A, kmols/m^2 .s

C_{Ai} = concentration of component A at the interface, kmols/m^3

C_{Al} = concentration of component A in the bulk liquid, kmols/m^3

R_A = resistance to mass transfer of component A from gas phase to the bulk liquid, s/m

Defining the local liquid side mass transfer coefficient as the reciprocal of the resistance to mass transfer yields Equation 3.2.

$$N_A = k_l(C_{Ai} - C_{Al}) \qquad (Eq\ 3.2)$$

where,

k_l = local liquid side mass transfer coefficient, m/s

The local liquid side mass transfer coefficient can be determined either experimentally or through correlations based on theory. Experimental determination requires knowledge of mass transfer flux and the component concentration at the interface and in the bulk liquid. It is difficult to measure the interfacial concentration of the component. Commonly, the liquid side mass transfer coefficient is determined through correlations based on theory and sharpened through experiments.

As concentrations at the interface cannot be measured, the flux can be defined based on the overall driving force.

$$N_A = K_L(C_A^* - C_{Al}) \qquad (Eq\ 3.3)$$

where,

K_L = overall liquid side mass transfer coefficient, m/s

C_A* = concentration of component A in equilibrium with the bulk gas phase concentration, kmols/m^3

The relationship between the overall liquid side mass transfer coefficient and the local coefficients is

$$K_L = \frac{1}{\frac{1}{m\,k_g} + \frac{1}{k_l}} \qquad (Eq\ 3.4)$$

where,
k_g = local gas side mass transfer coefficient, m/s

m = slope of the equilibrium curve

When both the liquid side and gas side resistances are appreciable, the form of Equation 3.4 remains. For liquid side controlling systems ($1/k_l >> 1/m\ k_g$), the overall mass transfer coefficient can be approximated as shown in Equation 3.5.

$$K_L \cong k_l \qquad (Eq\ 3.5)$$

Packed columns are widely used for distillation and absorption service. The film theory, penetration theory and the surface renewal theory are commonly used to characterize mass transfer coefficients in packed columns.

III.1.1. i.a - Film Theory

Film theory (Lewis and Whitman 1924) assumes the presence of a stagnant film adjacent to the gas-liquid interface (See Figure 3.1). The film is infinitely thin such that steady state mass transfer occurs across it solely due to molecular diffusion. Since the remainder of the liquid layer is assumed to be well mixed, the concentration gradient is limited to the stagnant film. The mass flux is given by,

$$N_A = \frac{D_A\,(C_{Ai} - C_{Al})}{\delta} \qquad (Eq\ 3.6)$$

As a result,

$$k_l = \frac{D_A}{\delta} \qquad (Eq\ 3.7)$$

where,
D_A = liquid phase diffusion coefficient for component A, m^2/s

δ = effective film thickness, m

As the effective film thickness cannot be measured, the liquid side mass transfer coefficient becomes completely empirical. As seen from Equation 3.7, the film theory proposes that liquid

side coefficient varies as the first power of diffusivity. Sherwood and Holloway (1940) showed that in a packed column, the liquid side coefficient varies to the 0.47 power of diffusivity. Thus, the film theory fails to predict the correct dependency of liquid side mass transfer coefficient with diffusivity. This failure was attributed to the nature of liquid flow in packed columns (Vivian and Peaceman 1956). As the liquid flows over the packing, the stagnant film should be adjacent to the solid wall rather than at the gas-liquid interface.

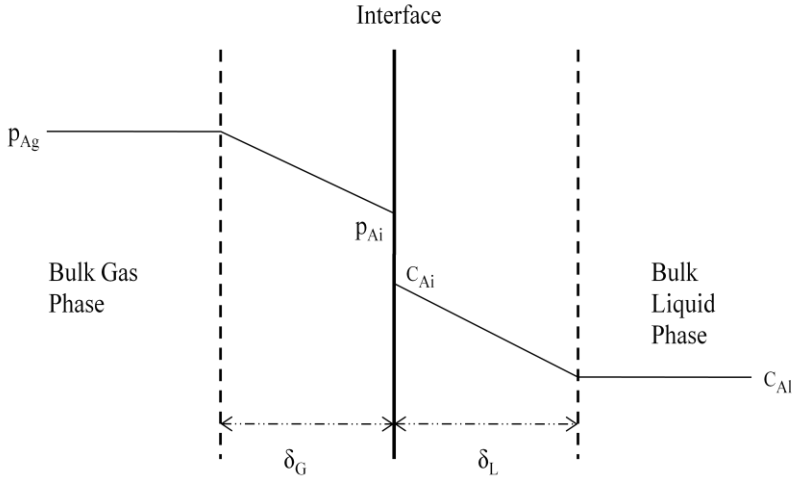

Figure 3.2 – Film Theory

III.1.1.i.b - Penetration Theory

Higbie (1935) proposed the penetration theory to account for liquid side mass transfer resistance. According to this theory, the liquid (with uniform velocity) flows over each element (packing) in laminar flow and gets mixed at the surface of discontinuity. Mass transfer occurs during a series of brief contacts between the gas and the liquid during which the solute gas "penetrates" a short distance into the liquid layer. The exposure time of the brief contacts is assumed to be constant. At the prevailing unsteady state conditions,

$$D_A \frac{\partial^2 C_A}{\partial x^2} = \frac{\partial C_A}{\partial t} \qquad (Eq\ 3.8)$$

Solution of above partial differential equation results in,

$$N_A = 2\,(C_{Ai} - C_{Al})\sqrt{\frac{D_A}{\pi\, t_E}} \qquad (Eq\ 3.9)$$

where,

t_E = exposure time of component A at gas liquid interface, sec

As a result,

$$k_l = 2\sqrt{\frac{D_A}{\pi\, t_E}} \qquad (Eq\ 3.10)$$

Thus, the penetration theory predicts that the liquid side mass transfer coefficient varies to the 0.5 power of diffusivity which is in close agreement with the results of Sherwood and Holloway (1940).

III.1.1.i.c - Surface Renewal Theory

The surface renewal theory (Danckwerts 1951) is an extension of the penetration theory. According to this theory, each individual species of the solute gas gets exposed at the interface for varied durations. The gas liquid interface then becomes a collection of species with different exposure time histories. As a result, the average mass flux across the interface needs to be determined. Assuming that the chance of individual species being replaced from the interface is independent of the time spent at the interface, the mass flux is given by

$$N_{A,avg} = (C_{Ai} - C_{Al})\sqrt{D_A\, s} \qquad (Eq\ 3.11)$$

where,

s = fractional rate of replacement of individual species at the interface

Thus, the surface renewal theory, like the penetration theory, predicts that the liquid side mass transfer coefficient varies as the 0.5 power of diffusivity.

The film theory, penetration theory, and the surface renewal theory are simple mathematical models used to account for mass transfer across a gas liquid interface. However, each model requires knowledge of, effective film thickness (δ), exposure time (t_E), and fractional rate of replacement of species at the interface (s), respectively. These parameters are difficult to measure experimentally. Second, diffusivities cannot be measured accurately enough to verify their effect on mass flux. In spite of these limitations, these theories are used as starting points to develop empirical correlations.

III.1.1.ii – Effect of Gravity

The influence of gravity on mass transfer operations has been studied for gas absorption/desorption systems, which are liquid side controlling (primary resistance). The effect of gravity has been deduced either by developing dimensionless correlations for the liquid side coefficient (k_l), or through experimentation.

Van Krevelen and Hoftijer (1947) studied the influence of various variables on the liquid side mass transfer coefficient (k_l). They developed a dimensionless correlation for k_l by modifying the equation predicting the gas phase coefficient in a film reactor (Gilliland and Sherwood 1934). The nature of mass transfer in a fluid flowing over a packing and in the gas phase of a film reactor were presumed to be similar. The resulting expression was

$$\frac{k_l}{D} = 0.025 \left(\frac{\Gamma}{\mu_L}\right)^{2/3} \left(\frac{\mu_L}{\rho\, D}\right)^{1/3} \left(\frac{g\, {\rho_L}^2}{{\mu_L}^2}\right)^{1/3} \qquad (Eq\ 3.12)$$

where,

k_l =local liquid side mass transfer coefficient, m/s

D = diffusion coefficient, m/s^2

Γ = liquid mass flowrate per wetted perimeter, kg/m-s

μ_L = liquid viscosity, kg/m-s

ρ_L = liquid density, kg/m^3

g = gravitational acceleration, m/s^2

The liquid side coefficient varied as 1/3 power of gravity.

Vivian and Peaceman (1956) validated the use of penetration theory to characterize liquid side resistance to gas absorption. Carbon dioxide and chlorine were desorbed from water and dilute hydrochloric acid, respectively, in several short (0.5 in – 4 in) glass wetted-wall columns. The use of short wetted-wall columns ensured uniform liquid layer concentration and infinite depth of liquid layer, so the penetration theory could be applied. The short height of wetted wall columns also prevented wave formation (ripples) at the free surface of the liquid layer, which result in increased mass transfer areas with increasing liquid rates (Kapitsa 1948). Their results showed that the liquid side coefficient varied as the 0.47 power of diffusivity which agreed favorably with the penetration theory. Further, a non-dimensional equation was proposed to account for all the variables affecting k_l. The proposed correlation was developed solely on dimensional analysis and lacked experimental verification.

$$\frac{k_l\ h}{D} = 0.433\ \left(\frac{\mu_L}{\rho_L\ D}\right)^{1/2} \left(\frac{{\rho_L}^2 g\ h^3}{{\mu_L}^2}\right)^{1/6} \left(\frac{4\ \Gamma}{\mu_L}\right)^{0.4} \qquad (Eq\ 3.13)$$

where,

k_l =local liquid side mass transfer coefficient, m/s

h = length of wetted wall column, m

D = diffusion coefficient, m/s^2

Γ = liquid mass flowrate per wetted perimeter, kg/m-s

μ_L = liquid viscosity, kg/m-s

ρ_L = liquid density, kg/m^3

g = gravitational acceleration, m/s^2

Equation 3.13 could be utilized for systems which have viscosity and density different from those of water at 25 °C. Since no experimental evidence was provided for the effects of dimensional

groups, the above equation should be used with caution. The liquid side mass transfer coefficient varied as the 1/6 power of gravity.

Vivian, Brian and Krukonis (1965) measured the effect of gravity on gas absorption experimentally in a packed column under the influence of a centrifugal field. The packed column (1 ft in height, 6 inches in diameter and packed with ¾ inch Raschig rings) was mounted on the arm of a centrifuge at a distance of 21 ft from the axis of rotation. The gravitational force was varied from 1 to 6.4 times the force of gravity. Their results indicated that the liquid side volumetric mass transfer coefficient varied with gravitational force as follows,

$$k_l a_e \propto g^{0.41-0.48} \qquad (Eq\ 3.14)$$

Where,

$k_l a_e$ = liquid side volumetric mass transfer coefficient, s^{-1}

a_e = effective interfacial area, m^2/m^3

Equations 3.12 and 3.13 show the effect of gravity on the local liquid side mass transfer coefficient, while Equation 3.14 shows the effect of gravity on the product of the local liquid side mass transfer coefficient and the effective interfacial area. The greater effect of gravity (in Equation 3.14) was attributed to increasing interfacial area with increasing gravitational force.

III.1.1.iii - Previous work on Mass Transfer in Higee

The first reported mass transfer correlations for Higee originate from the work done at ICI (Ramshaw 1981). Both liquid side and gas side mass transfer coefficients were determined using laboratory scale Higee units.

The liquid side mass transfer coefficient was determined by absorbing oxygen into water. The rotor used had an inner radius of 4 cm and an outer radius of 9 cm. The axial height of the rotor was not specified. Two types of packing were tested. The first packing was made of 1 mm glass beads with specific surface area of 3300 m^2/m^3. The second was made of 12 filament copper

gauze (Knitmesh 9031) having a specific surface area of 1650 m^2/m^3. It was assumed that the interfacial area was equal to the specific surface area of the packing. The rotational speed was varied from 1250 rpm to 1750 rpm. Deoxygenated water was fed at the eye of the rotor. Oxygen concentrations at the inlet and outlet were measured. Gas rates utilized were not reported. The liquid side overall mass transfer coefficient was calculated using the following correlation.

$$K_L = \frac{Q}{V\, a_e} \ln\left(\frac{C_{e1} - C_1}{C_{e1} - C_2}\right) \qquad (Eq\ 3.15)$$

where,

K_L = overall liquid side mass transfer coefficient, m/s

Q = volumetric flow rate of water, m^3/s

V = volume of packing, m^3

C_1 = concentration of oxygen in inlet water

C_2 = concentration of water in outlet water

C_{e1} = equilibrium concentration of oxygen in water at ambient temperature

a_e = interfacial area of packing, m^2/m^3

The results from the tests are presented in Table 3.1 and Table 3.2. It can be seen that increasing the rotational speed for any liquid flowrate results in an increased value of the mass transfer coefficient.

Table 3.1 – Mass Transfer Coefficients for Water/Oxygen System on 1mm Glass Beads (Ramshaw 1981)

Water flowrate	**Rotational speed**	***Mean acceleration**	**Mass transfer coefficient, K_L**	****$K_L a_e$ /$(K_L a_e)_I$**
m^3/s x 10^5	rpm	m/s	m/s x 10^5	
3	1250	1197	21.2	37
3	1500	1727	24.9	42
5	1500	1727	20.3	41
5	1750	2354	21.7	44

*Mean acceleration is calculated at mean radius. Mean radius = $(\{\text{outer radius}^2 + \text{inner radius}^2\}/2)^{1/2}$

** $(K_L a_e)_I$ refers to the value of mass transfer coefficient calculated for ½ in Intalox Saddle, 625 m^2/m^3 stationary column at same liquid rates employed for rotational experiments.

Table 3.2 - Mass Transfer Coefficients for Water/Oxygen System on Knitmesh Copper Gauze (Ramshaw 1981)

Water flowrate	**Rotational speed**	***Mean acceleration**	**Mass transfer coefficient, K_L**	****$K_L a_e$ /$(K_L a_e)_I$**
$m^3/s \times 10^5$	rpm	m/s	m/s x 10^5	
4	1500	1727	19.4	27
4	1750	2354	20.6	28
6	1500	1727	26.7	29
6	1750	2354	31.5	34

*Mean acceleration is calculated at mean radius. Mean radius = ({outer radius^2 + inner radius^2}/2)$^{1/2}$

** $(K_L a_e)_I$ refers to the value of mass transfer coefficient calculated for ½ in Intalox Saddle, 625 m^2/m^3 stationary column at same liquid rates employed for rotational experiments.

The gas side coefficient was determined by absorbing ammonia into water. The first set of experiments utilized 1.5 mm glass beads of specific surface area 2400 m^2/m^3, while the second set of experiments used stainless steel wire gauze (Knitmesh 9031) with a specific surface area of 1650 m^2/m^3. The gas side mass transfer coefficient was calculated using Equation 3.16 below.

$$K_G = \frac{M_w\, Q\, (C_2 - C_1)}{V\, a_e\, P_T} \left[\frac{\ln\left(\frac{y_1 - y_{e1}}{y_2 - y_{e2}}\right)}{(y_1 - y_{e1}) - (y_2 - y_{e2})} \right] \qquad (Eq\ 3.16)$$

where,

K_G = overall gas side mass transfer coefficient, m/s

M_w = molecular weight of ammonia, kg

Q = volumetric flow of water, m^3/s

C_1 = ammonia concentration in inlet liquid, $kmols/m^3$

C_2 = ammonia concentration in outlet liquid, $kmols/m^3$

V = volume of packing, m^3

a_e = effective interfacial area of packing, m^2/m^3

P_T = total pressure of the system, N/m^2

y_1 = mole fraction of ammonia in inlet gas

y_{e1} = mole fraction of ammonia in the gas phase which in equilibrium with an ammonia/water solution of concentration C_1

y_2 = mole fraction of ammonia in outlet gas

y_{e2}= mole fraction of ammonia in the gas phase which in equilibrium with an ammonia/water solution of concentration C_2

The results from the ammonia-water tests are tabulated below. The gas side mass transfer coefficient was found to increase with increasing rotational speed.

Table 3.3 – Mass Transfer Coefficients for Water/Ammonia System (Ramshaw 1981)

Packing	Rotational speed	*Mean acceleration	Mass transfer coefficient, K_G	**$K_G a_e$ /$(K_G a_e)_I$
	rpm	m/s^2	s/m x 10^8	
Glass beads	1000	760	3.94	4
Glass beads	1750	2354	4.83	5
Stainless steel gauze	1000	760	10.80	8
Stainless steel gauze	1750	2354	12.69	9

*Mean acceleration is calculated at mean radius. Mean radius = ({outer radius^2 + inner radius^2}/2)$^{1/2}$
** $(K_G a_e)_I$ refers to the value of mass transfer coefficient calculated for ½ in Intalox Saddle, 625 m^2/m^3 stationary column at same liquid rates employed for rotational experiments.
Liquid flowrate = 1.7 x 10^{-5} m^3/s
Gas flowrate = 0.88 x 10^{-3} m^3/s
$(K_G a_e)_I$ = 2.35 x 10-5 sec/m

To demonstrate the use of Higee for distillation, ICI performed tests on methanol/ethanol system using a rotor packed with stainless steel gauze having a specific surface area of 1650 m^2/m^3. The rotor had an internal radius of 6 cm and an outer radius of 9 cm. The rotational velocity was set at 1600 rpm. A mixture of 70 mole % methanol was charged to the reboiler. Distillation was carried out at total reflux. The steady state composition of methanol in the condenser was found to be 91 mole %. The gas side mass transfer coefficient was found using

$$K_G = \frac{Vapor\ flowrate}{Interfacial\ area} \times Height\ of\ transfer\ unit \qquad (Eq\ 3.17)$$

$$Height\ of\ transfer\ unit = \frac{Radial\ distance\ of\ rotor\ packing}{Number\ of\ transfer\ units} \qquad (Eq\ 3.18)$$

Results for the methanol/ethanol tests are presented in Table 3.4 below. Again, increasing radial velocity resulted in higher values of mass transfer coefficient.

Table 3.4 – Mass Transfer Coefficients for Methanol/Ethanol System (Ramshaw 1981)

Vapor flowrate	**Mean acceleration**	**Mass transfer coefficient**	**Volumetric mass transfer coefficient**
moles/m^2-s x 10^3	m/s^2	m^2/s x 10^5	moles/m^3-s
8.60	2147	44	0.72
8.42	9.8	5.4	0.034

Tung and Mah (Tung and Mah 1985) applied the penetration theory to model the liquid side mass transfer coefficient in Higee. Predictions by the penetration theory were compared against the data from ICI experiments and the predictions from Onda correlation (Equation 3.34). It was assumed that the exposure time be estimated by

$$t_E = \frac{\pi\, d_p}{2\, u} \qquad (Eq\ 3.19)$$

$$u = \frac{3^{2/3}}{2}\left(\frac{g\,\Gamma^2}{\rho_L\,\mu_L}\right)^{1/3} \qquad (Eq\ 3.20)$$

where,

t_E = exposure time, s

d_p = specific diameter of packing, m

u = free surface velocity of falling liquid film, m/s

g = gravitational acceleration, m/s^2

Γ = liquid mass flowrate per wetted perimeter, kg/m-s

ρ_L = liquid density, kg/m^3

μ_L = liquid viscosity, kg/m-s

Combining Equations 3.20, 3.19 and 3.10 results in the following correlation for the liquid side mass transfer coefficient:

$$\frac{k_l\, d_p}{D_A} = \left(\frac{2.3^{1/3}}{\pi}\right)\left(\frac{\mu_L}{\rho_L\, D_A}\right)^{1/2}\left(\frac{a_e\, \Gamma}{a_p\, \mu_L}\right)^{1/3}\left(\frac{a_p}{a_e}\right)^{1/3}\left(\frac{{d_p}^3\, {\rho_L}^2\, g}{{\mu_L}^2}\right)^{1/6} \qquad (Eq\ 3.21)$$

where,

D_A = diffusion coefficient of component A, m/s

a_e = effective interfacial area, m^2/m^3

a_p = specific surface area of the packing, m^2/m^3

Results from their analysis showed that the penetration theory predicted the data within 25 %. The variation of liquid side mass transfer coefficient as the 1/6 or 0.16 power of gravity was not in agreement with the experimental results of Vivian, *et al.* (1965). The Onda (1968) correlation was seen to under predict the data by about 80 %.

Munjal, *et al.* (1989 a) developed a theoretical correlation for predicting mass transfer coefficient in Higee. The correlation was based on the theoretical model of Davidson (1959), which assumes liquid film flow over randomly inclined packing surfaces under gravity. The mass transfer coefficient was determined by reactive absorption of carbon dioxide into sodium hydroxide solution. The packing employed for the mass transfer tests was 3 mm glass beads. The developed correlation is presented as Equation 3.22. Again, it is seen that the liquid mass transfer coefficient varied as the1/6 power of acceleration.

$$k_l = 2.6\,\frac{Q_w}{(\Delta X)}\left(\frac{\nu_L}{D}\right)^{-1/2}\left(\frac{4\,Q_w}{\nu_L}\right)^{-2/3} {G_{ravg}}^{1/6} \qquad (Eq\ 3.22)$$

where,

k_l = local liquid side mass transfer coefficient, m/s

Q_w = liquid flowrate per unit width of packed bed, m^2/s

ΔX = surface renewal parameter or the distance traveled by liquid film, m

ν_L = kinematic viscosity, m^2/s

D = diffusion coefficient, m^2/s

G_{ravg} = average Grashof number

$= \{r_{avg}\, \omega^2\, \Delta X^3\} / \{(\mu_L/\rho_L)^2\}$

r_{avg} = average radius of rotor, m

$= (r_i + r_o)/2$

r_i = inner radius of rotor, m

r_o = outer radius of rotor, m

ω = rotational speed, rad/s

$g = r_{avg}\, \omega^2$, m/s^2

Munjal, *et al.* (1989 b) also measured the effective gas-liquid interfacial area based on the method developed by Danckwerts and Sharma (1966). The gas-liquid interfacial area was found to increase with rotational speed. The observed relationship between the interfacial area and the rotational speed was

$$a_{e1} \propto \omega^{0.28-0.42} \qquad (Eq\ 3.23)$$

where,

a_{e1} = gas-liquid interfacial area inside the packed bed. m^2/m^3

ω = rotational speed, rpm

Munjal, *et al.* (1989 b) offered the following qualitative reasons for increasing interfacial area:

1. Spreading of liquid in the azimuthal direction because of Coriolis force,
2. lowering of the minimum wetting rate,
3. lowering of the static holdup, and
4. good initial distribution of liquid

The need for more work to quantify these effects was suggested.

Keyvani (1989) studied the operating characteristics of rotating packed beds using a rigid foamed aluminum packing. Three different specific surface areas of the aluminum packing were used; 656, 1476, and 2952 m^2/m^3, respectively. The porosity of the packing was 0.92. The

corresponding three rotors had an inner diameter of 25.4 cm, outer diameter of 45.7 cm, and axial height of 4.4 cm. The mean acceleration (at mean radius) was varied from 50 to 300 g. The effect of acceleration and packing specific surface area on the height of the tansfer unit (HTU) was evaluated by desorbing carbon dioxide from air to water. The HTU was defined by

$$HTU = \frac{L'}{\rho_L \, k_l a_e} \qquad (Eq\ 3.24)$$

Where,
HTU = height of a transfer unit, m

L' = superficial mass flowrate of liquid, kg/ m^2-s

ρ_L = liquid density, kg/m^3

$k_l a_e$ = volumetric liquid side mass transfer coefficient, s^{-1}

In Equation 3.24, the liquid side mass transfer coefficient was determined from the penetration theory while the Onda correlation (1968) was used for the interfacial area (Equation 3.34). HTU predictions were found to be within 30 % of the measured HTU.

The relationship between the measured HTU and acceleration was

$$HTU \propto g^{-0.3\ to-0.4} \qquad (Eq\ 3.25)$$

The variation of volumetric mass transfer coefficient with the specific surface area of the packing is as shown in Figure 3.3.

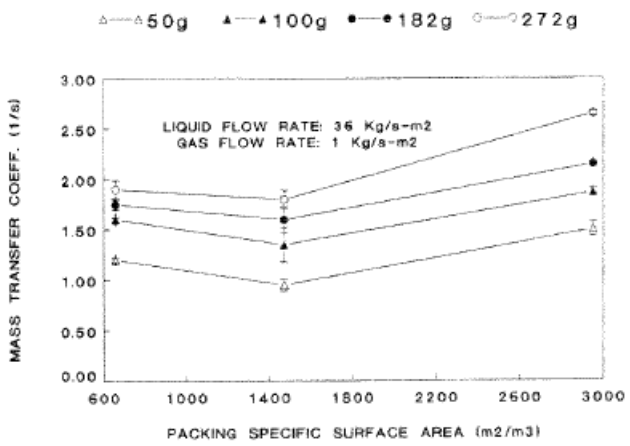

Figure 3.3 – Variation of Mass Transfer Coefficient with Specific Surface Area of Packing [Reference: Keyvani, M. (1989). "Operating characteristics of rotating beds." Chemical Engineering Progress **85**(9): 48-52.]

Figure 3.3 shows the volumetric mass transfer coefficient for lower specific surface to be greater than those for mid specific surfaces (around 1400 m^2/m^3). This anomaly was attributed to the Coriolis force, which caused the smaller packing to have greater wetted area.

Singh (1989) evaluated the performance of Higee for air stripping of jet fuel components from groundwater. Sumitomo packing having a specific surface area of 2500 m^2/m^3 and porosity of 0.95, and wire gauze packing with a specific surface area of 2067 m^2/m^3 and porosity of 0.934 were used. The outer radii of the rotors were 22.9 cm, 30.5 cm and 38.1 cm respectively. The inner radius was equal to the axial height of 12.7 cm. To account for the change in liquid loading with radius of the packing torus, Singh introduced the concept of area of transfer unit (ATU). ATU is analogous to HTU for conventional packed beds. ATU was defined by

$$ATU = \frac{L}{h\,K_L a_e} = \frac{\pi\,({r_o}^2 - {r_i}^2)}{NTU} \qquad (Eq\ 3.26)$$

where,

ATU = area of a transfer unit, m^2

L = mass flowrate of liquid, kg/s

h = axial height of rotor, m

$K_L a_e$ = overall volumetric mass transfer coefficient, s^{-1}

r_o = outer radius of rotor, m

r_i = inner radius of rotor, m

NTU = number of transfer units

The number of transfer units where defined by

$$NTU = \int_{x_1}^{x_2} \frac{dx}{(x - x^*)} \qquad (Eq\ 3.27)$$

Where,

x_1 = mole fraction of solute at inlet

x_2 = mole fraction of solute at outlet

$x - x^*$ = driving force for mass transfer

Singh (1989) plotted the variation of experimental ATU against the average acceleration. For a particular value of mean acceleration, the inlet and outlet concentrations of the solute were measured. The corresponding value of NTU was determined by evaluating the integral in Equation 3.27. The experimental ATU was then found using the values of the inner radius, outer radius, and NTU in Equation 3.26. The variation experimental ATU with mean acceleration is shown in Figure 3.4. The ATU was found to decrease with increasing acceleration.

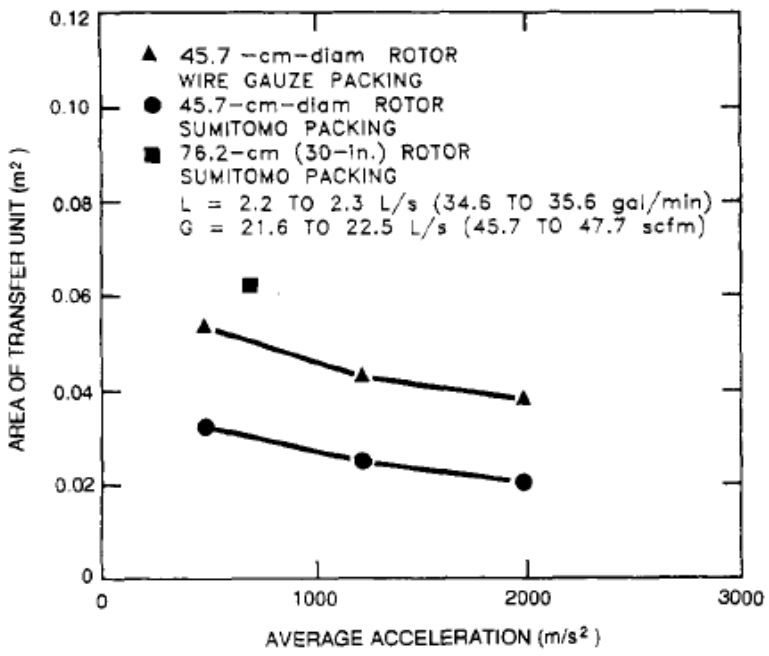

Figure 3.4 – Variation of ATU with Increasing Acceleration in Singh's Work
[Reference: Singh, S. (1989). Air Stripping of Volatile Organic Compounds from Groundwater: An Evaluation of A Centrifugal Vapor-Liquid Contactor. Knoxville, The University of Tennessee. Ph.D Dissertation]

Singh also calculated the value of ATU based on previously established correlations for the liquid side mass transfer coefficient. Expressions developed by Tung and Mah (1985) and used by Vivian, *et al.* (1965) were employed. The expression of Vivian, *et al.* (1965) over-predicted the value of ATU by a factor of 3 to 5. Predictions from the expression of Tung and Mah (1985) were found to be unreliable. A new correlation for the ATU was developed by performing dimensional analysis of all the variables influencing the ATU (liquid flowrate, liquid viscosity, liquid density, specific surface area of the packing and the acceleration). The correlation is presented as

$$ATU = \frac{337{,}143.86}{{a_p}^2}\left(\frac{L}{\mu_L\, a_p}\right)^{0.6}\left(\frac{{\rho_L}^2\, r\omega^2}{{\mu_L}^2 {a_p}^2}\right)^{-0.15} \qquad (Eq\ 3.28)$$

where,

a_p = specific surface area of packing, m^2/m^3

μ_L = liquid viscosity, kg/m-s

ρ_L = liquid density, kg/m^3

r = mean radius, m

ω = rad/s

Equation 3.28 fit the experimental data within 20 %. The main advantage of Equation 3.28 is that knowledge of interfacial area is not required.

Kelleher (1993) studied distillation in Higee using cyclohexane/n-heptane system at total reflux. The volumetric mass transfer coefficients were determined at 24 psia and 60 psia by varying the reboiler duty and rotational speed. Rotational speed was varied from 400 to 1200 rpm. Sumitomo Celmet packing having a specific surface area of 2500 m^2/m^3 and porosity of 0.92 was used as the rotor packing. The rotor had an inner radius of 8.75 cm, outer radius of 30 cm and axial height of 15 cm. The number of transfer units (NTU) and area of transfer unit (ATU) where found experimentally by varying the radial velocity.

As with Singh's work (1989), the NTU was found to increase with radial velocity. The experimental value of ATU was compared against the calculated ATU values based on Singh's work (1989), Onda correlation (1968), Davidson's model (1959) and the penetration theory (1935). None of the models correlated the data reasonably. Since many distillation systems are gas phase controlled, a new model to account for the gas-side resistance was developed. The new correlation for the local gas-side mass transfer coefficient is

$$k_g a_e = \left(\frac{a_p D_G}{d_p}\right)\left(\frac{G}{a_p\,\mu_G}\right)^2\left(\frac{{d_p}^3\,{\rho_G}^2\;r\,\omega^2}{{\mu_G}^2}\right)^{1/3}\left(\frac{\mu_G}{\rho_G\,D_G}\right)^{-1/3} \qquad (Eq\ 3.29)$$

where,

$k_g a_e$ = gas side volumetric mass transfer coefficient, s^{-1}

a_p = specific surface area of the packing, m^2/m^3

D_G =gas diffusivity, m/s^2

d_p = specific diameter of the packing, m

G = mass flowrate of vapor, kg/s

μ_G = gas viscosity, kg/m-s

ρ_G = gas density, kg/m^3

r = radius, m

ω = radial velocity, rad/s

The ATU calculated from Equation 3.29 fit the experimental ATU data within 30 %.

III.1.1.iv – Influence of Gravity on Interfacial Area

To understand the influence of gravity on interfacial area qualitatively, correlations for effective interfacial area in conventional packed columns are studied. The aim is to trace the origin of gravity term in these correlations to gain insight into how gravity might affect interfacial area.

Shulman, *et al.* (1955 a) measured the total and static holdup of liquid in ½ inch and 1 inch ceramic Berl saddles; ½ inch, 1 inch and 1 ½ inch ceramic Raschig rings; and 1 inch carbon Raschig rings under varying gas and liquid flowrates. The total holdup (h_t, m^3 of liquid / m^3 of packing) was defined as the total liquid holdup in the packing under operating conditions while the static holdup (h_s, mt^3 of liquid / m^3 of packing) was defined as the liquid which does not drain from the packing when the liquid flow to the packing is exhausted. The operating holdup (h_o, m^3 of liquid / m^3 of packing) was used to account for the liquid that would drain from the packing when the liquid flow was stopped. Thus,

$$h_t = h_s + h_o \qquad (Eq\ 3.30)$$

where,

h_t = total holdup, m^3 of liquid / m^3 of packing

h_s = static holdup, m^3 of liquid / m^3 of packing

h_o = operating or dynamic holdup, m^3 of liquid / m^3 of packing

Shulman, *et al.* (1955 a) concluded that the effective interfacial area during vaporization (as in distillation) consists of the pool of moving liquid and the liquid in stagnant zones. Thus, the

effective interfacial area is proportional to the total holdup (h_t). During absorption the stagnant pools of liquid become quickly saturated and are unavailable for further mass transfer. The effective interfacial area then becomes proportional to the operating holdup (h_o) which represents the pool of moving liquid. It was also proposed that,

$$\frac{(k_g a_e)_{vap}}{(k_g a_e)_{abs}} = 0.85 \frac{h_t}{h_o} \qquad (Eq\ 3.31)$$

where,
$(k_g a_e)_{vap}$ = volumetric gas side mass transfer coefficient for vaporization/distillation, s^{-1}

$(k_g a_e)_{abs}$ = volumetric gas side mass transfer coefficient for absorption, s^{-1}

Shulman, *et al.* (1955 b) used their holdup data to determine the void fraction in packings under operating conditions. The ultimate aim was to separate the mass transfer coefficients k_g and k_l from the volumetric mass transfer coefficients $k_g a_e$ and $k_l a_e$, respectively. They presented their findings in a series of plots (variation of fraction of total area wetted and effective interfacial area with respect to liquid and gas rates) for Raschig rings and Berl saddles of various sizes (0.5, 1.0, 1.5 inch naphthalene Raschig rings and 0.5, 1.0 inch Berl saddles). The wetted area of the packing was found to increase with increasing liquid rates and decrease with increasing gas rates up to the loading point. The following equations were used to correlate their data for Raschig rings and Berl saddles, respectively.

$$\frac{a_w}{a_p} = 0.24 \left[\frac{L'}{G'}\right]^{0.25} \qquad (Eq\ 3.32)$$

$$\frac{a_w}{a_p} = 0.35 \left[\frac{L'}{G'}\right]^{0.20} \qquad (Eq\ 3.33)$$

where,
a_w = wetted area of the packing, m^2/m^3

a_p = specific surface area of the packing, m^2/m^3

L' = superficial mass flowrate of liquid, kg/m^2-s

G' = superficial mass flowrate of gas, kg/m^2.s

Onda, Takeuchi and Okumoto (1968) proposed the following correlation for the wetted surface area of the packing (a_w).

$$\frac{a_w}{a_p} = 1 - \exp\left\{-1.45 \left(\frac{\sigma_c}{\sigma}\right)^{0.75} \left(\frac{L'}{a_p\, \mu_L}\right)^{0.1} \left(\frac{L'^2 a_p}{{\rho_L}^2 g}\right)^{-0.05} \left(\frac{L'^2}{\rho_L\, \sigma\, a_p}\right)^{0.2}\right\} \quad (Eq\ 3.34)$$

where,

a_w = wetted area of the packing, m^2/m^3

a_p = specific surface area of the packing, m^2/m^3

σ_c = critical surface tension of the packing material, N/m

σ = surface tension of the liquid, N/m

L' = superficial mass flowrate of liquid, kg/m^2-s

μ_L= liquid viscosity, kg-m/s^2

ρ_L = liquid density, kg/m^3

It was assumed that the wetted surface area of the packing was equal to the effective interfacial area. The liquid-side mass transfer coefficient and the gas side mass transfer coefficient were obtained by dividing $k_l a_e$ and $k_g a_e$ data in the literature by the wetted area found from Equation 3.34.

Wetted surface area and effective interfacial area are closely related, since only the wetted area can be effective (available) for mass transfer. However, the wetted surface area includes stagnant liquid pools or dead zones in the packing where the liquid does not re-mix or drain and is unavailable for mass transfer. Apart from the liquid hold up on the packing, the effective interfacial area also accounts for surfaces of drops and jets. Thus, the wetted surface area and the effective interfacial area, though closely related, differ (Wang 2005).

Puranik and Vogelpohl (1974) proposed a generalized correlation for the effective interfacial area during vaporization and absorption (with and without chemical reaction). The available data for effective interfacial area was analyzed based on the concept of static and dynamic/operating holdup or areas as developed by Shulman, *et al.* (1955 a). The maximum total effective interfacial area is the sum of the static and dynamic areas and is equal to the total wetted area.

$$a_{e\ max} = a_w = a_{st} + a_{dyn} \qquad (Eq\ 3.35)$$

where,

$a_{e,\ max}$ = maximum effective interfacial area of the packing, m^2/m^3

a_{st} = static area of liquid in the packing, m^2/m^3

a_{dyn} = dynamic area of liquid in the packing, m^2/m^3

As reported by Shulman, *et al.* (1955 a), the effective interfacial area during vaporization is the sum of the static and the dynamic areas. The effective interfacial area during absorption (without chemical reaction), is equal to the dynamic area (proportional to the operating holdup).

The generalized correlation for the predicted effective interfacial area is given by

$$\left(\frac{a_e}{a_p}\right)_{predicted} = 1.045\ (Re)^{0.041}\ (We)^{0.133}\ \left(\frac{\sigma}{\sigma_c}\right)^{-0.182} \qquad (Eq\ 3.36)$$

and the correlation for static area (a_{st}) is given by

$$\frac{a_{st}}{a_p} = 0.229 - 0.091 \ln\left(\frac{We}{Fr}\right) \qquad (Eq\ 3.37)$$

where,

$$Re = \frac{L}{a_p\ \mu_L}$$

$$We = \frac{L^2}{a_p\ \rho_L\ \sigma}$$

$$Fr = \frac{L^2\ a_p}{{\rho_L}^2\ g}$$

$$\frac{We}{Fr} = \frac{\rho_L \, g}{{a_p}^2 \sigma}$$

The ratio of Webber number to Froude number represents the ratio of gravitational force to the surface tension.

For specified liquid and gas rates, the specific wetted area of the packing attains a definite value (by Equation 3.32 or 3.33). By increasing the gravitational force, the specific static area of the packing can be reduced (see Equation 3.37), thereby increasing the dynamic area of the packing. Thus, the effective interfacial area of the packing would increase with increasing gravity.

Zech and Mersmann (1979) developed a method to separate the interfacial area (a_e) from the volumetric liquid-side mass transfer coefficients ($k_l a_e$) based on the theory of unsteady state diffusion and hydrodynamics of rivulets. In packed columns, the liquid flows down the packing surface in the form of rivulets at a contact angle (greater than zero) with the solid surface. The specific surface area of the rivulets ($a_{rivulet}$) is less than the specific surface area (a_p) of the packing ($a_{rivulet}/a_p < 1$). To calculate the specific surface area of the rivulets, the relationship between the width and the velocity of the rivulet, the flow rate of the liquid, and properties of both the liquid and the packing must be established.

The real packing was assumed to be replaced by a system of parallel cylindrical channels with the same specific surface area (a_p) and voidage (ε) as the real packing. The diameter of the real packing element was d_a while the hydraulic diameter of the channel was d_h. When a rivulet of width b and depth δ flows over the channel,

$$\frac{a_e}{a_p} = \frac{b}{d_h \, \pi}$$

where,
b = width, m

d_h = hydraulic diameter of channel, m

Theoretical considerations of rivulet hydrodynamics result in

$$\frac{a_e}{a_p} = f\ (Re, Ga, We/Fr)$$

where,
Ga = liquid Galilei number

$$\text{Ga} = \frac{\delta^3\ \text{g}}{{\nu_\text{L}}^2}$$

δ = film thickness, m

Based on experimental results for liquid-phase controlled distillation systems, a new correlation for the effective interfacial area was proposed (Equation 3.38). Experimentally, it was found that the liquid Galilei number had no effect on the effective interfacial area.

$$\frac{a_e}{a_p} = K_L\ Re^{0.5} \left(\frac{We}{Fr}\right)^{0.45} \qquad (Eq\ 3.38)$$

where,
K_L = overall liquid side mass transfer coefficients, m/s

$$\frac{We}{Fr} = \frac{\rho_L\ g\ {d_a}^2}{\sigma}$$

$$Re = \frac{u_L}{\nu_L\ d_a}$$

d_a = diameter of packing element, m

Thus, the effective interfacial area is proportional to gravity to the power of 0.45.

Billet and Schultes (1993) also proposed the following correlation for finding the ratio of effective interfacial area to the specific surface of the packing.

$$\frac{a_e}{a_p} = 1.5\ \left(a_p d_h\right)^{-0.5} \left(\frac{u_L d_h}{\nu_L}\right)^{-0.2} \left(\frac{{u_L}^2 \rho_L d_h}{\sigma}\right)^{0.75} \left(\frac{{u_L}^2}{g\ d_h}\right)^{-0.45} \qquad (Eq\ 3.39)$$

where,
d_h = hydraulic diameter of channel, m

u_L = linear velocity, m/s

v_L = kinematic viscosity of liquid, m^2/s

The correlation was developed based on dimensional analysis of parameters influencing the volumetric mass transfer coefficients. The proposed model was checked against an extensive database comprised of 31 different fluid systems and 67 different types and sizes of packings. As with the work of Zech and Mersmann (Zech 1979), the effective interfacial area was found to be proportional to 0.45 power of gravity.

III.1.2 – Flooding

III.1.2.i – Theory

Flooding may be defined as the upper capacity limit of packed column operation at which the pressure drop of gas flow through the packing increases to such an extent that the liquid is unable to flow downwards against the rising vapor (Stichlmair 1998). The increased holdup of liquid by gas results in decreased voidage and smaller effective interfacial area, causing a sharp decrease in separation efficiency (Kelleher 1993). The gas velocity at which flooding occurs is called the flooding velocity. The flooding velocity limits the hydraulic capacity of columns. As a factor of safety, conventional packed columns are designed to operate at 60 – 90 % of the flooding velocity.

In conventional packed columns, the hydraulic capacity is determined using the Sherwood chart (Sherwood, Shipley et al. 1938) or any other generalized pressure drop chart (GPDC) (Eckert 1970). From Figure 3.5, the abscissa of the Sherwood chart is

$$X = \frac{L}{G}\sqrt{\frac{\rho_G}{\rho_L}} \qquad (Eq\ 3.40)$$

where,

X = Sherwood chart abscissa

L = liquid mass flowrate, kg/s

G = gas mass flowrate, kg/s

ρ_G = gas density, kg/m^3

ρ_L = gas density, kg/m^3

The ordinate of the Sherwood chart is

$$Y = \frac{{U_G}^2 a_p}{g\,\varepsilon^3}\left(\frac{\rho_G}{\rho_L}\right)\left(\frac{\mu_L}{\mu_W}\right)^{0.2} \qquad (Eq\ 3.41)$$

where,

U_G = superficial velocity of gas, m/s

g = acceleration, m/s^2

a_p = specific surface area of the packing, m^2/m^3

ε = porosity of the packing

μ_L = viscosity of the liquid, kg/m-s

μ_W = viscosity of water, kg/m-s

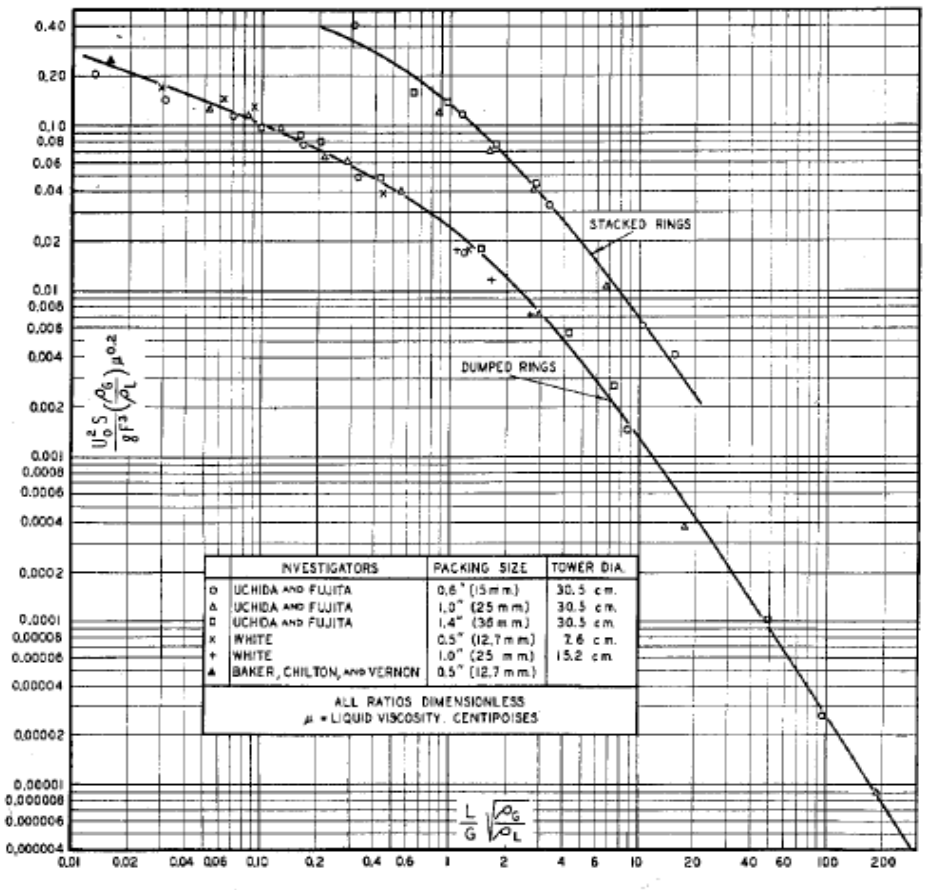

Figure 3.5 – Sherwood Flooding Chart
[Reference: Sherwood, T. K., G. H. Shipley, et al. (1938). "Flooding velocities in packed columns." Industrial and Engineering Chemistry **30**: 765-769.]

III.1.2.ii – Effect of Gravity

Flooding in Higee rotor is analogous to that in conventional columns. For a conventional packed column, the applied acceleration is constant and equal to the Earth's terrestrial acceleration (g = 9.81 m/s^2). For a fixed value of abscissa on the Sherwood chart, the acceleration limits superficial gas velocity, thereby limiting the hydraulic capacity of the column. For a Higee unit, the applied acceleration can be increased many fold by increasing the radial velocity as

$$g = r\,\omega^2 \qquad (Eq\ 3.42)$$

where,
r = radius of packing rotor of Higee unit, m
ω = radial velocity, rad/s

By increasing the gravitational acceleration, higher flooding velocities, and hence, higher operating gas velocities can be employed for normal operation. Thus, higher hydraulic capacity can be achieved in small sized equipment.

For a Higee rotor, flooding occurs first at the inner radius or the eye of the rotor where the acceleration is the lowest, while the liquid and vapor velocities are the highest. The hydraulic capacity of Higee is limited by the acceleration at the inner radius ($r_i\omega^2$) and the flow area at the inner radius ($2\pi r_i h$). Greater hydraulic capacity in Higee can be achieved by simply increasing the rotational velocity as opposed to increasing the diameter of a conventional packed column. Conversely, a reduction in the rotational velocity at constant liquid and gas flow rates will lead to flooding.

III.1.2.iii – Previous work on Flooding in Higee

Munjal (1986) evaluated the hydraulic performance of Higee by absorbing carbon dioxide from air into sodium hydroxide. The packing for his hydraulic tests were 1.09 mm spherical glass beads and 3 mm glass beads. The gravitational acceleration was varied from 35 to 135 times the terrestrial acceleration of the earth. The liquid flowrate was varied from 0.6 to 6 gallons per minute (GPM). The flood point or flooding condition was defined by,

1. formation of an opaque mist at the eye of the rotor,
2. heavy water spray in the gas exit pipe (indicating carryover of liquid), and
3. fluctuations in the pressure drop and flow readings.

It was found that the Sherwood chart underestimated the flooding gas velocity by about 40 to 70%. Munjal attributed this under-prediction to the difference in geometry of packings employed in development of the Sherwood chart, and his work.

Singh (1989) compared his flooding data with the Sherwood correlation. In his work, flooding was defined at a pressure drop of 498 Pa/100 rpm or greater. The normal operating pressure drop

was found to be 24.9 Pa/100 rpm. Consequently, the operating limit on the radial velocity was set at a pressure drop greater than 498 Pa. The results of Singh's hydraulic tests are shown in Figure 3.6. The Sherwood chart under-predicted the limit of operability by about 40 % for Sumitomo packing. However, predictions by the Sherwood chart were satisfactory for the wire gauze packing.

Kelleher (Kelleher 1993) performed hydraulic tests on Sumitomo packing having a specific surface area of 2500 m^2/m^3 and porosity of 0.92. The flood point was defined as the inflection point in the pressure drop against rotational speed at constant reboiler duty (as seen in Figure 3.7). The Sherwood correlation was found to predict the flood point to within 10 %. However, the accuracy of the Sherwood plot was checked against limited data points. The need for comparing the predictions of the Sherwood chart against extensive flooding data was highlighted.

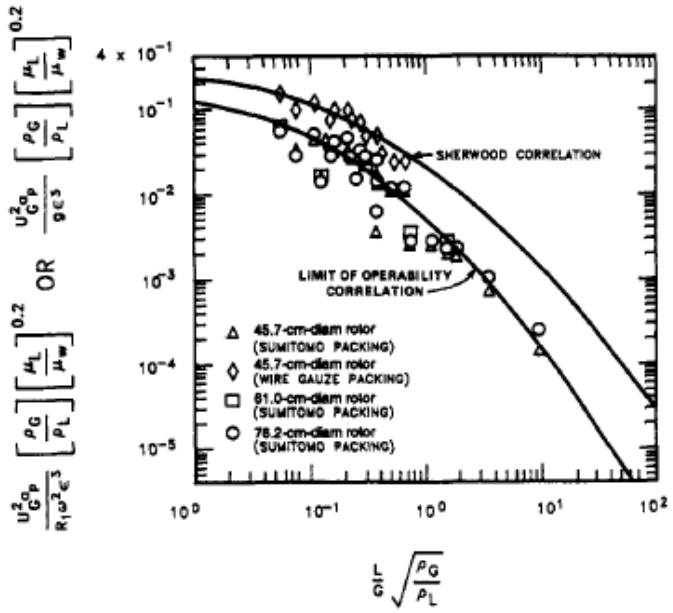

Figure 3.6 – Hydraulic Test Results of Singh's Work
[Reference: Singh, S. (1989). Air Stripping of Volatile Organic Compounds from Groundwater: An Evaluation of A Centrifugal Vapor-Liquid Contactor. Knoxville, The University of Tennessee. Ph.D Dissertation.]

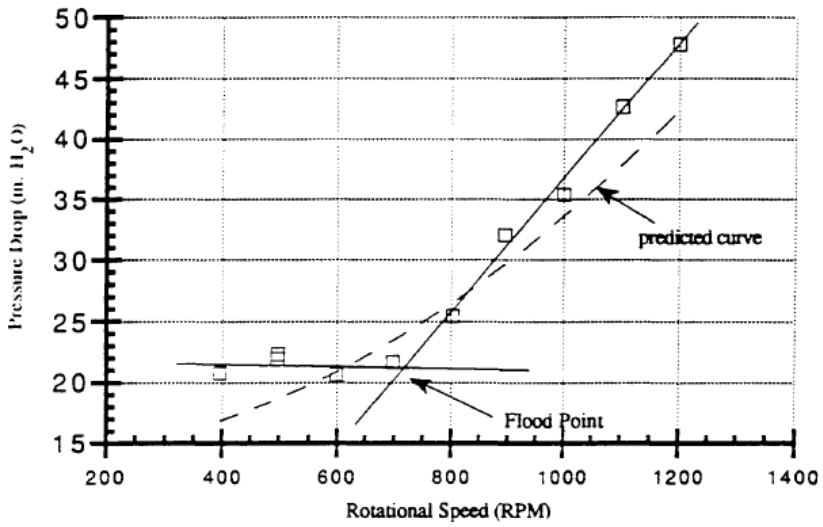

Figure 3.7 – Flood Point in Kelleher's Work at 60 psia and 0.9 MMBtu/hr Reboiler Duty [Reference: Kelleher, T. (1993). Mass Transfer and Hydraulic Operating Characteristics of a Pilot-Plant Scale High Gravity Contacting Unit. Austin, The University of Texas. M.S. Thesis]

III.1.3 – Power Consumption

Power required to rotate the packing (rotor) is a prime disadvantage of Higee. Calculating the amount of power required is crucial in making economic comparisons. Power in a Higee rotor is required to overcome

1. frictional loss as the liquid gets accelerated through the packing (Singh 1989), and
2. accelerating liquid from the eye to the outer rotor (Singh 1989)

The frictional losses vary greatly with the type of packing, material of packing, and design of machine (bearings, drives etc). The power required to overcome the accelerating liquid can be quantified based on the model of Leonard (1980). According to this model, the power consumption can be found using

$$P_C = Z_0 + Z_1 \rho_L {r_o}^2 \omega^2 Q_L \qquad (Eq\ 3.43)$$

where,

P_c = power consumption (kW)

ρ_L = liquid density (kg/m^3)

r_o = outer radius of rotor (m)

ω = radial velocity (rad/s)

Q_L = volumetric flow rate of liquid (m^3/s)

Z_0, Z_1 = constants (kW)

The constant Z_1 accounts for the slippage between the liquid and the rotating packing. The constants Z_0 and Z_1 were regressed by Singh (1989) to yield the expression for power consumed in a Higee. The regressed expression was

$$P_C = 1.222 + 0.0011\,\rho_L\, {r_o}^2 \omega^2\, Q_L \qquad (Eq\ 3.44)$$

The variation of power consumption with rotational velocity is shown in Figure 3.8 below. Equation 3.44 was found to correlate the experimental data within 20%.

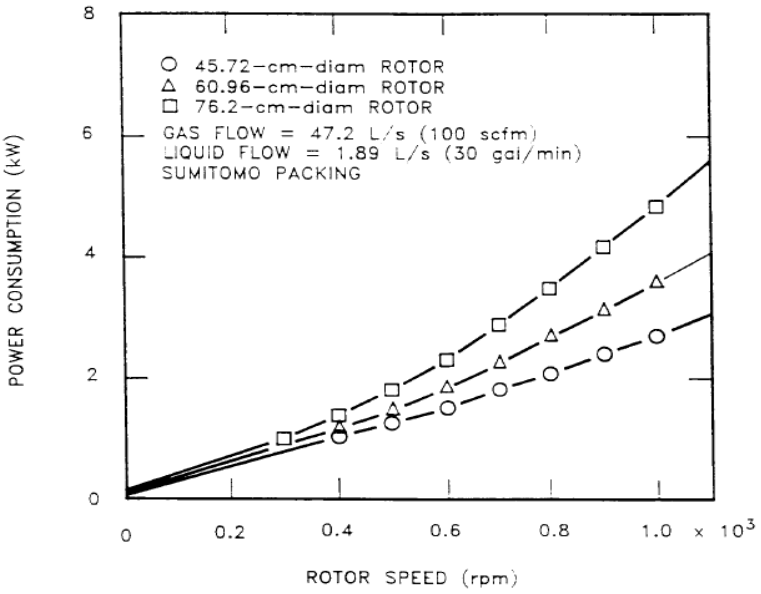

Figure 3.8 – Variation of Power Consumption with Radial Velocity in Singh's Work [Reference: Singh, S. (1989). Air Stripping of Volatile Organic Compounds from Groundwater: An Evaluation of A Centrifugal Vapor-Liquid Contactor. Knoxville, The University of Tennessee. PhD Dissertation]

III.1.4 – Pressure Drop

III.1.4.i – Theory

Kelleher (Kelleher 1993) developed a correlation for pressure drop through a Higee unit based on first principles. The pressure drop was modeled by using the volume average equations of motion (Bird 1960) to model the flow through Higee. The following assumptions were made:

1. Incompressible gas phase,
2. No axial or tangential variations in flow, and
3. Steady state operation.

Using these assumptions, the volume average radial momentum equation reduces to

$$\rho_G \left(u_r \frac{\partial u_r}{\partial r} - \frac{{u_\theta}^2}{r} \right) = - \frac{\partial P}{\partial r} + Drag \qquad (Eq\ 3.45)$$

where,
ρ_G = gas density, kg/m^3

u_r = radial vapor velocity, m/s

u_θ = tangential vapor velocity, m/s

P = pressure, Pa

r = radial distance, m

To integrate Equation 3.45 from the inner radius of the rotor to the outer radius, all variables were defined as functions of radius. The radial vapor velocity was related to the superficial gas velocity as

$$u_r = \varepsilon U_G = \frac{\varepsilon L}{2 \pi r h \rho_G} \qquad (Eq\ 3.46)$$

where,
ε = porosity of the packing

U_G = superficial gas velocity, m/s

L = liquid flowrate, kg/s

h = axial height of the packing rotor, m

The tangential velocity was defined by

$$u_\theta = r\,\omega \qquad (Eq\ 3.47)$$

where,

ω = radial velocity, rad/s

The drag model used (Kelleher 1993) was defined by

$$Drag = \left(\frac{8.5\,\mu_G\,{a_p}^2}{\varepsilon^3}\right)\bar{V} + \frac{a_p\,\rho_G}{\varepsilon^3}\left(\frac{L}{2\,\pi\,r\,h\,a_p\,\mu_g}\right)^{0.1}\bar{V}^2 \qquad (Eq\ 3.48)$$

where,

$\bar{V}$ = slip velocity between gas phase and second phase present, m/s

μ_G = gas viscosity, kg/m-s

a_p = specific surface area of packing, m^2/m^3

ε = porosity of packing

Substituting the derivative of Equation 3.46, Equation 3.47 (entire form), and Equation 3.48 (entire form) into Equation 3.45 yielded the following expression for change in pressure:

$$\frac{\partial P}{\partial r} = \rho_G\left[r\,\omega^2 + \left(\frac{\varepsilon\,L}{2\,\pi\,h\,\rho_G}\right)^2\frac{1}{r^3}\right] + A\,\bar{V} + \frac{B'}{r^{0.1}}\,\bar{V}^2 \qquad (Eq\ 3.49)$$

where,

$$A = \left(\frac{8.5\,\mu_G\,{a_p}^2}{\varepsilon^3}\right)$$

$$\frac{B'}{r^{0.1}} = \frac{a_p\,\rho_G}{\varepsilon^3}\left(\frac{L}{2\,\pi\,r\,h\,a_p\,\mu_g}\right)^{0.1}$$

Integrating Equation 3.49 from the inner radius to outer radius, while neglecting the liquid effects and the low Reynolds drag effect (constant A), resulted in the following the pressure drop correlation:

$$\Delta P = \frac{\rho_G \omega^2}{2}\left(r_o{}^2 - r_i{}^2\right) + \frac{5\,B'}{22}\left(\frac{\varepsilon\, L}{\pi\, h\, \rho_G}\right)^2\left(\frac{1}{r_i{}^{1.1}} - \frac{1}{r_o{}^{1.1}}\right) \qquad (Eq\ 3.50)$$

where,

ΔP = pressure drop across the Higee rotor, Pa

ω = radial velocity, rad/s

r_o = outer radius of rotor, m

r_i = inner radius of rotor, m

The first part of Equation 3.50 relates to the pressure drop due to rotation while the second part represents the high Reynolds number drag. The pressure drop is found to vary as the square of the rotational speed.

III.1.4.ii – Previous work on Pressure Drop in Higee

Keyvani (1989) modeled the pressure drop across Higee. The total pressure drop in a Higee unit was assumed to be the sum of pressure drops across the rotor and between the stationary casing and the spinning rotor. The pressure drop across the two regions was found by applying a momentum integral balance on each region and numerically solving the resulting equations for two cases: for the dry bed (with no liquid flow) and with liquid flow (irrigated bed). The resulting equation described the experimental data within 20% for dry bed. For an irrigated bed the equation under-predicted the experimental data within 20%. The experimental data showed a lower pressure drop for an irrigated bed compared to a dry bed for the same conditions as seen in Figure 3.9. The developed model could not explain this anomaly. It was suggested that the liquid might act as lubricant; thereby reducing the drag force between the vapor and the packing.

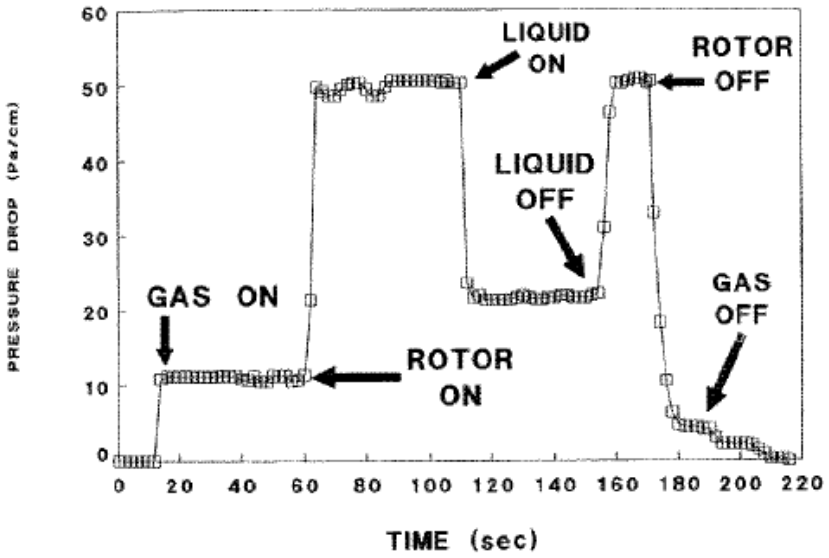

Figure 3.9 – Pressure Drop across Higee Rotor in Keyvani's Work
[Reference: Keyvani, M. (1989). "Operating characteristics of rotating packed beds." Chemical Engineering Progress **85**(9): 48-52.]

The pressure drop was found to increase as the square of the radial velocity as shown in Equation 3.51.

$$\Delta P \propto \omega^2 \qquad (Eq\ 3.51)$$

where,
ΔP = pressure drop across the Higee rotor, Pa

ω = radial velocity, rad/s

Singh (1989) developed a semi-empirical correlation to model the pressure drop across the Higee unit based on his experimental data. The pressure drop correlation had two terms: the first term accounts for the rotation of the packing and the second accounts for the fluids flowing through the packing. The correlation is

$$\Delta P_{tot} = 0.923\,\rho_G\ \omega^2\,(r_2{}^2 - r_1{}^2) + 0.992\,\rho_G \left(\frac{a_p}{\varepsilon}\right)(r_2{}^2 - r_1{}^2)\,U_{G,ave}{}^2 \qquad (Eq\ 3.52)$$

where,
ΔP_{tot} = pressure drop across the Higee rotor, Pa

ρ_G = gas density, kg/m^3

ω = radial velocity, rad/s

r_2 = outer radius of the rotor, m

r_1 = inner radius of rotor, m

a_p = specific surface area of the packing, m^2/m^3

ε = porosity of the packing

$U_{G,ave}$ = average superficial velocity of the gas, m/s

The expression fit the data within 30%. The correlation was semi-empirical in nature and based on many simplifications. However, it was easy to use and fairly accurate.

Kelleher (1993) collected pressure drop data by varying reboiler duties and rotational speed. As expected, the pressure drop was found to increase as the square of the radial velocity as shown in Figure 3.10. The pressure drop increased linearly with the reboiler duty. Increasing reboiler duty was a measure of the increasing vapor rates. The expression presented as Equation 3.50 in the theory section correlated the experimental data to within 20%. To compare the pressure drop in Higee and conventional packed columns, Kelleher suggested using the criteria of pressure drop per theoretical stage ($\Delta P/N_{theo}$) instead of pressure drop per inch of packing (ΔP/inch of packing). Pressure drop per theoretical stage ($\Delta P/N_{theo}$) is independent of the flow or cross sectional area.

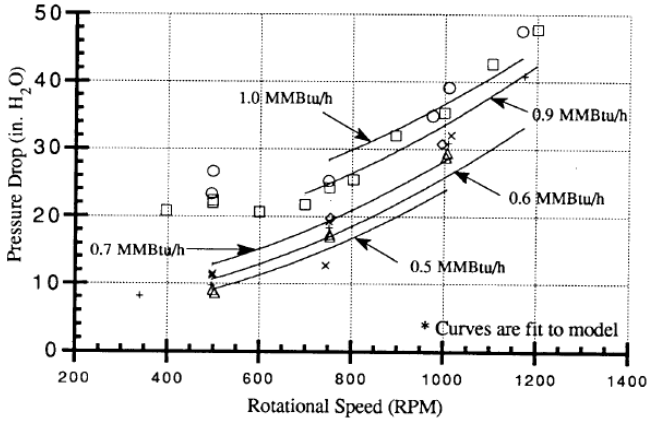

Figure 3.10 – Variation of Pressure Drop with Rotational Speed at 60 psia in Kelleher's work [Reference: Kelleher, T. (1993). Mass Transfer and Hydraulic Operating Characteristics of a Pilot-Plant Scale High Gravity Contacting Unit. Austin, The University of Texas. M.S. Thesis]

III.2 – Design

The design of conventional packed columns involves determining the required diameter and the depth of packing. The diameter of the column must be large enough to accommodate the desired liquid and gas rates and provide adequate hydraulic capacity. Similarly, the packing depth must be sufficient to achieve the desired separation. Analogous to conventional packed columns, the design of a Higee unit involves determining the flow area at the eye and the radial depth of the doughnut shaped packing. Since in a Higee rotor flooding is expected to occur first at the eye, the flow area at the eye limits the hydraulic capacity. Thus, determining the flow area for a given hydraulic capacity is equivalent to finding the diameter of a conventional packed column. Determining the radial depth of packing in a Higee rotor is equivalent to finding the vertical packed bed depth required to achieve desired separation. Hence, methods employed for finding the diameter and the packing depth in conventional packed columns can be utilized for determining the flow area at the eye and the radial depth of the Higee rotor with some modifications.

III.2.1 – Hydraulic Capacity

In design of conventional packed columns, the diameter is found based on flooding limit, by use of Sherwood (Sherwood, Shipley et al. 1938) or any other generalized pressure drop chart (GPDC) (Eckert 1970). Munjal (1986) and Singh (1989) verified the validity of using the Sherwood (1938) chart for determining flooding in Higee. Thus, the flow area at the eye can be found using a Sherwood type flooding chart.

III.2.2 – Packing Depth

Packing depth in a Higee rotor refers to the radial depth of packing (the difference between the outer radius and the inner radius of the packing). This distance needs to be calculated from a mass transfer point of view.

The mass transfer in a Higee rotor needs to be calculated on the basis of transfer unit concept similar to that for conventional columns. Singh (1989) performed material balance on a differential volume of the rotor (as shown in Figure 3.11) to find the overall mass transfer coefficient.

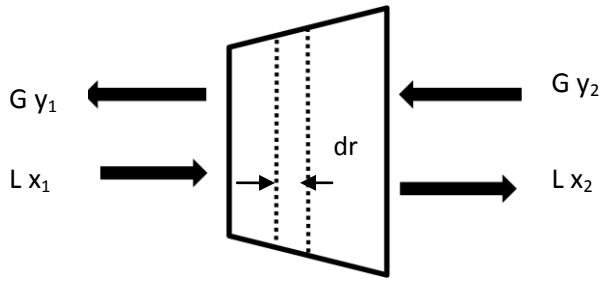

Figure 3.11 – Differential Volume Element of Higee Rotor
[Adapted from: Singh, S. (1989). Air Stripping of Volatile Organic Compounds from Groundwater: An Evaluation of A Centrifugal Vapor-Liquid Contactor. Knoxville, The University of Tennessee. Ph.D Dissertation]

A material balance for the liquid phase over the differential element leads to

$$\frac{d(L\,x_A)}{dV} = K_L a_e\,(x_A - x_A^*) \qquad (Eq\ 3.53)$$

where,

L = liquid mass flow rate, kg/s

x_A = mole fraction of component A in liquid phase

x_A*= mole fraction of component A in equilibrium with vapor mole fraction y_A

$K_L a_e$ = overall volumetric liquid side mass transfer coefficient, s^{-1}

The relationship between the volume of the differential element and the radius of the rotor is

$$dV = 2\,\pi\,r\,h\,dr \qquad (Eq\ 3.54)$$

where,

dV = volume of the differential element, m^3

r = radius of the element, m

h = axial height of the element, m

Substituting Equation 3.54 into Equation 3.53 and assuming the liquid flowrate to be constant resulted in

$$2\,\pi\,r\,dr\;=\;\frac{L}{\rho_L\;h\;K_L a_e}\int_{x_1}^{x_2}\frac{dx_A}{(x_A\;-\;x_A{}^*)} \qquad (Eq\ 3.55)$$

Equation 3.55 was integrated from the inner radius to the outer radius of the rotor yielding

$$\pi\,(r_o{}^2\;-\;r_i{}^2)\;=\;\frac{L}{\rho_L\,h\,K_L a_e}\int_{x_1}^{x_2}\frac{dx_A}{(x_A-\;x_A{}^*)} \qquad (Eq\ 3.56)$$

$$\pi\,(r_o{}^2\;-\;r_i{}^2)\;=ATU\;\times NTU \qquad (Eq\ 3.57)$$

where,

ATU = area of a transfer unit, m^2

NTU = number of transfer units

The Number of Transfer Units (NTU) defined above is the same as that for conventional packed columns. The NTU is a measure of the efficiency of separation. Greater value of NTU is desirable. From Equations 3.56 and 3.57, NTU is defined as

$$NTU=\int_{x_1}^{x_2}\frac{dx_A}{(x_A-\;x_A{}^*)} \qquad (Eq\ 3.58)$$

The Area of Transfer Unit (ATU) is analogous to the concept of Height of a Transfer Unit (HTU) in conventional packed columns. The ATU accounts for the difference in liquid loading with the increasing radius. The concept of HTU needs to be modified for Higee as the HTU required to achieve a step of separation would decrease with increasing radius. The ATU defined in Equation 3.59 below maintains a constant value over the entire rotor (from inner to the outer radius).

$$ATU=\frac{L}{\rho_L\;h\,K_L a_e} \qquad (Eq\ 3.59)$$

Using the definition of ATU shown in Equation 3.59, the overall volumetric mass transfer coefficient can be defined as below.

$$K_L a_e = \frac{L}{\rho_L \, h \, ATU} = \frac{L \times NTU}{\rho_L \, h \, \pi \, (r_o{}^2 - r_i{}^2)} \qquad (Eq\ 3.60)$$

III.2.3 – Stepwise Design Procedure

Kelleher (1993) outlined the preliminary stepwise design procedure for Higee rotor. The aim is to find the inner radius, outer radius and the axial height of the rotor for given operating conditions; flow rates, temperatures and pressure. The radial velocity and packing properties have to be assumed. The steps involved in the procedure are as follows:

1. The abscissa value of the flooding correlation of Sherwood *et al.* (1938) needs to be determined.

$$X = \frac{L}{G} \sqrt{\frac{\rho_G}{\rho_L}} \qquad (Eq\ 3.61)$$

2. Find the ordinate (Y) from the flooding correlation of Sherwood *et al.* (1938). This can be done either graphically or by curve fitting.
3. The flooding velocity is then calculated from the ordinate term by using

$$U_G = \sqrt{\frac{Y \, r_i \, \omega^2 \, \varepsilon^3}{a_p} \left(\frac{\rho_L}{\rho_G}\right) \left(\frac{\mu_W}{\mu_L}\right)^{0.2}} \qquad (Eq\ 3.62)$$

4. The area at the eye of the rotor can be found using

$$Area_{eye} = 2 \, \pi \, r_i \, h = \frac{L}{\rho_G \, U_G} \qquad (Eq\ 3.63)$$

5. The gas diffusivity is determined using the Fuller-Schettler-Giddings (1966) correlation,

$$D_G = \frac{0.0001\, T^{1.75} \left(\frac{1}{M_A} + \frac{1}{M_B}\right)^{1/2}}{P \left(\sum {v_A}^{1/3} + \sum {v_B}^{1/3}\right)^2} \qquad (Eq\ 3.64)$$

6. The Area of Transfer Unit (ATU) needs to be determined. The ATU is a function of both the rotor size and mass transfer coefficients.

$$ATU = \frac{L}{\rho_L\ h\ K_L a_e} = \frac{\pi\ ({r_o}^2 - {r_i}^2)}{NTU} \qquad (Eq\ 3.65)$$

where,

$$K_L a_e = \frac{1}{\left(\frac{1}{k_G a_e} + \frac{1}{k_L a_e}\right)} \qquad (Eq\ 3.66)$$

$$k_G a_e = 2.3\ E-07 \left(\frac{a_p D_G}{d_p}\right)\left(\frac{G}{a_p \mu_G}\right)^2 \left(\frac{{d_p}^3 {\rho_G}^2\ r\ \omega^2}{{\mu_G}^2}\right)^{0.33} \left(\frac{\mu_G}{\rho_G D_G}\right)^{-0.33} \qquad (Eq\ 3.67)$$

$$k_L a_e = \frac{L\ {a_p}^2}{337143.86\ \rho_L\ h}\left(\frac{L}{\mu_L a_p}\right)^{-0.6} \left(\frac{{\rho_L}^2\ r\ \omega^2}{{\mu_L}^2\ {a_p}^3}\right)^{0.15} \qquad (Eq\ 3.68)$$

7. The Number of Transfer Units (NTU) is the measure of ease in achieving desired separation. The NTU is defined by Equation 3.58.

$$NTU = \int_{x_1}^{x_2} \frac{dx}{x - x^*} \qquad (Eq\ 3.58)$$

The number of transfer units can be found by evaluating the integral defined above.

8. The axial height was related to the outer radius by the following correlation based on previously studied Higee units.

$$h = \frac{r_o}{2} \qquad (Eq\ 3.69)$$

Equations 3.63, 3.65 and 3.69 need to be solved simultaneously to obtain r_i, r_o and h. This requires an iterative procedure, as the local and overall mass transfer coefficient correlations are a function of the mean radius defined as

$$r = \sqrt{\left(\frac{{r_o}^2 + {r_i}^2}{2}\right)} \qquad (Eq\ 3.70)$$

Shortcomings of the design procedure are as follows:

1. The above developed procedure has three variables: the inner radius (r_i), outer radius (r_o) and the axial height (h). The radial velocity (ω) is fixed initially. The rationale behind selecting a specific radial velocity is not provided.
2. No limit is imposed on the minimum acceleration at the eye. For a fixed radial velocity, a set of values of r_i, r_o and h can be found where the inner radius r_i is very small, while the outer radius and the axial height are very large. This can result in extremely low acceleration ($r_i\omega^2$) at the eye. Liquid discharged from the distributor gets attached to the inner periphery of the packing as the liquid does not have the same radial velocity as the rotor (at the inner radius). Low acceleration at the eye may not be able to force this attached liquid radially outwards. This may result in blockage of available void spaces.
3. Small value of the inner radius (r_i) may prevent the liquid distributor system being installed in the casing.
4. Large value of the axial height requires multiple projections on the liquid distributor to wet the entire depth of the packing. This ensures that all of the exiting vapor contacts the liquid. Initial wetting of packing greatly influences packing performance (Trent 1999).

These drawbacks can be removed by making minor adjustments to the design procedure as seen in Chapter IV.

CHAPTER IV

DESIGN OF HIGEE UNIT

Design of a Higee distillation unit involves sizing the rotor; determining the inner radius, the outer radius, axial height of the rotor, and the radial velocity for a given hydraulic capacity as seen in Figure 4.1.

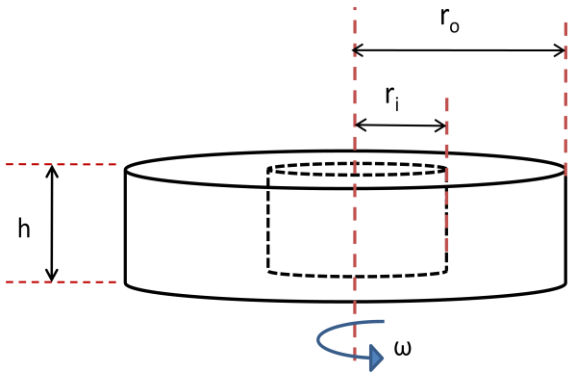

Figure 4.1 – Design Variables for Higee Rotor

The hydraulic capacity dictates a specific flow area at the eye or the center of the rotor. This flow area can be determined by using flooding charts. The radial distance between the inner and outer radii is analogous to the depth of packing required in vertical columns to achieve desired separation. This distance is calculated from mass transfer considerations. The design requires an iterative procedure since the value of the mean radius is required to find the mass transfer coefficients and the outer radius.

The design variables; the inner radius, outer radius, axial height, and the radial velocity need to satisfy the following constraints.

1. The inner radius and the radial velocity determine the acceleration at the eye of the rotor. A minimum value of 100 g (presumed value at the mean radius) or more needs to be maintained to ensure significant increase in mass transfer flux (Martin 1992).
2. The inner radius and the axial height determine the flow area at the eye of the rotor. Flooding of the rotor occurs first at the eye, where the acceleration is lowest while the liquid and vapor rates per unit area are the greatest (Fowler 1989; Kelleher 1993). The flow area at the eye must be sufficiently large to provide adequate hydraulic capacity.
3. The inner radius must be large enough to accommodate the liquid distribution system. The axial height must be appropriate, so that the liquid exiting the distributor wets the entire depth of the rotor.
4. The outer radius should not be large enough to exceed the stress limitations of the support system (Kelleher 1993).

Thus, the design of Higee involves finding the optimum values of design variables which satisfy the various constraints mentioned above. If more than one value of a design variable is found to satisfy all the constraints, then a new criterion must be utilized to select a unique configuration for the unit. In absence of reliable cost estimates, rate of increase of mass transfer coefficients with acceleration, power requirement, pressure drop, and flow area (limits flooding) are additional criteria which can be used to select the final configuration in such situations.

Unlike conventional distillation columns, the mechanical set up of the rotor does not allow feed to be introduced at some intermediate radial distance. As a result, two separate rotors are required for rectification and stripping service for any application, respectively (Wang, Xu et al. 2008). Thus in the present study, two rotors, Rectification Higee and Stripping Higee, are designed.

IV.1 – Design Basis

Sizing of a conventional distillation column is based on certain pre-specified conditions such as feed rate and composition, distillate recovery and purity, and other constraints. The design of Higee unit for ethanol dewatering is also based on the following minimum pre-specified conditions:

1. Feed rate and composition
2. Distillate purity and recovery
3. Bottoms purity
4. Overhead pressure

The feed rate for the dewatering step depends upon the amount of fermented juice available and the duration of operation. The OSU farm scale ethanol model is to be operated year round (Mukherjee 2009). The amount of fermented juice available for processing is calculated based on the yield of sweet sorghum and the fermentation efficiency. A 500 acre sweet sorghum farm with yield of 30 tons per acre, 55 % juice extraction and 15 % sugar in juice, and a fermentation efficiency of 85 %, results in 2,000,000 gallons of fermented juice available for dewatering (Holcomb 2008). This translates to a feed rate of 250 gallons per hour.

Tests conducted by the Department of Biosystems and Agricultural Engineering at Oklahoma State University on sweet sorghum have found the ethanol content of the fermented juice to vary from 6.5 – 10 vol % (Mukherjee 2009). For design, the lower value of 6.5 % (vol %) ethanol in the fermented juice is selected.

The aim of the farm scale model is to produce at least 190 proof, or azeotropic, ethanol. The final product purity is thus fixed at 190 proof or 95 % (vol %) ethanol (corresponds to 93 wt % ethanol). The ethanol content in the stillage is to be limited to 500 ppm (wt). This ensures that the bottoms can simply be run off onto the farm itself (Mukherjee 2010). This sets the ethanol

recovery such that the minimum final product flowrate is to be around 15 gallons per hour. The rectification Higee is to operate at an overhead pressure of 1 atmosphere (1.033 kg/cm^2). Steam at 150 psia is to be used as the stripping agent. No side stream draw to remove fusel oil is provided. The design basis for the Higee dewatering unit is summarized in Figure 4.2 below.

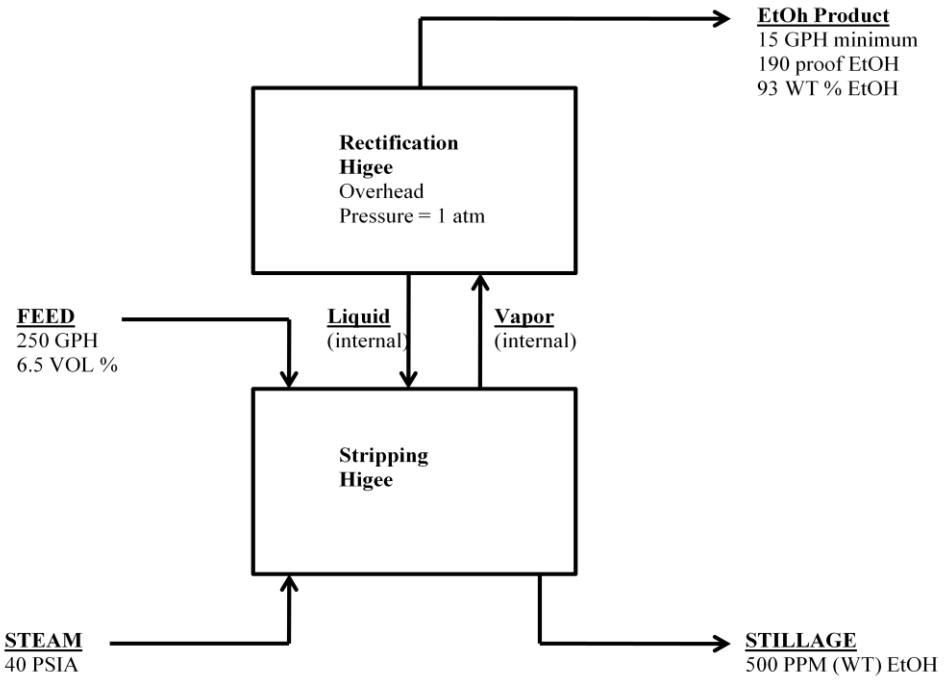

Figure 4.2 – Ethanol Dewatering Design Basis

IV.2- Design Procedure

As mentioned earlier, the rotor sizing involves finding the inner radius, outer radius, axial height and the radial velocity. A primary limitation of a Higee rotor is that the liquid is always introduced at the eye of the rotor or the inner periphery.

The limitations of the design procedure outlined by Kelleher (Kelleher 1993) can be overcome by making minor adjustments and simplifications as follows:

1. The minimum acceleration at the eye is specified instead of the radial velocity. This ensures that the inner radius of the rotor does not become too small.

2. The axial height is set equal to the inner radius (instead of half of the outer radius). This limits the axial height from being excessively large. Large axial height results in multiple projections on the liquid distributor. Coincidentally, the inner radius then can be found simply based on the operating velocity (derived from flooding charts). The iterative process becomes limited to only finding the outer radius.

The detailed step-wise procedure for designing the rotor is as follows:

1. Process parameters: the liquid and gas flow rates, densities and viscosities are found by simulating the ethanol dewatering process in ChemCad using an SCDS column with 27 computational stages (26 theoretical stages in the column and a condenser) with feed introduced on the 14th computational stage. The average liquid and gas rates, densities and viscosities in each section are selected for design of the two rotors respectively (See section IV.3 for details).
2. Packing to be used for the rotor needs to be selected. The packing properties: specific surface area (a_p), void fraction (ε) and specific diameter (d_p) of the packing need to be specified (See section IV.4 for details).
3. The acceleration at the eye of the rotor (a_c) is specified. The minimum value of acceleration at the eye is fixed at 10 g while the maximum acceleration at the eye is limited to 140 g (See section IV.5 for details).
4. Using a flooding chart like Sherwood *et.al.* (1938), the flooding velocity (U_G') can be determined. The operational velocity (U_G) is then defined as some fraction (75 %) of the flooding velocity (See section IV.6 for details).
5. Based on previous published configurations of Higee rotors (Tung and Mah 1985; Singh 1989), the axial height is set equal to the inner radius.

$$h = r_i \qquad (Eq\ 4.1)$$

6. Based on the flooding velocity and the flow area at the eye of the rotor, the inner radius (r_i) is calculated.

$$r_i = \sqrt{\frac{L}{2\,\pi\,\rho_G\,U_G}} \qquad (Eq\ 4.2)$$

7. The radial velocity is then calculated using

$$\omega = \sqrt{\frac{a_c}{r_i}} \qquad (Eq\ 4.3)$$

8. The gas diffusivity is determined using the Fuller-Schettler-Giddings (Fuller 1966) correlation (Equation 3.64, see section IV.7 for details).
9. An initial guess for the outer radius ($r_{o,\ guess}$) is made. The mean radius (r, defined by Equation 3.70) and the corresponding mean acceleration ($r\omega^2$) are calculated.
10. The liquid side volumetric mass transfer coefficient and the gas side coefficient can be determined using the Equations 3.68and 3.67, respectively. The overall liquid side mass transfer coefficient can then be established using Equation 3.66. Finding the mass transfer coefficients requires prior knowledge of the acceleration at the mean radius.
11. The area of the transfer unit (ATU) needs to be determined using Equation 4.4 below.

$$ATU = \frac{L}{\rho_L\,K_L a_e\,h} \qquad (Eq\ 4.4)$$

12. The number of transfer units for each section is found by evaluating the integral in Equation 3.58 using Polymath (See section VI.8 for details).
13. Finally, the outer radius is established using Equation 4.5 below. The difference (Δr) between the calculated value of outer radius and the guess for outer radius is defined. The Solver tool in Microsoft Excel is then used to make this difference zero by changing the

initial guess for the outer radius. A visual check is performed to ensure that the values of the initial guess and the calculated value of the outer radius match.

$$r_o = \sqrt{\left(\frac{ATU \times NTU}{\pi}\right) + r_i^2} \qquad (Eq\ 4.5)$$

14. The height equivalent of a theoretical plate (HETP) is then determined by dividing the radial distance (difference between the outer radius and the inner radius) by the number of theoretical stages (N_{theo}) in that section as seen in equation 4.6 (Ramshaw 1981; Martin 1992). The resulting HETP is then checked against previously published HETP values for Higee rotors as a safeguard.

$$HETP = \frac{\Delta r}{N_{theo}} \qquad (Eq\ 4.6)$$

15. The entire procedure (steps 4-14) is repeated for different values of the acceleration at the eye. The acceleration at the eye is increased from 10 g to 140 g in increments of ten. Thus, each value of a_c yields a unique value of r_o, r_i, h, ω, ATU and K_La_e (See section IV.9 for results).
16. The power consumed for each configuration is determined using Equation 3.44 (See section IV.10 for results).
17. The rate of increase in mass transfer coefficient with respect to acceleration ($\Delta K_La_e/\Delta a_c$) and the power consumption (P_c) are plotted against the acceleration at the eye (a_c) as seen in Figure 4.6 and Figure 4.7. The rate of increase in mass transfer coefficient levels off at some value of acceleration. The lowest acceleration (which results in lowest power consumption) at which this occurs along with the corresponding configuration (r_o, r_i, h and ω) is selected for design (See section IV.11 for details).

IV.3- Simulation

The simulation of the ethanol dewatering process was based on the previous work of Mukherjee (2009). The two column system (Beer or Stripping column and the Rectifier or Rectification column in the previous study) is simulated as a single SCDS column with 27 computational stages (26 theoretical stages inside the column and a condenser). The feed is introduced on the 14th computational stage. Dry saturated steam at 150 psia, used as the stripping agent, is introduced at the bottom of the column. The process schematic of the simulation is shown in Figure 4.3. Detailed results of the simulation can be found in Appendix A.

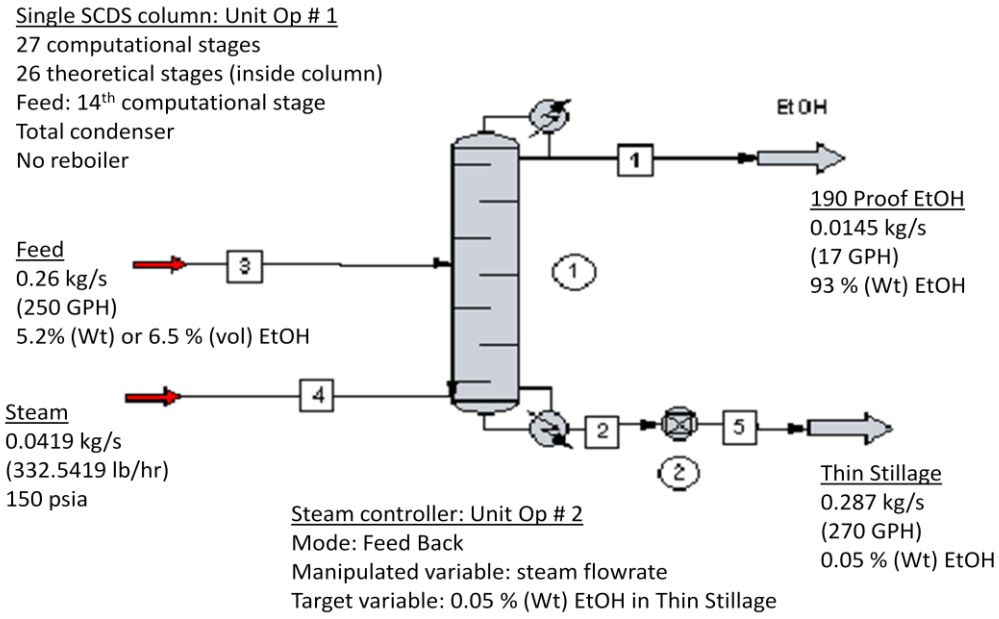

Figure 4.3 – Process Schematic for Simulation

IV.3.1- Component Selection

The sweet sorghum juice, apart from ethanol and water, contains other compounds in small volumes along with solids. Typical representative feed composition of sweet sorghum juice is shown in Table 4.1 (Mukherjee 2009). Solids in the sweet sorghum juice are not in the simulation.

Table 4.1- Representative Feed Composition

Component #	ChemCad ID #	Name	Formula	Composition	
				Vol %	Mole %
1	134	Ethanol	C_2H_6O	6.5	2.132
2	62	Water	H_2O	92.51	97.646
3	680	Lactic Acid	$C_3H_6O_3$	0.24	0.062
4	268	Glycerol	$C_3H_8O_3$	0.35	0.091
5	130	Acetic Acid	$C_2H_4O_2$	1.86	0.063
6	277	Succinic Acid	$C_4H_6O_4$	0.02	0.004

IV.3.2- Thermodynamic Model

For the process of ethanol dewatering, the Non-Random-Two-Liquids (NRTL) model was used to estimate the K-values. The Latent Heat (LATE) model was used to estimate the enthalpies for the system. The NRTL model is suitable for highly non-ideal systems and for two liquid systems (Chemstations 2009).

The binary interaction parameters used by ChemCad are shown in Table 4.2 below.

Table 4.2 - Binary Interaction Parameters for NRTL

i	j	B_{ij}	B_{ji}	α	A_{ij}	A_{ji}	C_{ij}	C_{ji}	D_{ij}	D_{ji}
1	2	-55.17	670.44	0.303	0	0	0	0	0	0
1	4	398.44	79.51	0.296	0	0	0	0	0	0
1	5	-147.79	105.31	0.299	0	0	0	0	0	0
2	4	258.11	-274.35	1.011	0	0	0	0	0	0
2	5	424.02	-110.57	0.3	0	0	0	0	0	0

IV.3.3- Input Data

The single column was simulated using a SCDS column. SCDS is a rigorous, multi stage, vapor-liquid equilibrium module designed to simulate non-ideal chemical systems (Chemstations 2009).

The inputs for the SCDS column are summarized in Table 4.3.

Table 4.3 - Inputs for SCDS Column

Parameter	Value
Number of Computational stages	27
Feed Stage	14
Condenser type	Total
Top pressure	1.033 kg/cm^2
Column pressure drop	0.173 kg/cm^2
Reflux Ratio (molar)	3.108
Distillate Rate	0.001675 kmol/s
Reflux Rate	0.015245 kmol/s

The controller unit operation was used to adjust the steam flow rate to ensure not more than 0.05% (wt) ethanol leaves the column through the thin stillage stream. The inputs for the Controller unit operation are specified in Table 4.4.

Table 4.4 – Inputs for Controller

Parameter	Value
Controller Mode	Feed-backward
Variable	Steam mass flow rate
Variable minimum value	149.7 (kg/h)
Variable maximum value	158.8 (kg/h)
Target stream	Thin Stillage
Target property	Ethanol mass fraction
Target property value	0.0005

IV.3.4 - Simulation Results

The simulation results of the SCDS column are summarized below in Table 4.5.

Table 4.5 - Simulation Results

Parameter	Symbol	Unit	Value
Distillate purity	x_D	mass fraction	93 %
Thin Stillage purity	x_B	mass fraction	0.05 %
Rectification*:			
Liquid flow rate	L	kg/s	0.059
Gas flow rate	G	kg/s	0.053
Liquid Density	ρ_L	kg/m^3	794.020
Gas Density	ρ_G	kg/m^3	1.386
Liquid viscosity	$\mu_{L,}$	kg/(m-s)	0.0004
Gas viscosity	$\mu_{G,}$	kg/(m-s)	0.00001
Stripping*:			
Liquid flow rate	L	kg/s	0.2927
Gas flow rate	G	kg/s	0.0484
Liquid Density	ρ_L	kg/m^3	947.900
Gas Density	ρ_G	kg/m^3	0.8067
Liquid viscosity	μ_L	kg/(m-s)	0.0003
Gas viscosity	μ_G	kg/(m-s)	0.00001
* Average values in each section			

The values of above parameters are used for sizing the Higee rotor, and calculating the power requirement and pressure drop.

IV.4 - Packing

As mentioned in the Background section, various types of packing have been used to fabricate the Higee rotors. The type of packing selected was based on:

1. Essential attributes required: specific surface areas greater than 2500 m^2/m^3 and void fractions greater than 0.9 (Fowler 1989).

2. Material of construction: For ethanol dewatering service, column internals are made up of 316 SS. Similarly, the packing used in Higee rotor should be made up of 316 SS. Acetic acid present in the feed and the product rapidly corrodes 304 SS (Starskey 2009).

Based on the developed criteria, the Celmet packing (Sumitomo Electric, Hyogo, Japan) was selected. Currently, a Celmet packing made of 316 SS is being developed (sumitomoelectricusa.com 2009). The properties exhibited by the packing are summarized below.

Table 4.6 - Packing Properties of Celmet

Packing: Celmet packing, Grade # 4, Sumitomo Electric		
Specific surface area	a_p	2500 m^2/m^3
Void fraction	ε	0.92
MOC		316 SS

IV.5 - Acceleration at Eye

A minimum value of acceleration at the eye is required to ensure proper functioning of the rotor. In the previous study (Kelleher 1993), the acceleration at the eye was varied from 15 g to 140 g. For this work, the acceleration at the eye is varied from 10 g to 140 g in increments of ten.

IV.6 - Flooding Chart

The operation velocity is determined using the Sherwood *et al.* (1938) flooding chart. The abscissa on this chart is determined by the system properties: the liquid rate, gas rate, and the densities. Based on the value of the ordinate on the chart, the flooding velocity is determined. The operating velocity was defined as 75 % of the flooding velocity. The results from the flooding chart are summarized below.

Table 4.7 - Flooding Chart Results

Rectification section		
Abscissa value	X	0.05
Ordinate value	Y	0.28
Stripping section		
Abscissa value	X	0.18
Ordinate value	Y	0.15

IV.7 - Diffusivity

The gas diffusivity was determined using the Fuller-Schettler-Giddings correlation (Fuller 1966). The gas diffusivity for the ethanol-water system was found to be 2.36426×10^{-5} m^2/s. Calculation of gas diffusivity is shown in Appendix B.

IV.8 - Number of Transfer Units

In general, the number of transfer units is found by evaluating the integral in Equation 3.58. The integrals to be evaluated for the Rectification Higee and the Stripping Higee are presented as Equations 4.7 & 4.8, respectively.

$$NTU = \int_{0.0213}^{0.83} \frac{dx}{x - x^*} \qquad (Eq\ 4.7)$$

$$NTU = \int_{0.0002}^{0.0213} \frac{dx}{x - x^*} \qquad (Eq\ 4.8)$$

Initially, equilibrium data generated by ChemCad is used to plot the x-y data in Excel. The operating lines for both the rectification and stripping sections are drawn based on the simulation results. The operating line equations for the rectification and stripping sections are presented as Equations 4.9 and 4.10, respectively.

$$y = 0.75652\,x + 0.20208 \qquad (Eq\ 4.9)$$

$$y = 7.55601\,x - 0.001316 \qquad (Eq\ 4.10)$$

For every value of x (on the operating line), the corresponding value for x* (on the equilibrium curve) is obtained as shown in Figure 4.4.

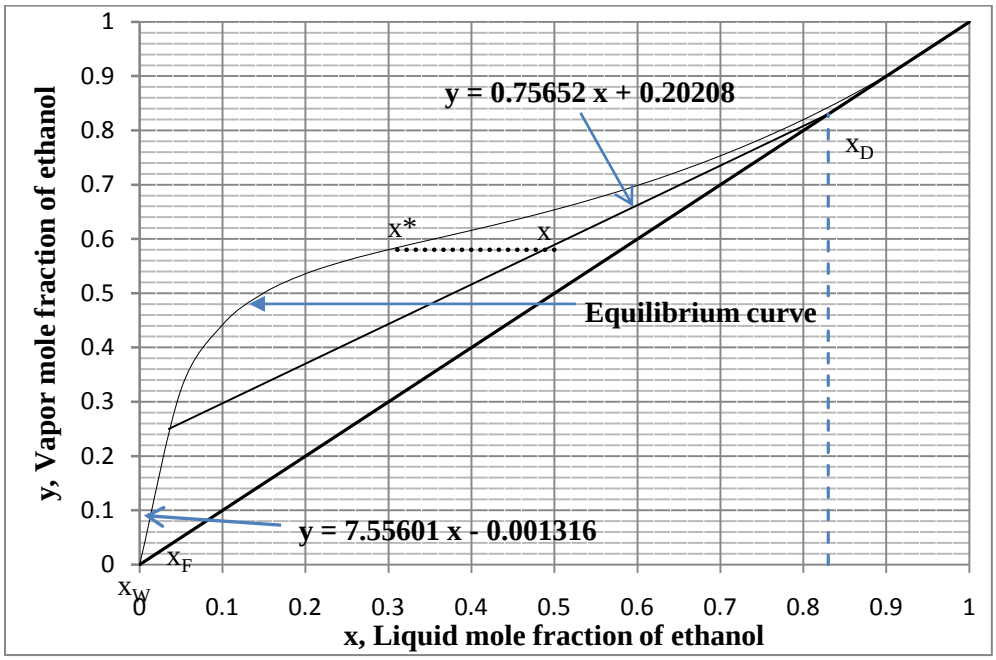

Figure 4.4 – Equilibrium Curve with Operating Lines
[Adapted from: Treybal, R. E. (1981). Mass Transfer Operations, Pg 427]

As seen in Figure 4.4, x and x* cannot be distinguished for the stripping section. Hence, another exaggerated plot for the stripping section is made to graphically distinguish x and x* values, as shown in Figure 4.5. The integral function in Equation 4.8 and Equation 4.9 is calculated for each value of x and x*. These values are presented in Tables 4.8 and 4.9, respectively. In Figure 4.4, both the rectification and striping lines appear to intersect the equilibrium curve. However, this is not the case as seen in Figure 4.5 below.

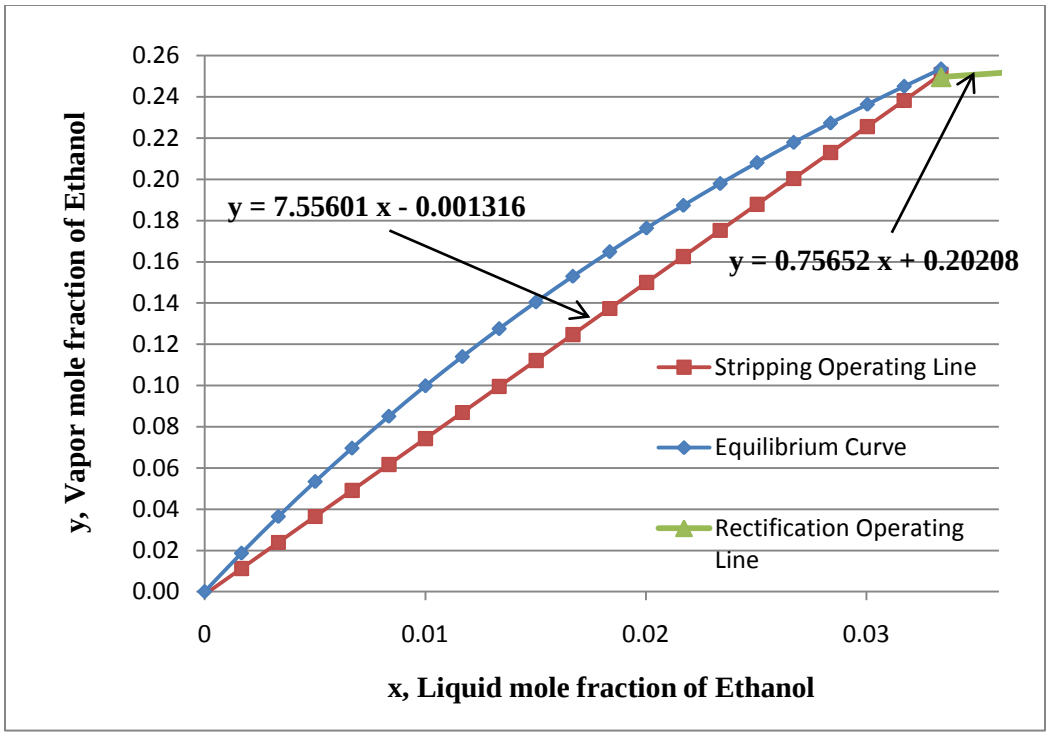

Figure 4.5 – Equilibrium Curve with Stripping Operating Line

Table 4.8 – Data for x* in Rectification NTU Calculation

x	x*	f (x) = (x-x*)$^{-1}$
0.83	0.82	100.00
0.80	0.78	50.00
0.75	0.73	50.00
0.70	0.66	25.00
0.75	0.58	14.29
0.60	0.50	10.00
0.55	0.40	6.67
0.50	0.30	5.00
0.45	0.21	4.17
0.40	0.15	4.00
0.35	0.12	4.35
0.30	0.09	4.76
0.25	0.07	5.56
0.20	0.06	7.14
0.15	0.05	10.00
0.10	0.04	16.67
0.05	0.03	50.00

Table 4.9 – Data for x* in Stripping NTU Calculation

x	x*	f (x) = (x-x*)$^{-1}$
0.0330	0.0322	1250.00
0.0310	0.0292	549.45
0.0290	0.0263	370.374
0.0270	0.0244	378.78
0.0250	0.0215	289.01
0.0230	0.0195	289.01
0.0210	0.0174	274.72
0.0190	0.0154	274.72
0.0170	0.0132	261.78
0.0150	0.0115	289.01
0.0130	0.0097	304.87
0.0110	0.0079	322.58
0.0090	0.0064	384.61
0.0070	0.0048	454.54
0.0050	0.0033	588.23
0.0030	0.0019	909.09
0.0010	0.0005	2000.00

Plot of 1/(x-x*) against x is made in Excel for both the rectification section and the stripping section, respectively. The curve is fitted to a polynomial equation (trendline). The degree of the polynomial fit is adjusted to give the highest value of coefficient of determination (R^2).

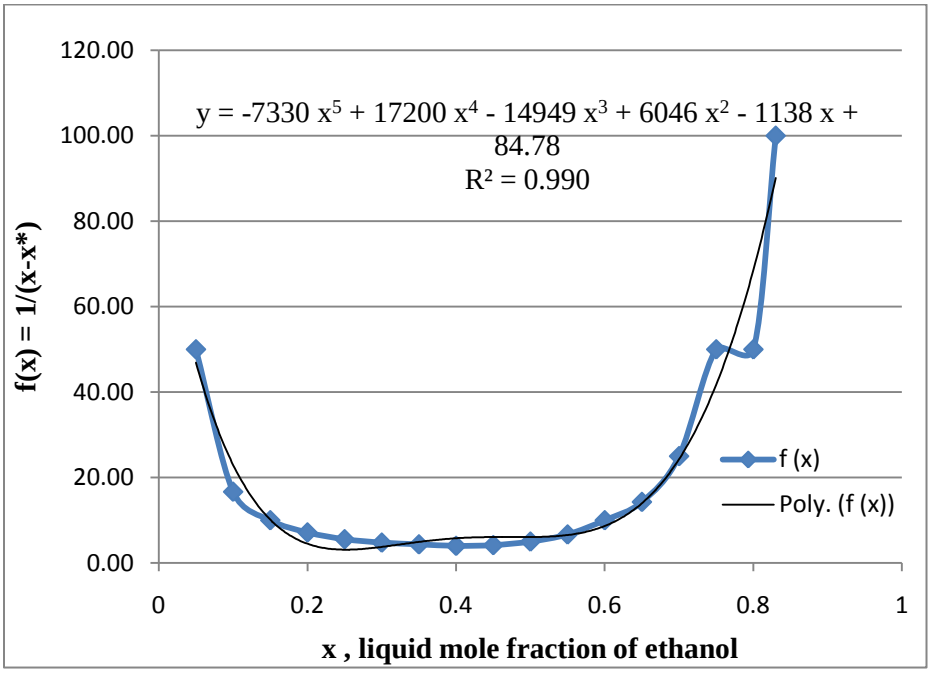

Figure 4.6 – Curve Fitting for Rectification NTU Calculation

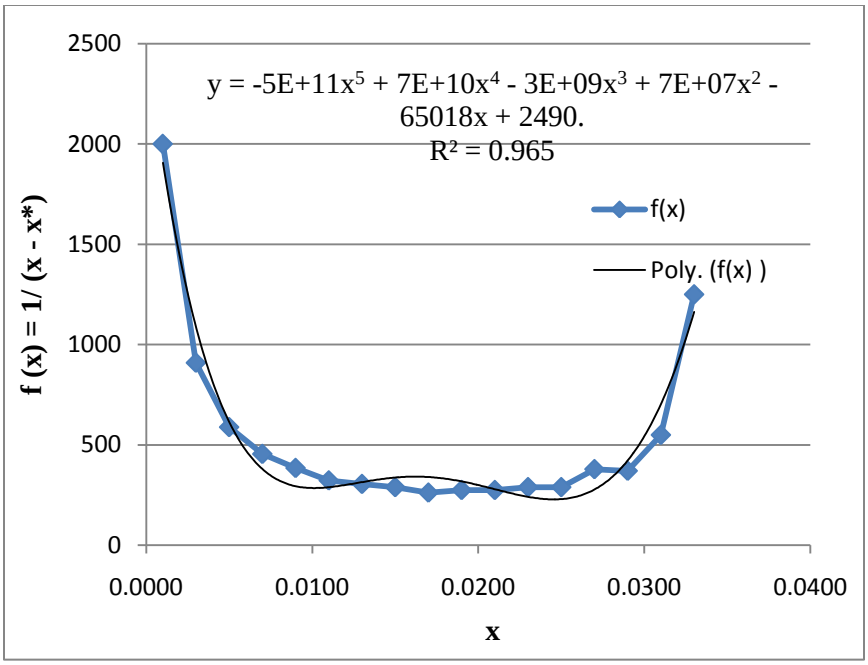

Figure 4.7 – Curve Fitting for Stripping NTU Calculation

Using the polynomial integration tool (Regression for polynomial) in POLYMATH 6.10, the value of integral in Equations 4.7 and 4.8 is obtained. The results for the number of transfer units in each section are tabulated below. Refer to Appendix C for the POLYMATH results sheet.

Table 4.10 – NTU Results

Section	NTU
Rectification	14.72
Stripping	11.74

For the stripping NTU, x* corresponding to the stillage liquid mole fraction (x = 0.0002) cannot be graphically distinguished as shown in Figure 4.5. The integral is evaluated by projecting the polynomial function beyond the final data point in Table 4.9 (corresponding to x = 0.0010).

IV.9 - Design Results

As mentioned earlier, the design procedure is repeated for values of acceleration at the eye (a_c) from 10 g to 140 g. The results for these are tabulated below for the Rectification Higee (Table 4.11) and the Stripping Higee (Table 4.12). Both design spreadsheets are attached as Appendix D.

Table 4.11 – Rectification Higee Results

Acceleration at eye	**Outer radius**	**Inner radius**	**Axial height**	**Radial velocity**	**Overall mass transfer Coefficient**	**Area of transfer unit**
a_c (g)	r_o (in)	r_i (in)	h (in)	ω (rpm)	$K_L a_e \times 10^2$ (s^{-1})	ATU (m^2)
1*	46.45	29.27	29.27	35	0.0558	0.1792
10	35.53	16.46	16.46	150	0.1302	0.1365
20	33.17	13.84	13.84	230	0.1689	0.1251
30	31.92	12.51	12.51	295	0.1969	0.1188
40	31.09	11.64	11.64	350	0.2196	0.1144
50	30.47	11.01	11.01	400	0.2391	0.1112
60	29.98	10.52	10.52	450	0.2563	0.1085
70	29.58	10.12	10.12	495	0.2718	0.1064
80	29.23	9.79	9.79	540	0.2860	0.1045
90	28.94	9.50	9.50	580	0.2992	0.1029
100	28.68	9.26	9.26	620	0.3115	0.1014
110	28.44	9.04	9.04	655	0.3231	0.1002
120	28.23	8.84	8.84	695	0.3341	0.0990
130	28.04	8.67	8.67	730	0.3445	0.0979
140	27.87	8.51	8.51	765	0.3544	0.0970

* Values at 1 g are presented merely to show the increase in mass transfer coefficient with increasing acceleration and will not be considered for design.

Table 4.12 – Stripping Higee Results

Acceleration at eye	**Outer radius**	**Inner radius**	**Axial height**	**Radial velocity**	**Overall mass transfer Coefficient**	**Area of transfer unit**
a_c (g)	r_o (in)	r_i (in)	h (in)	ω (rpm)	$K_L a_e \times 10^2$ (s^{-1})	ATU (m^2)
1*	94.55	72.29	72.29	25	0.0262	0.6410
10	67.48	40.65	40.65	95	0.0597	0.5008
20	62.01	34.19	34.19	145	0.0769	0.4623
30	59.21	30.89	30.89	185	0.0893	0.4405
40	57.37	28.75	28.75	225	0.0994	0.4255
50	56.01	27.19	27.19	255	0.1080	0.4141
60	54.95	25.98	25.98	285	0.1156	0.4050
70	54.09	24.99	24.99	315	0.1224	0.3973
80	53.36	24.17	24.17	345	0.1287	0.3908
90	52.73	23.47	23.47	370	0.1345	0.3851
100	52.19	22.86	22.86	395	0.1399	0.3800
110	51.70	22.32	22.32	420	0.1450	0.3755
120	51.26	21.84	21.84	440	0.1499	0.3714
130	50.87	21.41	21.41	465	0.1545	0.3676
140	50.51	21.02	21.02	485	0.1588	0.3642

* Values at 1 g are presented merely to show the increase in mass transfer coefficient with increasing acceleration and will not be considered for design.

Results from Tables 4.11 and 4.12 are summarized below:

1. Increasing acceleration at the eye results in a more compact rotor configuration. The values of outer radius, inner radius and axial height are seen to decrease with increasing acceleration. This is due to the increasing value of the flooding velocity found from the Sherwood chart.
2. The radial velocity is found to increase with acceleration at the eye. This is expected, since the acceleration at the eye is a product of the inner radius and the square of the radial velocity.
3. For the same value of acceleration at the eye, the Stripping Higee rotor is far larger compared to the Rectification Higee. This can be attributed to the large liquid load handled by the Stripping Higee. The average liquid rate in the Stripping Higee (0.2927 kg/s) is a magnitude greater than that in the Rectification Higee (0.059 kg/s) as seen in Table 4.5.
4. The overall liquid side mass transfer coefficient is found to increase with increasing acceleration at the eye for both the Rectification Higee and the Stripping Higee, respectively. Equations 3.67 and 3.68 show that the gas side local mass transfer coefficients and liquid local side mass transfer coefficients to vary as the 1/3 and 1/6 power of acceleration, respectively.

IV.10 - Power Consumption

The power consumption was computed using Equation 3.43 for each value of acceleration at the eye. The purchased power (P_p) was found by dividing the power consumption (P_c) by the motor efficiency. Motor efficiency was assumed to be 80 % (Peters 1991). Results for power consumption are tabulated in Table 4.13 and Table 4.14. The power consumption calculation spreadsheet is shown in Appendix E.

Table 4.13 – Power Consumption for Rectification Higee

Acceleration at eye	**Outer radius**	**Angular velocity**		**Consumed Power**	**Purchased Power**
a_c (g)	r_o (in)	ω (rpm)	ω (rad/s)	P_c (kW)	P_p (kW)
10	35.53	150	15.7100	1.2350	1.5438
20	33.17	230	24.0887	1.2487	1.5609
30	31.92	295	30.8963	1.2627	1.5784
40	31.09	350	36.6567	1.2764	1.5955
50	30.47	400	41.8933	1.2902	1.6128
60	29.98	450	47.1300	1.3056	1.6320
70	29.58	495	51.8430	1.3231	1.6539
80	29.23	540	56.5560	1.3364	1.6705
90	28.94	580	60.7453	1.3514	1.6893
100	28.68	620	64.9347	1.3672	1.7090
110	28.44	655	68.6003	1.3814	1.7267
120	28.23	695	72.7897	1.3988	1.7485
130	28.04	730	76.4553	1.4144	1.7680
140	27.87	765	80.1210	1.4308	1.7885

Table 4.14 – Power Consumption for Stripping Higee

Acceleration at eye	**Outer radius**	**Angular velocity**		**Consumed Power**	**Purchased Power**
a_c (g)	r_o (in)	ω (rpm)	ω (rad/s)	P_c (kW)	P_p (kW)
10	67.48	95	9.9497	1.3156	1.6445
20	62.01	145	15.1863	1.4062	1.7578
30	59.21	185	19.3757	1.4954	1.8692
40	57.37	225	23.5650	1.6017	2.0021
50	56.01	255	26.7070	1.6868	2.1085
60	54.95	285	29.8490	1.7808	2.2260
70	54.09	315	32.9910	1.8835	2.3543
80	53.36	345	36.1330	1.9942	2.4927
90	52.73	370	38.7513	2.0893	2.6116
100	52.19	395	41.3697	2.1903	2.7379
110	51.70	420	43.9880	2.2963	2.8704
120	51.26	440	46.0827	2.3811	2.9764
130	50.87	465	48.7010	2.4969	3.1211
140	50.51	485	50.7957	2.5894	3.2367

For both the Rectification Higee and the Stripping Higee, the power consumption increases with increasing acceleration at the eye. The power consumption varies as the square of the radial velocity, as seen in Equation 3.44. The larger outer radius and liquid rate handled by the Stripping Higee result in greater power consumption compared to the Rectification Higee.

IV.11 - Final Design Selection

To select one unique configuration for each section, the incremental rate of increase in mass transfer coefficient with respect to acceleration at the eye ($\Delta K_L a_e/\Delta a_c$) is plotted against the acceleration at the eye (a_c). The lowest value of acceleration at which the rate of increase in mass transfer coefficient is seen to level off, is selected as the design configuration. The lowest value of acceleration corresponds to lowest power consumption. Leveling off indicates the point or points beyond which more power is needed to gain a step increase in the overall mass transfer coefficient. For any Higee unit, increasing acceleration results in higher value of overall mass transfer coefficient but results in increased power consumption. Thus, the optimum configuration

for any Higee unit needs to be a compromise between the mass transfer coefficients and the power consumed.

The incremental increase in the overall mass transfer coefficient is defined by Equation 4.11.

$$\Delta K_L a_e = K_L a_e \; at \; a_{c2} - K_L a_e \; at \; a_{c1} \qquad (Eq\ 4.11)$$

where, $a_{c2} > a_{c1}$

Similarly, the incremental increase in acceleration is defined by Equation 4.12.

$$\Delta a_c = a_{c2} - a_{c1} \qquad (Eq\ 4.12)$$

Plots for the incremental increase in mass transfer coefficient and acceleration for both the Rectification and Stripping sections is shown in Figure 4.8 & Figure 4.9 respectively. Data for the plots is presented in Appendix F.

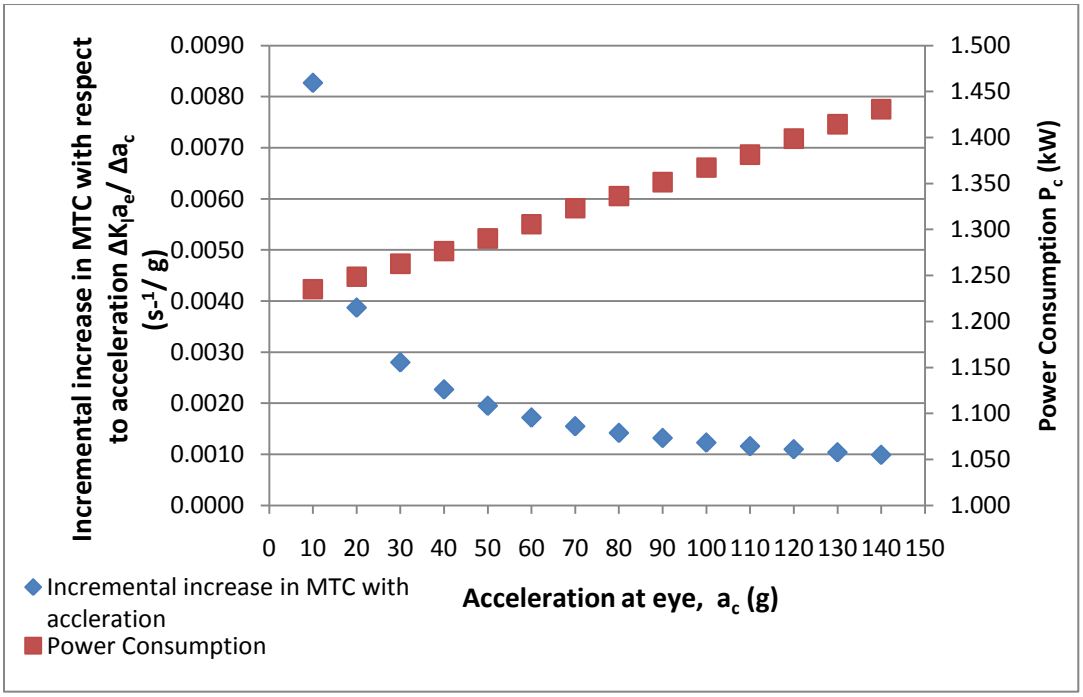

Figure 4.8 – Incremental Increase in Mass transfer Coefficient and Power Consumption for Rectification Higee

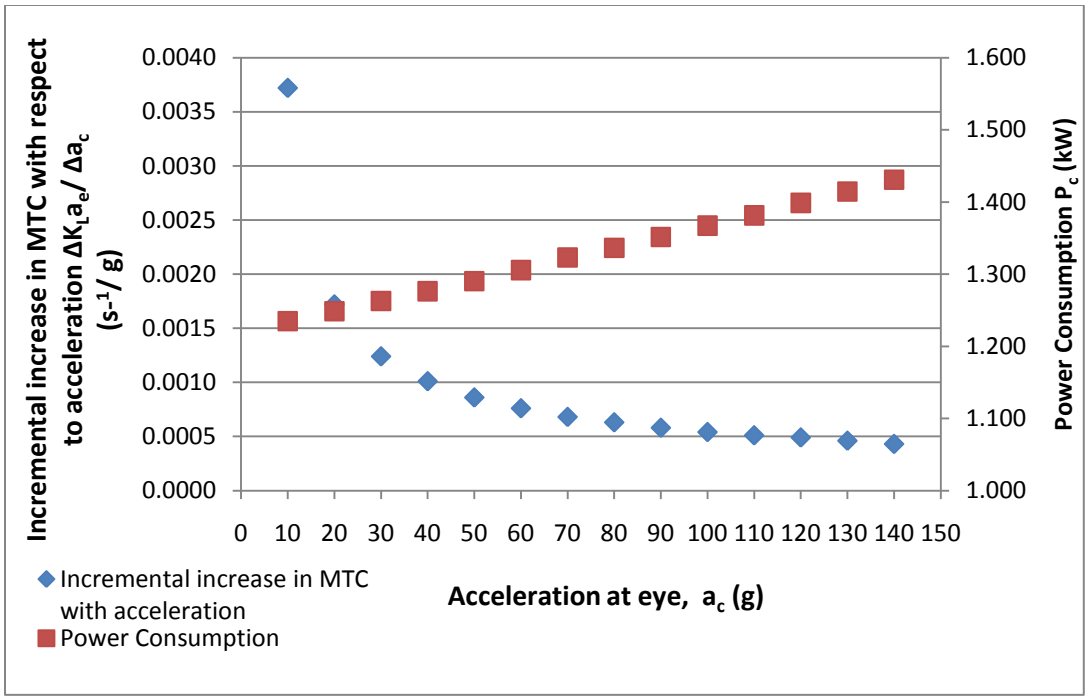

Figure 4.9 – Incremental Increase in Mass transfer Coefficient and Power Consumption for Stripping Higee

As seen in Figure 4.8, the incremental change in mass transfer coefficient with respect to acceleration levels off in the region of 50 g, indicating a drop in mass transfer coefficient increase for a step increase in the acceleration at the eye. For the Rectification section, configuration of the Higee rotor corresponding to acceleration at the eye of 50 g is selected for design. The details of this configuration are tabulated below.

Table 4.15 – Selected Configuration for Rectification Higee

Configuration of rotor	**Acceleration**			**Angular velocity**	**Overall Mass Transfer Coefficient**	**Power consumed**	**Height Equivalent of a Theoretical Plate**
	Eye	Mean radius	Outer radius				
r_o x r_i x h (in x in x in)	a_c (g)	a_m (g)	a_o (g)	ω (rpm)	$K_L a_e$ x 10^2 (s^{-1})	P_c (kW)	HETP (in)
30.47 x 11.01 x 11.01	50	104	138	400	0.2391	1.613	1.50

For the Stripping section, the incremental change in mass transfer coefficient levels off at around 50 g as seen in Figure 4.9. Thus, the selected design corresponds to an acceleration of 50 g at the eye. Details of this configuration are presented in Table 4.16.

Table 4.16 - Selected Configuration for Stripping Higee

Configuration of rotor	**Acceleration**			**Angular velocity**	**Overall Mass Transfer Coefficient**	**Power consumed**	**Height Equivalent of a Theoretical Plate**
r_o x r_i x h (in x in x in)	Eye a_c (g)	Mean radius a_m (g)	Outer radius a_o (g)	ω (rpm)	$K_L a_e$ x 10^2 (s^{-1})	P_c (kW)	HETP (in)
56.01 x 27.19 x 27.19	50	81	103	255	0.1080	2.109	2.22

IV.12 - Pressure Drop

The pressure drop across the two Higee rotors was modeled using Equation 4.13.

$$\Delta P = \frac{\rho_g \omega^2}{2} \left(r_o{}^2 - r_i{}^2\right) + \frac{5\,B'}{22} \left(\frac{\varepsilon\, G}{\pi\, h\, \rho_g}\right)^2 \left(\frac{1}{r_i{}^{1.1}} - \frac{1}{r_o{}^{1.1}}\right) \qquad (Eq\ 4.13)$$

Where,

$$B' = \frac{a_p\, \rho_g\, r^{0.1}}{\varepsilon^3} \left(\frac{G}{2\,\pi\, r\, h\, a_p\, \mu_g}\right)^{0.1} \qquad (Eq\ 4.14)$$

ω = radial velocity, rad/s

Pressure drop results for both the selected rotors are tabulated below. Spreadsheet for pressure drop calculation is provided in Appendix G.

Table 4.17 – Pressure Drop Results for Selected Rotors

Section	Higee rotor configuration (r_o x r_i x h) (in x in x in)	Mean radius r (in)	Radial velocity ω (rpm)	Pressure drop ΔP (Pa)	Pressure drop ΔP (psi)	Pressure drop per theoretical stage $\Delta P/N_{theo}$ (psi/stage)
Rectification	30.47 x 11.01 x 11.01	22.91	400	637.7493	0.0925	0.0071
Stripping	56.01 x 27.19 x 27.19	44.03	255	445.3410	0.0022	0.0050

The pressure drop across a Higee rotor varies as the square of both the radial velocity and vapor rate. Larger vapor rates and higher designed radial velocity result in greater pressure drop across the Rectification Higee compared to the Stripping Higee.

IV.13 - Sensitivity Analysis

In case the present design is found inadequate, the design can be corrected by simply increasing the acceleration of both the Higee units as required. As the rotor configuration is fixed, the acceleration can only be increased by increasing the radial velocity. The purpose of sensitivity analysis is to predict the effect of increasing acceleration on the performance of selected Higee rotors.

Performance of the rotor is measured in terms of the overall mass transfer coefficient (K_La_e), power consumed (P_c) and pressure drop per theoretical stage ($\Delta P/N_{theo}$). Decreasing the radial velocity below the design value would result in the radial depth of the packing being insufficient to accommodate the number of theoretical stages required for desired separation. This, in turn, would alter the outlet compositions. On the hydraulic side, lowering of the radial velocity would result in flooding at the eye of the rotor. Thus, use of radial velocities below the design value, is not considered for the sensitivity analysis.

The radial velocity of each rotor is increased from the designed value (400 rpm for the Rectification Higee and 255 rpm for the Stripping Higee) up to 1600 rpm. The performance parameters for each rotor are plotted against increasing radial velocity. The variation of overall mass transfer coefficient with radial velocity is presented in Figures 4.10 and 4.11. Figures 4.12

and 4.13 show the variation of power consumed with increasing radial velocity for the Rectification and Stripping sections, respectively. Variation of pressure drop per theoretical stage for the Rectification and Stripping sections are presented in Figure 4.14 and Figure 4.15, respectively. Data for all the sensitivity plots (Figure 4.10 – 4.15) is provided in Appendix H.

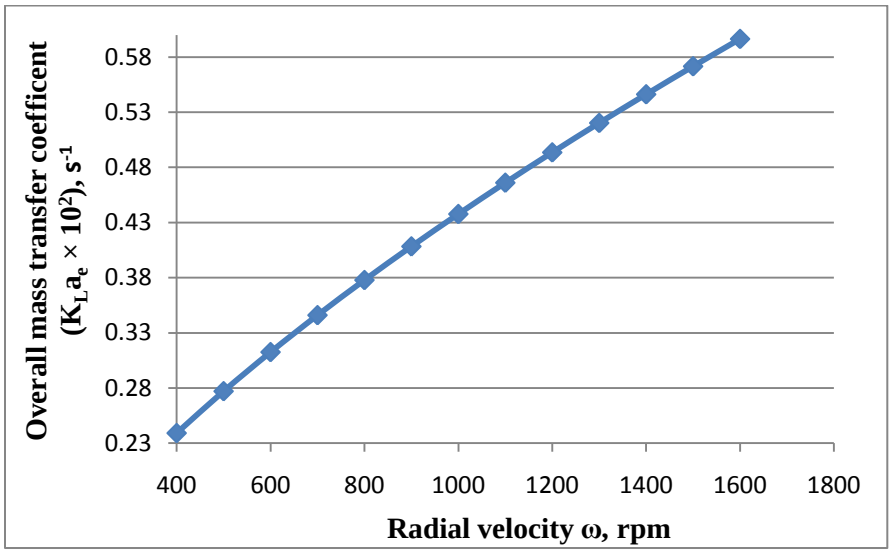

Figure 4.10 – Variation of Overall Mass Transfer Coefficient for Rectification Higee

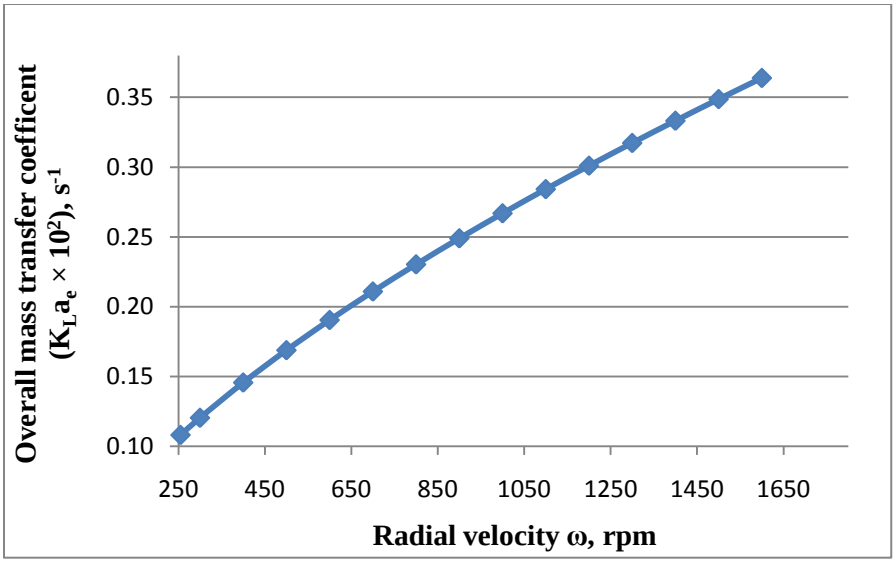

Figure 4.11 – Variation of Overall Mass Transfer Coefficient for Stripping Higee

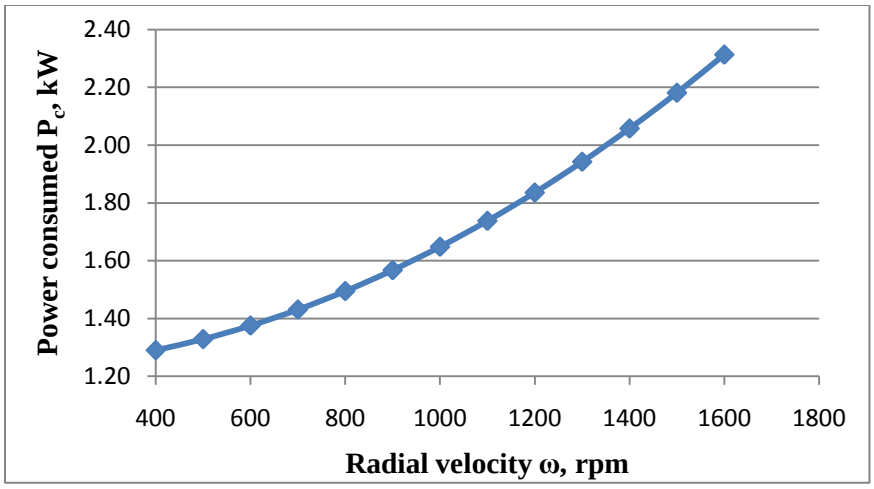

Figure 4.12 – Variation of Power Consumption for Rectification Higee

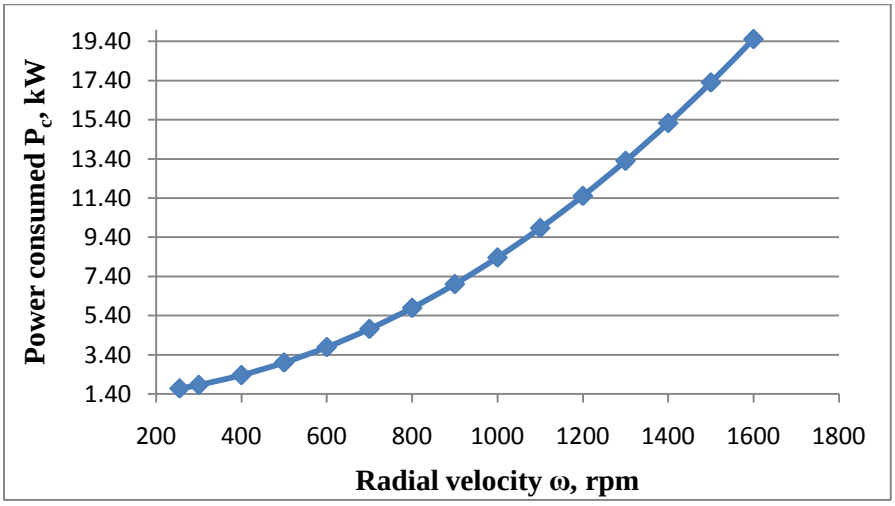

Figure 4.13 – Variation of Power Consumption for Stripping Higee

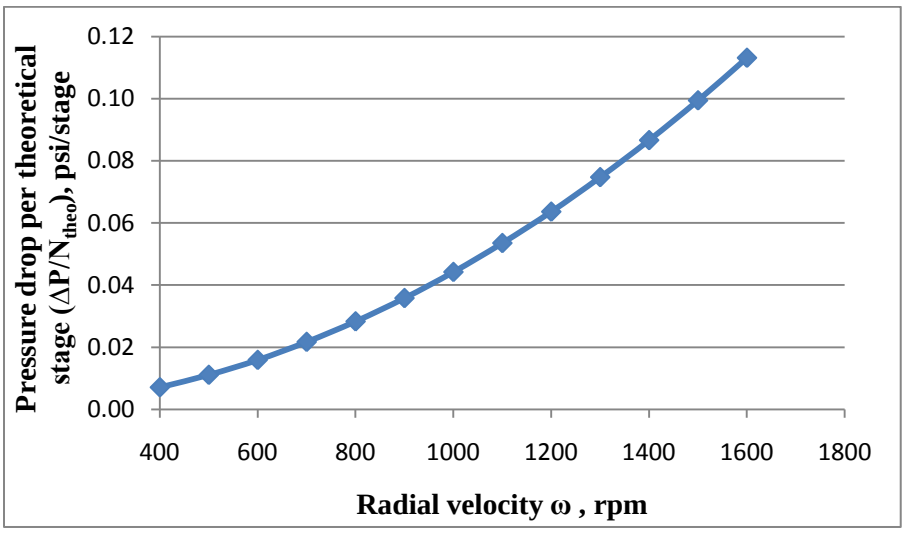

Figure 4.14 –Variation of Pressure Drop per Theoretical Stage for Rectification Higee

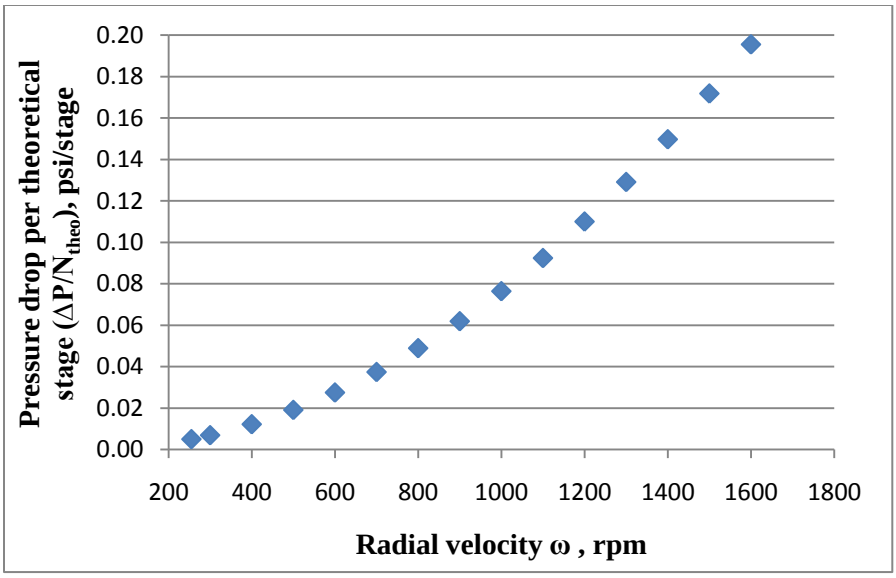

Figure 4.15 –Variation of Pressure Drop per Theoretical Stage for Stripping Higee

From Figures 4.10 and 4.11, it can be seen that the overall liquid mass transfer coefficient varies almost linearly with radial velocity. Equation 3.67 shows that the local gas side mass transfer coefficient varies as the 0.66 power of the radial velocity. Ethanol/water separation is primarily gas phase controlled (refer to the values of local mass transfer coefficients in the design spreadsheets attached as Appendix D). Hence, the overall mass transfer coefficient strongly depends on the local gas side mass transfer coefficient. This explains the observed near linear dependence of overall mass transfer coefficient with radial velocity.

The predicted power consumed is seen to increase with increasing radial velocity (Figures 4.12 and 4.13). The power consumed varies as the square of the radial velocity. As before, the power consumed by the Stripping Higee is greater than the Rectification Higee on account of the high liquid rate.

Increasing radial velocity results in increased pressure drop per theoretical stage across the Higee rotor (refer to Figures 4.14 and 4.15). The pressure drop curve appears to break off or level off at the lowest value of radial velocity (design value). Below this point, the eye of the rotor is likely to flood.

VI.14- Process Schematic with Control Loops

A simplified process schematic is developed to show a possible control strategy for the two Higee units. A detailed piping and instrumentation diagram (PID) is beyond the scope of this study.

The process schematic is based on the previous control scheme for ethanol dewatering developed by Mukerjee (Mukherjee 2009). An indirect material balance scheme is chosen for control. Most distillation columns employ material balance schemes for controlling product compositions (Kister 1990). In the present control scheme, the product composition is controlled by manipulating the reflux flow into the Rectification Higee. Both the product streams are controlled by level. Detailed description of such control schemes can be found in Kister (Kister 1990) and Rousseau (Rousseau 1987).

The primary disadvantage of such a scheme is the slow speed of response to composition change (Kister 1990). The speed of response is improved by coupling the temperature controller with a flow controller (cascade control with temperature controller as the primary controller) to manipulate the reflux flow into the Rectification Higee unit. As seen in Figure 4.16 below, the two retention tanks at the liquid outlet of the two Higee units ensure the use of level control to maintain product streams.

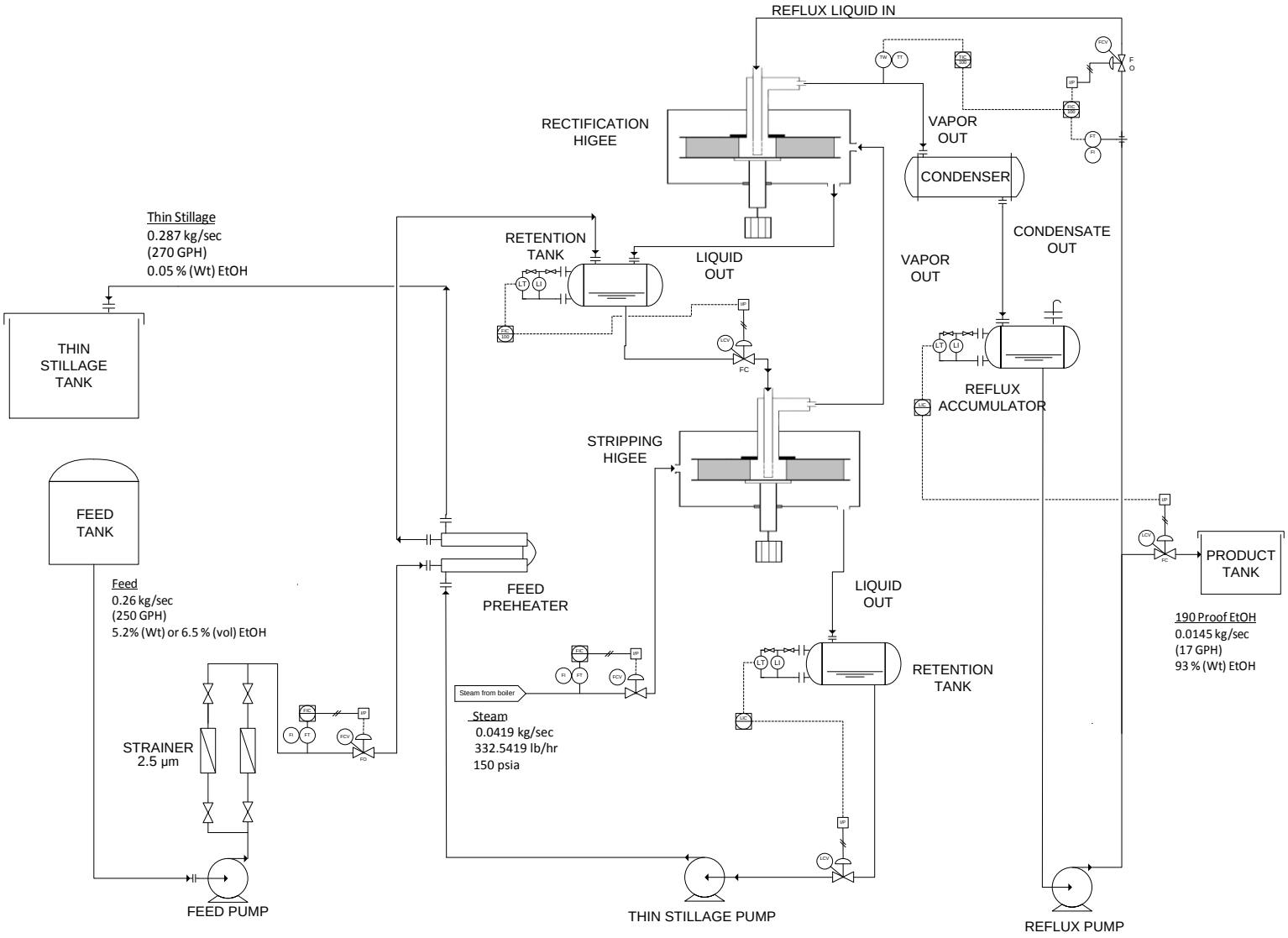

Figure 4.16 – Process Schematic with Control Loops

CHAPTER V

CONCLUSION AND RECOMMENDATIONS

The design of Higee rotor (Chapter IV) shows that methods and concepts used to size conventional packed columns can be applied with appropriate modifications.

The present study involves a forward design of Higee rotor for distillation service at finite reflux. Forward design implies sizing the rotor for fixed liquid and gas rates in order to achieve pre-defined outlet compositions. As seen, two rotors heave been designed, Rectification Higee and Stripping Higee, respectively. No previous study has demonstrated a forward design of Higee.

Lack of rationale for selecting a pre-defined radial velocity for design, no limit on the minimum acceleration at the eye, possibility of designing rotor configuration with very low inner radius, and large outer and axial height, were the primary drawbacks of the previously established design procedure (Kelleher 1993). Leveling off the incremental increase in overall mass transfer coefficient with respect to acceleration is the new criterion used for selecting one unique configuration of the rotor. This new criterion fixes the acceleration at the eye rather than the radial velocity. The resulting procedure is simpler, robust, and rectifies the drawbacks of the design procedure established previously (Kelleher 1993).

The outer radius of Rectification Higee and Stripping Higee are 30.47 inches and 56.01 inches, respectively. The corresponding space requirement will be of the order of 3000 – 10000 sq. inches, respectively. Thus, the footprint of both Higee units is relatively small.

The designed radial velocity of both units is low. As a result, the predicted power requirement of both units is low. A standard motor of 3 HP (brake) is sufficient to drive both the rotors at their designed radial velocities.

Process schematic illustrates how an indirect material balance control philosophy for conventional columns can be adopted for Higee units.

Qualitative explanation for reduction in the static area and increasing interfacial area has been provided based on previous work in packed columns.

In spite of these positives, the present study has the following limitations.

1. The present study is limited to sizing of the two rotors. Mechanical design of the Higee units was beyond the scope of this work.
2. The liquid distributor is of critical importance in operation of Higee units. Design of liquid distributor needs to be completed during the detailed design phase.

The following steps are recommended for future work:

1. A detailed design of Higee for ethanol dewatering is warranted. The detailed design should encompass the mechanical design, liquid distributor design, instrumentation and supports. Sufficient details must be provided in the design to be able to build a unit.
2. Effect of solids in the feed stream on packing performance needs to be evaluated. Effectiveness of strainers in removing solids from the feed stream needs to be checked.

3. Validation of the present design procedure or the design is required. This can either be done by designing a Higee unit for a pre-existing unit employing the present procedure or through experimentation.
4. Different liquid distributor designs and geometries need to be tested. Effectiveness of these on wetting the entire inner periphery and distribution of liquid needs to be checked.
5. Information on cost of building Higee units needs to be established. The influence of type and material of construction of packing, fabrication procedure and assembly on cost needs to be studied. Sumitomo packing in the present work is a specialized packing and is likely to be expensive. Other packings for ethanol dewatering should be tested in field.
6. Higee is supposed to achieve steady state more rapidly than conventional columns (Fowler 1989). In the present study, an indirect material balance control scheme is adopted for maintaining product flow rates and purities. Effect of other control schemes on product purity, stability, and achievement of steady state need to be studied. So far, no study on the control of Higee units has been reported.

REFERENCES

Billet, R. and M. Schultes (1993). "Predicting mass transfer in packed columns." Chemical Engineering and Technology **16**: 1-9.

Bird, R., W. Stewart, E. Lightfoot (1960). Transport Phenomena. New York, John Wiley & Sons Ltd.

Chemstations (2009) "ChemCad Help Topics."

Cross, W. T. and C. Ramshaw (1986). "Process intensification – laminar flow heat – transfer." Chemical Engineering Research & Design **64**(4): 293-301.

Danckwerts, P. V. (1951). "Significance of liquid – film coefficients in gas absorption." Industrial and Engineering Chemistry **43**(6): 1460-1467.

Danckwerts.P.V. and M. M. Sharma (1966). "Absorption of carbon dioxide into solutions of alkalis and amines (with some notes on hydrogen sulphide and carbonyl sulphide." Transactions of the Institution of Chemical Engineers and the Chemical Engineer **44**(8): 244.

Davidson, J. F. (1959). "The hold-up and liquid film coefficient of packed towers, Part 2: Statistical models of the random packing." Chemistry & Industry (9): 283.

Eckert, J. S. (1970). "Selecting the proper distillation column packing." Chemical Engineering Progress **66**(3): 39-44.

Fowler, R. (1989 a). "Higee – a status report." Chemical Engineer-London (456): 35-37.

Fowler, R., Gerdes, K. F., and Nygaard, H.F. (1989 b). "A commercial-scale demonstration of Higee for bulk CO_2 removal and gas dehydration." Offshore Technology Conference. Houston, TX.

Fuller, E., Schettler, P. and Giddings, J. (1966). "A new method for prediction of binary gas phase diffusion coefficients." Industrial and Engineering Chemistry **58**(5): 19-27.

Gilliland, E. R. and T. K. Sherwood (1934). "Diffusion of vapors into air streams." Industrial and Engineering Chemistry **26**: 516-523.

Higbie, R. (1935). "The rate of absorption of a pure gas into a still liquid during short periods of exposure." Transactions of the American Institute of Chemical Engineers **31**: 365-389.

Holcomb, R. (2008). Capital Cost for Sorganol Production.

Kapitsa, P. L. (1948). J. Exptl. Theoret. Phys. (U.S.S.R) **18**: 3-18.

Kelleher, T. (1993). Mass Transfer and Hydraulic Operating Characteristics of a Pilot-Plant Scale High Gravity Contacting Unit. Austin, The University of Texas. M.S. Thesis.

Keyvani, M. (1989). Operating Characteristics of Rotating Beds. Cleveland, Ohio, Case Western Reserve University PhD. Dissertation.

Kister, H. (1990). Distillation Operation, McGraw-Hill.

Leonard, R. A. (1980). "Prediction of Hydraulic Performance in Annular Centrifugal Contactors." Argonne National Laboratory ANL-80-57.

Lewis, W. K. and W. G. Whitman (1924). "Principles of gas absorption." Industrial and Engineering Chemistry **16**: 1215-1220.

Martin, C. L. (1992). "Preliminary distillation mass transfer and pressure drop results using a pilot-plant high gravity contacting unit." AIChE Spring National Meeting. New Orleans, LA.

Mukherjee, A. (2009). On Farm Ethanol Dewatering: Detailed Design of Distillation Unit. School of Chemical Engineering. Stillwater, Oklahoma State University. M.S. Thesis.

Mukherjee, A. (2010). Personal Communication. Y. Tamhankar. Stillwater, Ok.

Munjal, S. (1986). Fluid Flow and Mass Transfer in Rotating Packed Beds with Countercurrent Gas-Liquid Flow. Department of Chemical Engineering. St. Louis, Washington University. PhD Dissertation.

Munjal, S., M. P. Dudukovic, et al. (1989 a). "Mass-transfer in rotating packed beds. I. Development of gas-liquid and liquid-solid mass-transfer correlations." Chemical Engineering Science **44**(10): 2245-2256.

Munjal, S., M. P. Dudukovic, et al. (1989 b). "Mass-transfer in rotating packed beds. II. Experimental results and comparison with theory and gravity flow." Chemical Engineering Science **44**(10): 2257-2268.

Öhgren, K., A. Rudolf, et al. (2006). "Fuel ethanol production from steam-pretreated corn stover using SSF at higher dry matter content." Biomass and Bioenergy **30**(10): 863-869.

Onda, K., Takeuchi, H. and Okumoto, Y. (1968). "Mass transfer coefficients between gas and liquid phases in packed columns." Journal of Chemical Engineering of Japan **1**(1): 56-62.

Peters, M.S., K.D. Timmerhaus (1991). Plant Design and Economics for Chemical Engineers, McGraw-Hill.

Puranik, S. S. and Vogelpoh.A (1974). "Effective interfacial area in irrigated packed-columns." Chemical Engineering Science **29**(2): 501-507.

Ramshaw, C., Mallinson R. (1981). Mass Transfer Process. United States Patent and Trademarks Office, 4,283,255.

Rousseau, R. W. (1987). Handbook of Separation Process Technology, John Wiley & Sons**:** 328-330.

Seader, J. D., E.J. Henley (2006). Separation Process Principles, John Wiley and Sons, Inc.

Sherwood, T. K. and F. A. L. Holloway (1940). "Performance or packed towers - liquid film data for several packings." Transactions of the American Institute of Chemical Engineers **36**(1): 0039-0070.

Sherwood, T. K., G. H. Shipley, et al. (1938). "Flooding velocities in packed columns." Industrial and Engineering Chemistry **30**: 765-769.

Shulman, H. L., C. F. Ullrich, et al. (1955 a). "Performance of packed columns, Part 1: Total, static, and operating holdups." AIChE Journal **1**(2): 247-253.

Shulman, H. L., C. F. Ullrich, et al. (1955 b). "Performance of packed columns, Part 2: Wetted and effective interfacial areas, gas and liquid phase mass transfer rates." AIChE Journal **1**(2): 253-258.

Singh, S. (1989). Air Stripping of Volatile Organic Compounds from Groundwater: An Evaluation of A Centrifugal Vapor-Liquid Contactor. Knoxville, The University of Tennessee. PhD Dissertation.

sorganol.com. (2010). "Sorganol: What is it?" from http://www.sorganol.com/. Retrieved November 1, 2010.

Starskey, P. (2009). Personal Communication. Y. Tamhankar. Stillwater, Ok.

Stichlmair, J., J. Fair (1998). Distillation: Principles and Practice. New York, Wiley-VCH.

sumitomoelectricusa.com. (2009). "Products, Celmet (Porous Metal)" from http://www.sumitomoelectricusa.com/scripts/products/ncp/default.cfm. Retrieved November 01, 2009.

Trent, D., Tirtowidjojo, D. and G. Quarderer (1999). "Reactive stripping in a rotating packed bed for the production of Hypochlorous acid. 3rd International Conference on Process Intensification for The Chemical Industry. Antwerp, Belgium, BHR Group**:** 217-231.

Tung, H. H. and R. S. H. Mah (1985). "Modeling liquid mass-transfer in Higee separation process." Chemical Engineering Communications **39**(1-6): 147-153.

Vankrevelen, D. W. and P. J. Hoftijzer (1947). "Studies of gas absorption, Part 1: Liquid film resistance to gas absorption in scrubbers." Recueil Des Travaux Chimiques Des Pays-Bas-Journal of the Royal Netherlands Chemical Society **66**(1-2): 49-66.

Vivian, J. E., P. L. T. Brian, et al. (1965). "Influence of gravitational force on gas absorption in a

packed column." AIChE Journal **11**(6): 1088.

Vivian, J. E. and D. W. Peaceman (1956). "Liquid-side resistance in gas absorption." AIChE Journal **2**(4): 437-443.

Wang, G. Q., O. G. Xu, et al. (2008). "New Higee - rotating zigzag bed and its mass transfer performance." Industrial and Engineering Chemistry Research **47**(22): 8840-8846.

Wang, G. Q., X. G. Yuan, et al. (2005). "Review of mass-transfer correlations for packed columns." Industrial and Engineering Chemistry Research **44**: 8715-8729.

Whiteley, J. (2010). Personal Communication. Y. Tamhankar. Stillwater, Ok.

Zech, J. B. M., A.B. (1979). "Liquid flow and mass transfer in irrigated packed columns." Institute of Chemical Engineers Symposium Series **56**: 39-47.

APPPENDIX A

CHEMCAD SIMULATION REPORT

CHEMCAD 6.1.3
Job Name: CONSOLIDATED REPORT_OSU_BIOENERGY_STEAM

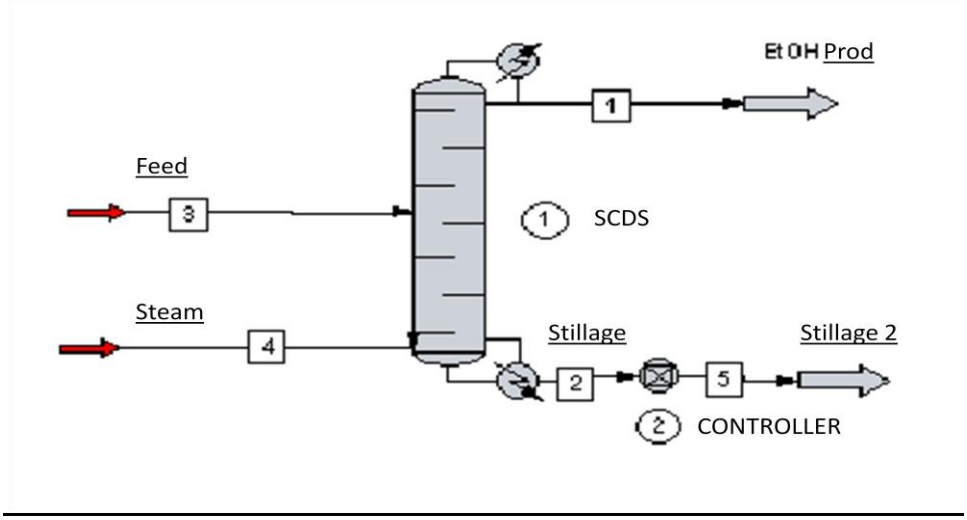

FLOWSHEET SUMMARY

Equipment Label Stream Numbers

1	SCDS	3	4	-1	-2	
2	CONT	2	-5			

Stream Connections

Stream	Equipment	
	From	To
1	1	
2	1	2
3		1
4		1
5	2	

Calculation mode : Sequential
Flash algorithm : Normal

Equipment Calculation Sequence
1 2

No recycle loops in the flowsheet.

Overall Mass Balance

	kmol/sec		kg/sec	
	Input	Output	Input	Output
Ethanol	0.000	0.000	0.014	0.014
Water	0.016	0.016	0.286	0.286
Lactic Acid	0.000	0.000	0.001	0.001
Glycerol	0.000	0.000	0.001	0.001
Acetic Acid	0.000	0.000	0.001	0.001
Succinic Acid	0.000	0.000	0.000	0.000
Total	0.016	0.016	0.302	0.302

COMPONENTS

	ID #	Name	Formula
1	134	Ethanol	C2H6O
2	62	Water	H2O
3	680	Lactic Acid	C3H6O3
4	268	Glycerol	C3H8O3
5	130	Acetic Acid	C2H4O2
6	277	Succinic Acid	C4H6O4

THERMODYNAMICS

K-value model : NRTL
No correction for vapor fugacity
Enthalpy model : Latent Heat
Liquid density : Library

Std vapor rate reference temperature is 0 C.
Atmospheric pressure is 1.0332 kg/cm2.

NRTL Parameters: Tij = Aij + Bij/T + Cij * Ln(T) + Dij * T (T Deg K)

I	J	Bij	Bji	Alpha	Aij	Aji	Cij	Cji	Dij	Dji
1	2	-55.17	670.44	0.303	0.00	0.00	0.00	0.00	0.00	0.00
1	4	398.44	79.51	0.296	0.00	0.00	0.00	0.00	0.00	0.00
1	5	-147.79	105.31	0.299	0.00	0.00	0.00	0.00	0.00	0.00
2	4	258.11	-274.35	1.011	0.00	0.00	0.00	0.00	0.00	0.00
2	5	424.02	-110.57	0.300	0.00	0.00	0.00	0.00	0.00	0.00

Warning : BIP matrix is less than 50 % full.

EQUIPMENT SUMMARIES

Scds Rigorous Distillation Summary

Equip. No.	1
Name	
No. of stages	27
1st feed stage	14
2nd feed stage	27
Condenser mode	6
Condenser spec	0.8300
Cond comp i pos.	1
Reboiler spec.	0.0100
Reboiler comp i	1
Cond press drop (kg/cm2)	0.0422
Colm press drop (kg/cm2)	0.1730
Est. dist. rate (kmol/sec)	0.0017
Est. reflux rate (kmol/sec)	0.0152
Est. T top K	367.5944
Est. T bottom K	374.2611
Top pressure (kg/cm2)	1.0335
Calc Cond duty (MJ/sec)	-0.0567
Calc Reflux mole (kmol/sec)	0.0011
Calc Reflux ratio	3.1079
Calc Reflux mass (kg/sec)	0.0452
Calc. tolerance	0.0001

Controller Summary

Equip. No.	2
Name	
Mode	2
Local variable H	
Stream No. adj.	4
Variable No. adj.	6
Minimum Value	330.0000
Maximum Value	350.0000
Rel Step Size	0.0010
Tolerance	1.0000e-004
Iterations	250
Measured variables:	
Number 1	2
Variable 1	-801
Constant	0.0005

STREAM PROPERTIES

Stream No	1	2	3	4	5
Stream Name	EtOH Prod	Stillage	Feed	Steam	Stillage 2
Overall Stream Properties					
Temperature deg K	351.449	378.528	338.706	454.594	378.528
Pressure kg/cm2	1.034	1.249	2.109	10.546	1.249
Vapor fraction	0.000	0.000	0.000	1.000	0.000
Critical T deg K	523.56	647.95	640.90	647.35	647.95
Critical P kg/cm2	71.18	226.46	211.91	225.54	226.46
Std sp. gr. * wtr = 1	0.809	1.001	0.988	1.000	1.001
Vpress kg/cm2	1.03	1.25	0.33	10.55	1.25
Enthalpy MJ/sec	-9.601E-002	-4.436E+000	-3.922E+000	-5.530E-001	-4.436E+000
Molar flow kmol/sec	0.000	0.016	0.014	0.002	0.016
Mass flow kg/sec	0.015	0.287	0.260	0.042	0.287
Avg. mol. wt.	41.300	18.146	18.757	18.015	18.146
Actual dens kg/m3	748.374	954.984	965.744	5.197	954.984
Actual vol m3/h	0.070	1.083	0.969	29.060	1.083
Std liq vol gph	17.105	272.790	250.000	39.895	272.790

FLOW SUMMARIES

Stream No.	1	2	3	4	5
Stream Name	EtOH Prod	Stillage	Feed	Steam	Stillage 2
Temp K	351.4489	378.5281	338.7055	454.5945	378.5281
Pres kg/cm2	1.0335	1.2487	2.1092	10.5460	1.2487
Enth MJ/sec	-0.096013	-4.4361	-3.9224	-0.55295	-4.4361
Vapor mole fraction	0.00000	0.00000	0.00000	1.0000	0.00000
Total kmol/sec	0.000	0.016	0.014	0.002	0.016
Component mole %					
Ethanol	83.000	0.020	2.132	0.000	0.020
Water	17.000	99.787	97.647	100.000	99.787
Lactic Acid	0.000	0.054	0.062	0.000	0.054
Glycerol	0.000	0.080	0.091	0.000	0.080
Acetic Acid	0.000	0.055	0.063	0.000	0.055
Succinic Acid	0.000	0.004	0.005	0.000	0.004
Total kg/sec	0.015	0.287	0.260	0.042	0.287
Component mass %					
Ethanol	92.585	0.050	5.237	0.000	0.050
Water	7.415	99.065	93.785	100.000	99.065
Lactic Acid	0.000	0.271	0.299	0.000	0.271
Glycerol	0.000	0.405	0.448	0.000	0.405
Acetic Acid	0.000	0.183	0.203	0.000	0.183
Succinic Acid	0.000	0.026	0.028	0.000	0.026
Total std L gph	17.105	272.790	250.000	39.895	272.790
Component std liq volume %					
Ethanol	94.005	0.062	6.500	0.000	0.062
Water	5.995	99.204	92.700	100.000	99.204

Lactic Acid	0.000	0.220	0.240	0.000	0.220
Glycerol	0.000	0.321	0.350	0.000	0.321
Acetic Acid	0.000	0.174	0.190	0.000	0.174
Succinic Acid	0.000	0.018	0.020	0.000	0.018

DISTILLATION PROFILE

Unit type : SCDS Unit name: Eqp # 1

* Net Flows *

Stg	Temp K	Pres kg/cm2	Liquid kg/sec	Vapor kg/sec	Feeds kg/sec	Product kg/sec	Duties MJ/sec
1	351.4	1.03	0.05		0.01		-0.05674
2	352.5	1.08	0.04	0.06			
3	352.7	1.08	0.04	0.06			
4	352.9	1.09	0.04	0.06			
5	353.1	1.10	0.04	0.06			
6	353.4	1.10	0.04	0.06			
7	353.6	1.11	0.04	0.06			
8	354.0	1.12	0.04	0.06			
9	354.3	1.12	0.04	0.05			
10	354.9	1.13	0.04	0.05			
11	356.0	1.14	0.03	0.05			
12	358.8	1.14	0.02	0.05			
13	365.2	1.15	0.02	0.04			
14	369.0	1.16	0.30	0.04	0.26		
15	369.4	1.17	0.30	0.06			
16	370.0	1.17	0.30	0.05			
17	370.8	1.18	0.30	0.05			
18	371.8	1.19	0.30	0.05			
19	373.0	1.19	0.29	0.05			
20	374.2	1.20	0.29	0.05			
21	375.3	1.21	0.29	0.05			
22	376.3	1.21	0.29	0.05			
23	377.0	1.22	0.29	0.05			
24	377.5	1.23	0.29	0.04			
25	378.0	1.23	0.29	0.04			
26	378.3	1.24	0.29	0.04			
27	378.5	1.25		0.04	0.04	0.29	

Mass Reflux ratio 3.108
Total liquid entering stage 14 at 340.616 K, 0.280 kg/sec.
Total liquid entering stage 27 at 378.528 K, 0.289 kg/sec.

Mole Reflux ratio 3.108
Total liquid entering stage 14 at 340.616 K, 0.015 kmol/sec.

Total liquid entering stage 27 at 378.528 K, 0.016 kmol/sec.

TRAY PROPERTIES

Unit type : SCDS Unit name: Eqp # 1

LIQUID Stg	Average mol wt	Actual vol rate gph	Actual density kg/m3	viscosity kg/m-sec	Thermal conduct. W/m-K	Surface tension N/m	Liq H MJ/sec
1	41.30	57.43	748.37	0.0004	0.166	0.019	-0.2984
2	40.84	56.86	748.81	0.0004	0.167	0.019	-0.29897
3	40.37	56.04	750.19	0.0004	0.169	0.019	-0.29883
4	39.87	55.18	751.69	0.0004	0.170	0.019	-0.29867
5	39.33	54.23	753.40	0.0004	0.172	0.020	-0.29849
6	38.71	53.16	755.43	0.0004	0.175	0.020	-0.29827
7	37.98	51.88	758.00	0.0004	0.178	0.020	-0.298
8	37.05	50.27	761.45	0.0004	0.182	0.021	-0.29763
9	35.79	48.06	766.59	0.0004	0.188	0.021	-0.29708
10	33.87	44.71	775.41	0.0004	0.199	0.022	-0.29612
11	30.41	38.67	795.20	0.0004	0.228	0.025	-0.29396
12	23.86	27.62	854.54	0.0003	0.344	0.035	-0.29013
13	19.86	21.36	917.00	0.0003	0.520	0.048	-0.29032
14	19.13	305.63	934.93	0.0003	0.579	0.052	-4.4061
15	19.08	304.69	935.90	0.0003	0.583	0.052	-4.4086
16	19.00	303.22	937.40	0.0003	0.589	0.053	-4.412
17	18.90	301.20	939.53	0.0003	0.598	0.053	-4.4164
18	18.77	298.70	942.20	0.0003	0.610	0.054	-4.4221
19	18.63	296.01	945.17	0.0003	0.623	0.055	-4.4288
20	18.50	293.50	948.02	0.0003	0.636	0.055	-4.4358
21	18.38	291.45	950.43	0.0003	0.647	0.056	-4.4425
22	18.30	289.94	952.24	0.0003	0.656	0.057	-4.4482
23	18.24	288.95	953.46	0.0003	0.663	0.057	-4.4527
24	18.20	288.35	954.23	0.0003	0.667	0.057	-4.4561
25	18.17	288.01	954.67	0.0003	0.670	0.057	-4.4587
26	18.16	287.84	954.89	0.0003	0.671	0.057	-4.4607
27	18.15	286.05	954.98	0.0003	0.673	0.057	-4.4361

VAPOR Stg	Average mol wt	Actual vol rate m3/h	Actual density kg/m3	viscosity kg/m-sec	Thermal conduct. W/m-K	Compr. factor	Vap H MJ/sec
1	0.00	0	0.0000	0.0000	0.000	0.000	0
2	41.30	142	1.5170	0.0000	0.021	0.980	-0.33767
3	40.95	141	1.5128	0.0000	0.021	0.980	-0.33824
4	40.59	140	1.5082	0.0000	0.021	0.980	-0.3381
5	40.22	139	1.5027	0.0000	0.021	0.980	-0.33794
6	39.81	138	1.4956	0.0000	0.021	0.980	-0.33776
7	39.34	138	1.4860	0.0000	0.021	0.981	-0.33755
8	38.79	137	1.4727	0.0000	0.021	0.981	-0.33728

9	38.09	136	1.4531	0.0000	0.021	0.981	-0.33691
10	37.14	135	1.4227	0.0000	0.021	0.981	-0.33636
11	35.70	134	1.3708	0.0000	0.021	0.982	-0.3354
12	33.12	133	1.2673	0.0000	0.022	0.984	-0.33323
13	28.27	133	1.0663	0.0000	0.023	0.986	-0.3294
14	25.29	133	0.9486	0.0000	0.023	0.988	-0.32959
15	25.04	211	0.9435	0.0000	0.023	0.988	-0.52295
16	24.65	211	0.9326	0.0000	0.024	0.988	-0.52549
17	24.08	211	0.9142	0.0000	0.024	0.988	-0.52885
18	23.30	212	0.8874	0.0000	0.024	0.988	-0.53329
19	22.37	214	0.8537	0.0000	0.024	0.989	-0.53895
20	21.36	215	0.8170	0.0000	0.024	0.989	-0.54563
21	20.41	218	0.7826	0.0000	0.025	0.990	-0.55271
22	19.63	219	0.7547	0.0000	0.025	0.990	-0.5594
23	19.04	221	0.7348	0.0000	0.025	0.990	-0.56509
24	18.64	221	0.7222	0.0000	0.025	0.990	-0.56959
25	18.37	222	0.7152	0.0000	0.025	0.990	-0.57301
26	18.21	222	0.7122	0.0000	0.025	0.990	-0.57559
27	18.10	221	0.7115	0.0000	0.025	0.990	-0.57755

TRAY COMPOSITIONS

Unit type : SCDS Unit name: Eqp # 1

Stage # 1	351.45 K	1.03 kg/cm2	
	Vap kg/sec	Liq kg/sec	Y/X
Ethanol	0.00000	0.04184	0.00000
Water	0.00000	0.00335	0.00000
Lactic Acid	0.00000	0.00000	0.00000
Glycerol	0.00000	0.00000	0.00000
Acetic Acid	0.00000	0.00000	0.00000
Succinic Acid	0.00000	0.00000	0.00000
Total kg/sec	0.0000	0.0452	

Stage # 2	352.50 K	1.08 kg/cm2	
	Vap kg/sec	Liq kg/sec	Y/X
Ethanol	0.05531	0.04109	1.02025
Water	0.00443	0.00368	0.91164
Lactic Acid	0.00000	0.00000	0.00000
Glycerol	0.00000	0.00000	0.00000
Acetic Acid	0.00000	0.00000	0.20921
Succinic Acid	0.00000	0.00000	0.00000
Total kg/sec	0.0597	0.0448	

Stage # 3	352.71 K	1.08 kg/cm2	
	Vap kg/sec	Liq kg/sec	Y/X
Ethanol	0.05455	0.04019	1.02609
Water	0.00476	0.00401	0.89771
Lactic Acid	0.00000	0.00000	0.00000
Glycerol	0.00000	0.00000	0.00000

Acetic Acid	0.00000	0.00000	0.20907
Succinic Acid	0.00000	0.00000	0.00000
Total kg/sec	0.0593	0.0442	

Stage # 4	352.92 K	1.09 kg/cm2	
	Vap kg/sec	Liq kg/sec	Y/X
Ethanol	0.05366	0.03926	1.03308
Water	0.00509	0.00435	0.88335
Lactic Acid	0.00000	0.00000	0.00000
Glycerol	0.00000	0.00000	0.00000
Acetic Acid	0.00000	0.00000	0.20906
Succinic Acid	0.00000	0.00000	0.00000
Total kg/sec	0.0587	0.0436	

Stage # 5	353.14 K	1.10 kg/cm2	
	Vap kg/sec	Liq kg/sec	Y/X
Ethanol	0.05272	0.03824	1.04174
Water	0.00543	0.00473	0.86801
Lactic Acid	0.00000	0.00000	0.00000
Glycerol	0.00000	0.00000	0.00000
Acetic Acid	0.00000	0.00000	0.20920
Succinic Acid	0.00000	0.00000	0.00000
Total kg/sec	0.0582	0.0430	

Stage # 6	353.38 K	1.10 kg/cm2	
	Vap kg/sec	Liq kg/sec	Y/X
Ethanol	0.05170	0.03708	1.05295
Water	0.00581	0.00515	0.85100
Lactic Acid	0.00000	0.00000	0.00000
Glycerol	0.00000	0.00000	0.00000
Acetic Acid	0.00000	0.00000	0.20955
Succinic Acid	0.00000	0.00000	0.00000
Total kg/sec	0.0575	0.0422	

Stage # 7	353.64 K	1.11 kg/cm2	
	Vap kg/sec	Liq kg/sec	Y/X
Ethanol	0.05054	0.03570	1.06836
Water	0.00623	0.00566	0.83130
Lactic Acid	0.00000	0.00000	0.00000
Glycerol	0.00000	0.00000	0.00000
Acetic Acid	0.00000	0.00000	0.21027
Succinic Acid	0.00000	0.00000	0.00000
Total kg/sec	0.0568	0.0414	

Stage # 8	353.95 K	1.12 kg/cm2	
	Vap kg/sec	Liq kg/sec	Y/X
Ethanol	0.04916	0.03396	1.09127
Water	0.00673	0.00629	0.80728
Lactic Acid	0.00000	0.00000	0.00000
Glycerol	0.00000	0.00000	0.00000
Acetic Acid	0.00000	0.00000	0.21165

Succinic Acid	0.00000	0.00000	0.00000
Total kg/sec	0.0559	0.0402	

Stage # 9	354.34 K	1.12 kg/cm2	
	Vap kg/sec	Liq kg/sec	Y/X
Ethanol	0.04742	0.03159	1.12951
Water	0.00737	0.00714	0.77605
Lactic Acid	0.00000	0.00000	0.00000
Glycerol	0.00000	0.00000	0.00000
Acetic Acid	0.00000	0.00000	0.21448
Succinic Acid	0.00000	0.00000	0.00000
Total kg/sec	0.0548	0.0387	

Stage # 10	354.91 K	1.13 kg/cm2	
	Vap kg/sec	Liq kg/sec	Y/X
Ethanol	0.04506	0.02802	1.20648
Water	0.00822	0.00843	0.73178
Lactic Acid	0.00000	0.00000	0.00000
Glycerol	0.00000	0.00000	0.00000
Acetic Acid	0.00000	0.00001	0.22117
Succinic Acid	0.00000	0.00000	0.00000
Total kg/sec	0.0533	0.0365	

Stage # 11	355.96 K	1.14 kg/cm2	
	Vap kg/sec	Liq kg/sec	Y/X
Ethanol	0.04148	0.02162	1.42859
Water	0.00951	0.01070	0.66170
Lactic Acid	0.00000	0.00000	0.00076
Glycerol	0.00000	0.00000	0.00000
Acetic Acid	0.00001	0.00002	0.24310
Succinic Acid	0.00000	0.00000	0.00000
Total kg/sec	0.0510	0.0323	

Stage # 12	358.78 K	1.14 kg/cm2	
	Vap kg/sec	Liq kg/sec	Y/X
Ethanol	0.03508	0.00994	2.59431
Water	0.01177	0.01484	0.58305
Lactic Acid	0.00000	0.00000	0.00097
Glycerol	0.00000	0.00000	0.00000
Acetic Acid	0.00002	0.00004	0.36356
Succinic Acid	0.00000	0.00000	0.00000
Total kg/sec	0.0469	0.0248	

Stage # 13	365.21 K	1.15 kg/cm2	
	Vap kg/sec	Liq kg/sec	Y/X
Ethanol	0.02340	0.00309	5.64289
Water	0.01592	0.01746	0.67909
Lactic Acid	0.00000	0.00000	0.00190
Glycerol	0.00000	0.00000	0.00005
Acetic Acid	0.00004	0.00004	0.67191
Succinic Acid	0.00000	0.00000	0.00001

Total kg/sec	0.0394	0.0206	
Stage # 14	368.96 K	1.16 kg/cm2	
	Vap kg/sec	Liq kg/sec	Y/X
Ethanol	0.01655	0.02548	7.34445
Water	0.01854	0.27237	0.76945
Lactic Acid	0.00000	0.00078	0.00264
Glycerol	0.00000	0.00116	0.00007
Acetic Acid	0.00004	0.00060	0.84493
Succinic Acid	0.00000	0.00007	0.00002
Total kg/sec	0.0351	0.3005	
Stage # 15	369.42 K	1.17 kg/cm2	
	Vap kg/sec	Liq kg/sec	Y/X
Ethanol	0.02534	0.02417	7.47777
Water	0.02976	0.27306	0.77735
Lactic Acid	0.00000	0.00078	0.00272
Glycerol	0.00000	0.00116	0.00007
Acetic Acid	0.00007	0.00060	0.85876
Succinic Acid	0.00000	0.00007	0.00002
Total kg/sec	0.0552	0.2998	
Stage # 16	370.02 K	1.17 kg/cm2	
	Vap kg/sec	Liq kg/sec	Y/X
Ethanol	0.02402	0.02221	7.68671
Water	0.03045	0.27405	0.78961
Lactic Acid	0.00000	0.00078	0.00284
Glycerol	0.00000	0.00116	0.00007
Acetic Acid	0.00007	0.00061	0.88033
Succinic Acid	0.00000	0.00007	0.00002
Total kg/sec	0.0546	0.2989	
Stage # 17	370.82 K	1.18 kg/cm2	
	Vap kg/sec	Liq kg/sec	Y/X
Ethanol	0.02207	0.01953	7.99240
Water	0.03145	0.27540	0.80761
Lactic Acid	0.00000	0.00078	0.00301
Glycerol	0.00000	0.00116	0.00008
Acetic Acid	0.00008	0.00061	0.91185
Succinic Acid	0.00000	0.00007	0.00002
Total kg/sec	0.0536	0.2976	
Stage # 18	371.83 K	1.19 kg/cm2	
	Vap kg/sec	Liq kg/sec	Y/X
Ethanol	0.01939	0.01622	8.40254
Water	0.03280	0.27708	0.83202
Lactic Acid	0.00000	0.00078	0.00324
Glycerol	0.00000	0.00116	0.00008
Acetic Acid	0.00008	0.00062	0.95418
Succinic Acid	0.00000	0.00007	0.00002
Total kg/sec	0.0523	0.2959	

Stage # 19	372.99 K	1.19 kg/cm2	
	Vap kg/sec	Liq kg/sec	Y/X
Ethanol	0.01607	0.01260	8.89616
Water	0.03447	0.27895	0.86191
Lactic Acid	0.00000	0.00078	0.00354
Glycerol	0.00000	0.00116	0.00009
Acetic Acid	0.00009	0.00062	1.00524
Succinic Acid	0.00000	0.00007	0.00002
Total kg/sec	0.0506	0.2942	

Stage # 20	374.20 K	1.20 kg/cm2	
	Vap kg/sec	Liq kg/sec	Y/X
Ethanol	0.01246	0.00914	9.41938
Water	0.03634	0.28079	0.89421
Lactic Acid	0.00000	0.00078	0.00386
Glycerol	0.00000	0.00116	0.00010
Acetic Acid	0.00010	0.00063	1.05956
Succinic Acid	0.00000	0.00007	0.00003
Total kg/sec	0.0489	0.2926	

Stage # 21	375.32 K	1.21 kg/cm2	
	Vap kg/sec	Liq kg/sec	Y/X
Ethanol	0.00900	0.00621	9.90426
Water	0.03819	0.28240	0.92474
Lactic Acid	0.00000	0.00078	0.00419
Glycerol	0.00000	0.00116	0.00011
Acetic Acid	0.00010	0.00064	1.11010
Succinic Acid	0.00000	0.00007	0.00003
Total kg/sec	0.0473	0.2913	

Stage # 22	376.26 K	1.21 kg/cm2	
	Vap kg/sec	Liq kg/sec	Y/X
Ethanol	0.00607	0.00399	10.30004
Water	0.03980	0.28367	0.95013
Lactic Acid	0.00000	0.00078	0.00447
Glycerol	0.00000	0.00116	0.00012
Acetic Acid	0.00011	0.00064	1.15156
Succinic Acid	0.00000	0.00007	0.00003
Total kg/sec	0.0460	0.2903	

Stage # 23	377.00 K	1.22 kg/cm2	
	Vap kg/sec	Liq kg/sec	Y/X
Ethanol	0.00385	0.00244	10.58999
Water	0.04106	0.28459	0.96911
Lactic Acid	0.00000	0.00078	0.00469
Glycerol	0.00000	0.00116	0.00012
Acetic Acid	0.00011	0.00064	1.18211
Succinic Acid	0.00000	0.00007	0.00003
Total kg/sec	0.0450	0.2897	

Stage # 24	377.54 K	1.23 kg/cm2	
	Vap kg/sec	Liq kg/sec	Y/X
Ethanol	0.00230	0.00142	10.78499
Water	0.04199	0.28524	0.98218
Lactic Acid	0.00000	0.00078	0.00485
Glycerol	0.00000	0.00116	0.00013
Acetic Acid	0.00012	0.00064	1.20282
Succinic Acid	0.00000	0.00007	0.00003
Total kg/sec	0.0444	0.2893	

Stage # 25	377.96 K	1.23 kg/cm2	
	Vap kg/sec	Liq kg/sec	Y/X
Ethanol	0.00128	0.00078	10.90763
Water	0.04263	0.28568	0.99068
Lactic Acid	0.00000	0.00078	0.00496
Glycerol	0.00000	0.00116	0.00013
Acetic Acid	0.00012	0.00064	1.21601
Succinic Acid	0.00000	0.00007	0.00004
Total kg/sec	0.0440	0.2891	

Stage # 26	378.27 K	1.24 kg/cm2	
	Vap kg/sec	Liq kg/sec	Y/X
Ethanol	0.00064	0.00038	10.98117
Water	0.04307	0.28598	0.99601
Lactic Acid	0.00000	0.00078	0.00505
Glycerol	0.00000	0.00116	0.00013
Acetic Acid	0.00012	0.00063	1.22404
Succinic Acid	0.00000	0.00007	0.00004
Total kg/sec	0.0438	0.2890	

Stage # 27	378.53 K	1.25 kg/cm2	
	Vap kg/sec	Liq kg/sec	Y/X
Ethanol	0.00024	0.00014	11.02640
Water	0.04338	0.28456	0.99929
Lactic Acid	0.00000	0.00078	0.00511
Glycerol	0.00000	0.00116	0.00013
Acetic Acid	0.00010	0.00053	1.22897
Succinic Acid	0.00000	0.00007	0.00004
Total kg/sec	0.0437	0.2872	

APPENDIX B

GAS DIFFUSIVITY CALCULATION SPREADSHEET

Gas Diffusivity Calculation
-- Yash Tamhankar

D_g = gas diffusivity (to be found from Fueller-Schettler-Giddings correlation)

$Dg^{1} = (0.001\ T^{1.75}\ M_{AB}{}^{1/2})/(P\ \{[\sum v]_A{}^{1/3} + [\sum v]_B{}^{1/3}\}^2)$

Parameter	Symbol	Formula	Unit	Value
Temperature	T	-	K	352.4493
Pressure	P	-	atm	1
Molecular weight of A (EtOh)	M_A	-	-	46
Molecular weight of A (EtOh)	M_B	-	-	18
Molecular weight of gas	M_{AB}	((1/MA) + (1/MB))		0.077294686
Atomic Diffusion Volumes[2]				
C	v_C		cm^3/gatom	16.5
H	v_H		cm^3/gatom	1.98
O	v_O		cm^3/gatom	5.48
Molecular Volumes				
A (Ethanol) (C_2H_5 - OH)	$(\sum v)_A$	v_C* 2 + v_H * 6 + v_O *1	cm^3/mol	50.36
B (Water) (H_2O)	$(\sum v)_B$	v_H*2 + v_O * 1	cm^3/mol	9.44
Gas Diffusivity	D_g	$(0.001\ T^{1.75}\ M_{AB}{}^{1/2})/(P\ \{[\sum v]_A{}^{1/3} + [\sum v]_B{}^{1/3}\}^2)$	cm^2/s	0.236426236
Gas Diffusivity	D_g		m^2/s	2.36426E-05

References:
1. Perry's Chemical Engineering Handbook, 7th edition, Tables 5-13, 5-14 and 5-16, Pages 5-48 to 5-49

APPENDIX C

POLYMATH INTEGRATION – NUMBER OF TRANSFER UNITS

POLYMATH Report NTU – Rectification section
Linear Regression 28-Sep-2010

Model: Fx = a0 + a1*x + a2*x^2 + a3*x^3 + a4*x^4 + a5*x^5

Variable	Value	95% confidence
a0	86.49125	44.24369
a1	-986.0277	908.67
a2	4259.772	5956.874
a3	-8177.756	1.661E+04
a4	6699.419	2.058E+04
a5	-1563.956	9327.557

Analytical polynomial integration

Fx = 86.49125 -986.0277 *x + 4259.772 *x^2 -8177.756 *x^3 + 6699.419 *x^4 -1563.956 *x^5
Integ(Fx,x1,x2) = 86.49125 *x -493.0139 *x^2 + 1419.924 *x^3 -2044.439 *x^4 + 1339.884 *x^5 -260.6594 *x^6
x(1) = 0.02132
x(2) = 0.83
Integ(Fx,x1,x2) = 14.7205

General

Degree of polynomial = 5
Regression including a free parameter
Number of observations = 17

Statistics

R^2	0.9472986
R^2adj	0.9233434
Rmsd	1.421721
Variance	53.1048

Source data points and calculated data points

	x	Fx	Fx calc	Delta Fx
1	0.83	100	90.09352	9.906478
2	0.8	50	68.51681	-18.51681
3	0.75	50	41.70522	8.294783
4	0.7	25	24.26614	0.7338554
5	0.65	14.29	13.93442	0.3555826
6	0.6	10	8.628693	1.371307
7	0.55	6.67	6.510111	0.1598885
8	0.5	5	6.040948	-1.040948
9	0.45	4.17	6.043257	-1.873257
10	0.4	4	5.757522	-1.757522
11	0.35	4.35	4.901304	-0.5513041
12	0.3	4.76	3.727891	1.032109
13	0.25	5.56	3.084945	2.475055
14	0.2	7.14	4.473149	2.666851
15	0.15	10	10.10486	-0.1048584
16	0.1	16.67	22.96275	-6.292748
17	0.05	50	46.85846	3.14154

POLYMATH Report NTU – Stripping section

Linear Regression 28-Sep-2010

Model: Fx = a0 + a1*x + a2*x^2 + a3*x^3 + a4*x^4 + a5*x^5

Variable	Value	95% confidence
a0	2490.426	363.6805
a1	-6.502E+05	2.177E+05
a2	7.003E+07	3.943E+07
a3	-3.354E+09	2.93E+09
a4	6.932E+10	9.488E+10
a5	-4.547E+11	1.111E+12

Analytical polynomial integration

Fx = 2490.426 -6.502E+05*x + 7.003E+07*x^2 -3.354E+09*x^3 + 6.932E+10*x^4 -4.547E+11*x^5

Integ(Fx,x1,x2) = 2490.426 *x -3.251E+05*x^2 + 2.334E+07*x^3 -8.386E+08*x^4 + 1.386E+10*x^5 -7.578E+10*x^6

x(1) = 0.0002

x(2) = 0.02132

Integ(Fx,x1,x2) = 11.74675

General

Degree of polynomial = 5
Regression including a free parameter
Number of observations = 17

Statistics

R^2	0.9656682
R^2adj	0.9500628
Rmsd	20.00917
Variance	1.052E+04

Source data points and calculated data points

	x	Fx	Fx calc	Delta Fx
1	0.033	1250	1163.339	86.66094
2	0.031	549.4505495	703.5009	-154.0504
3	0.029	370.3703704	422.1305	-51.76012
4	0.027	378.7878788	277.604	101.1838
5	0.025	289.017341	229.5987	59.41867
6	0.023	289.017341	240.8382	48.1791
7	0.021	274.7252747	278.8395	-4.114254
8	0.019	274.7252747	317.6583	-42.93299
9	0.017	261.7801047	339.6352	-77.8551
10	0.015	289.017341	337.1422	-48.12488
11	0.013	304.8780488	314.3283	-9.4503
12	0.011	322.5806452	288.8659	33.71476
13	0.009	384.6153846	293.6964	90.91894
14	0.007	454.5454545	378.777	75.76844
15	0.005	588.2352941	612.8261	-24.59077
16	0.003	909.0909091	1085.07	-175.9787
17	0.001	2000	1906.987	93.0128

APPENDIX D

HIGEE ROTOR DESIGN SPREADSHEETS

Rectification section

Farm scale Ethanol dewatering - Higee rotor design				
-- Yash Tamhankar			Inputs	
Rectification Higee			Outputs	
Step 1: Process parameters from ChemCad simulation				
Liquid mass flow-rate	L	0.059	kg/s	
Vapor mass flow rate	G	0.0528	kg/s	
Liquid density	ρ_l	794.020	kg/m^3	
Vapor bulk density	ρ_g	1.386	kg/m^3	
Liquid Viscosity	μ_l	0.0004	kg/ (m -s)	
Water viscosity	μ_w	0.00001	kg/ (m -s)	
Gas viscosity	μ_g	0.00001	kg/ (m -s)	
Step 2: Packing properties				
Packing selected: Sumitomo (Celmet); Reference - Kelleher 1992, M.S. Thesis. University of Texas				
Porosity	ε	0.92		
Specific surface area of packing	a_p	2500	m^2/m^3	
Effective diameter of packing	d_p	0.000192	m	$d_p = 6(1-\varepsilon)/a_p$
Step 3: Initial acceleration at the eye				
Acceleration required at eye	a_c	50	g	Acceleration varied from 10 g to 140 g for design
		490.5	m/s^2	
Step 4: Operational velocity determination using Sherwood flooding chart				
Sherwood Fl. Chart abscissa	X	0.05		$(L/G)*(\rho_g/\rho_l)^{0.5}$
Sherwood Fl. Chart ordinate	Y	0.28		Fig 2.2, Kelleher, UTA Thesis, Pg11
Superficial velocity of vapor @ Flooding	U_g'	0.1238	m/s	$\sqrt{\{Y r_i(\omega)^2 \varepsilon^3 / a_p\}*(\rho_l/\rho_g)*((\mu_w/\mu_l)\text{^}(0.2)\}}$
Operational velocity of vapor (@ 75 % Flood)	U_g	0.0866	m/s	$U_g' * (0.75)$
Step 5: Value of inner radius based on the operational velocity and flow area at the eye				
Inner radius required at the eye	r_i	0.2796	m	$\sqrt{[L / (2 \pi \rho_g U_g)]}$
(Based on area at eye)		0.92	ft	r_i (m) * 3.2808
		11.01	in	r_i (ft) * 3.2808
Step 6: Finding radial velocity based on acceleration at the eye and inner radius				
Rotational speed	ω	41.8820	rad/s	$\sqrt{\{a_c (m/s^2)/r_i\}}$
		6.6649	rps	ω (rad/s) /(2π)
		400	rpm	ω (rps) * 60
Step 7: Set axial height equal to the optimized inner radius				
Axial height	h	0.2796	m	$h=r_i$
		0.92	ft	h(m)*3.2808
		11.01	in	h(ft)*12
Step 8: Determination of gas diffusivity using Fueller-Schettler-Giddings corelation				
Gas Diffusivity	D_g	2.36426E-05	m^2/s	See Appendix B

Step 9: Initial guess for outer radius					
Initial guess for outer radius	$r_{o,\,guess}'$	0.7739	m		
Mean radius	r	0.5819	m		
Mean acceleration	$r\omega^2$	1020.6633	m/s^2		
Step 10: Determination of local and overall liquid side mass transfer coefficients					
	a1	307.8467		$a_p D_g/d_p$	Assuming the $r\omega^2$
	b1	2.112		$G/(a_p * \mu_g)$	in MTC calculations
	c1	138.7755		$(d_p^3 \rho_g^2 r \omega^2)/(\mu_g^2)$	is the mean acceleration
	d1	0.3052		$(\mu_g/(\rho_g D_g))$	
Local gas side MTC	$k_g a_e$	0.002424	s^{-1}	$(2.3\ E\text{-}07)\ (a1)\ (b1)^2\ (c1)^{1/3}\ (d1)^{-1/3}$	
	a2	0.0049		$(L\ a_p^2)/(337143.86\ \rho_l\ h)$	
	b2	0.0590		$L/\{a_p\ \mu_l\}$	
	c2	257398.1270		$\{\rho_l^2\ r\ \omega^2\}/\{\mu_l^2\ a_p^3\}$	
Local liquid side MTC	$k_l a_e$	0.174413	s^{-1}	$a2\ (b2)^{-0.6}\ (c2)^{0.15}$	
Overall liquid side MTC	$K_L a_e$	0.002391	s^{-1}	$(1/((1/k_g a_e)+(1/k_l a_e)))$	
Step 11: Determination of Area of Transfer Unit					
Area of transfer unit	ATU	0.1112	m^2	$L/(\rho_l\ h\ K_l a_e)$	
Step 12: Determination of Number of Transfer Units					
Number of Transfer Units	NTU	14.72		Polymath Integration, See Appendix C	
Step 13: Outer radius Solver calculation					
Outer Radius	r_o	0.7739	m	$\sqrt{\{(ATU*NTU/\pi)+ r_i^2\}}$	
		2.54	ft		
		30.47	in		
Difference in assumed outer radius and calculated outer radius	Δ	0.00000		$r_{o,calc} - r_{o,\,guess}'$	
Solver Inputs:					
Set $\Delta = 0$, by changing $r_{o,\,guess}'$					
Check: $r_{o,\,guess}' = r_o$					
Step 14: Calculation of HETP					
Radial distance	Δr	19.46	in	$r_o - r_i$	Martin, C. L. (1992). Preliminary distillation mass transfer and pressure drop
Number of theoretical stages	N_{theo}	13	-		results using a pilot-plant high gravity contacting unit.
Height Equivalent of Theoretical Plate	HETP	1.50	in	$\Delta r/N_{theo}$	AiChE Spring National Meeting. New Orleans, LA.

Design Summary			
Outer radius	r_o	0.7739	m
		30.47	in
Inner radius	r_i	0.2796	m
		11.01	in
Axial height	h	0.2796	m
		11.01	in
HiGee Configuration	r_o x r_i x h	30.47" x 11.01" x 11.01"	in
Radial velocity	ω	400	rpm
		42	rad/s
Acceleration at the eye	$r_i\omega^2$	50	g
Acceleration at outer radius	$r_o\omega^2$	138	g
Mean radius	r	0.5819	m
		22.9084	in
Mean acceleration	$r\omega^2$	1020.6633	m/s^2
		104	g
Radial distance	Δr	19.46	in
Height Equivalent of Theoretical Plate	HETP	1.50	in

Stripping Section

Farm scale Ethanol dewatering - Higee rotor design
-- Yash Tamhankar — Inputs
Stripping Higee — Outputs

Step 1: Process parameters from ChemCad simulation				
Liquid mass flow-rate	L	0.2927	kg/s	
Vapor mass flow rate	G	0.0484	kg/s	
Liquid density	ρ_l	947.9	kg/m^3	
Vapor bulk density	ρ_g	0.8067	kg/m^3	
Liquid Viscosity	μ_l	0.0003	kg/ (m -s)	
Water viscosity	μ_w	0.00001	kg/ (m -s)	
Gas viscosity	μ_g	0.00001	kg/ (m -s)	
Step 2: Packing properties				
Packing selected: Sumitomo (Celmet); Reference - Kelleher 1992, M.S. Thesis. University of Texas				
Porosity	ε	0.92		
Specific surface area of packing	a_p	2500	m^2/m^3	
Effective diameter of packing	d_p	0.000192	m	$d_p = 6(1-\varepsilon)/a_p$
Step 3: Initial acceleration at the eye				
Acceleration required at eye	a_c	50	g	Acceleration varied from 10 g to 140 g for design
		490.5	m/s^2	
Step 4: Operational velocity determination using Sherwood flooding chart				
Sherwood Fl. Chart abscissa	X	0.18		$(L/G)*(\rho_g/\rho_l)^{0.5}$
Sherwood Fl. Chart ordinate	Y	0.15		Fig 2.2, Kelleher, UTA Thesis, Pg11
Superficial velocity of vapor @ Flooding	U_g'	0.1730	m/s	$\sqrt{Yr_i(\omega)^2\varepsilon^3/ a_p)*(\rho_l/\rho_g)*((\mu_w/\mu_l)\text{^}(0.2)}$
Operational velocity of vapor (@ 75 % Flood)	U_g	0.1211	m/s	$U_g' * (0.75)$
Step 5: Value of inner radius based on the operational velocity and flow area at the eye				
Inner radius required at the eye	r_i	0.6906	m	$\sqrt{[L / (2 \pi \rho_g U_g)]}$
(Based on area at eye)		2.27	ft	r_i (m) * 3.2808
		27.19	in	r_i (ft) * 3.2808
Step 6: Finding radial velocity based on acceleration at the eye and inner radius				
Rotational speed	ω	26.6514	rad/s	$\sqrt{a_c (m/s^2)/r_i}$
		4.2412	rps	ω (rad/s) /(2π)
		254	rpm	ω (rps) * 60
Step 7: Set axial height equal to the optimized inner radius				
Axial height	h	0.6906	m	$h=r_i$
		2.27	ft	h(m)*3.2808
		27.19	in	h(ft)*12
Step 8: Determination of gas diffusivity using Fueller-Schettler-Giddings corelation				
Gas Diffusivity	D_g	2.36426E-05	m^2/s	See Appendix B

Step 9: Initial guess for outer radius

Initial guess for outer radius	$r_{o,\,guess}'$	1.4228	m	
Mean radius	r	1.1183	m	
Mean acceleration	$r\omega^2$	794.3145	m/s^2	
		80.9699	g's	

Step 10: Determination of local and overall liquid side mass transfer coefficients

	a1	307.8467	$a_p D_g/d_p$	Assuming the $r\omega^2$
	b1	1.9360	$G/(a_p * \mu_g)$	in MTC calculations
	c1	36.5865	$(d_p^3 \rho_g^2 r \omega^2)/(\mu_g^2)$	is the mean acceleration
	d1	0.5243	$(\mu_g/(\rho_g D_g))$	
Local gas side MTC	$k_g a_e$	0.001091 s^{-1}	$(2.3\text{ E-}07)\,(a1)\,(b1)^2\,(c1)^{1/3}\,(d1)^{-1/3}$	
	a2	0.0083	$(L\,a_p^2)/(337143.86\,\rho_l\,h)$	
	b2	0.3903	$L/\{a_p\,\mu_l\}$	
	c2	507522.1775	$\{\rho_l^2\,r\,\omega^2\}/\{\mu_l^2\,a_p^3\}$	
Local liquid side MTC	$k_l a_e$	0.104599 s^{-1}	$a2\,(b2)^{-0.6}\,(c2)^{0.15}$	
Overall liquid side MTC	$K_L a_e$	0.001080 s^{-1}	$(1/((1/k_g a_e)+(1/k_l a_e)))$	

Step 11: Determination of Area of Transfer Unit

Area of transfer unit	ATU	0.4141 m^2	$L/(\rho_l\,h\,K_l a_e)$	

Step 12: Determination of Number of Transfer Units

Number of Transfer Units	NTU	11.74		Polymath Integration, See Appendix C

Step 13: Outer radius Solver calculation

Outer Radius	r_o	1.4228	m	$\sqrt{\{(ATU*NTU/\pi)+ r_i^2\}}$
		4.67	ft	
		56.01	in	
Difference in assumed outer radius and calculated outer radius	Δ	0.00000		$r_{o,calc} - r_{o,\,guess}'$

Solver Inputs:

Set Δ = 0, by changing $r_{o,\,guess}'$

Check: $r_{o,\,guess}' = r_o$

Step 14: Calculation of HETP

Radial distance	Δr	28.83	in	$r_o - r_i$
Number of theoretical stages	N_{theo}	13	-	
Height Equivalent of Theoretical Plate	HETP	2.22	in	$\Delta r/N_{theo}$

Martin, C. L. (1992). Preliminary distillation mass transfer and pressure drop results using a pilot-plant high gravity contacting unit. AiChE Spring National Meeting. New Orleans, LA.

Design Summary

Outer radius	r_o	1.4228	m
		56.01	in
Inner radius	r_i	0.6906	m
		27.19	in
Axial height	h	0.6906	m
		27.19	in
HiGee Configuration	r_o x r_i x h	56.01" x 27.19" x 27.19"	in
Radial velocity	ω	254	rpm
		27	rad/s
Acceleration at the eye	$r_i\omega^2$	50	g
Acceleration at outer radius	$r_o\omega^2$	103	g
Mean radius	r	1.1183	m
		44.03	in
Mean acceleration	$r\omega^2$	81	g
Radial distance	Δr	28.83	in
Height Equivalent of Theoretical Plate	HETP	2.22	in

APPENDIX E

POWER CONSUMPTION SPREADSHEET

Ethanol Dewatering Process
Motor Shaft Power Requirement
Yash Tamhankar

Power consumption calculations are based on the model of Surinder Singh, Air Stripping of volatile organic compounds from groundwater: an evaluation of a centrifugal vapor - liquid contactor, PhD Dissertation, University of Tennessee, Knoxville, August 1989, pg 141, equation 6-19.

$P_c = 1.222 + 0.0011\ \rho_L\ r_o^2\ \omega^2\ Q_L$

where

P_c - power consumption during operation (kW)

ρ_L - liquid density (kg/m^3)

r_o - outer radius of the rotor (m)

ω - angular velocity (rad/s)

Q_L - volumetric flow rate of the liquid (m^3/s)

L - Liquid mass flowrate (kg/s) = $\rho_L * Q_L$

Parameter	Symbol	Value	Unit	Formula	Reference
Section - Rectification					
Liquid mass flow-rate	L	0.059	kg/s	-	ChemCad simulation output, Appendix A
Outer radius of packing	r_o	30.47	in	-	Higee Rectification Design Spreadsheet, Appendix D
		0.773938	m	r_o (in)*0.0254	
Angular velocity	ω	400	rpm		Higee Rectification Design Spreadsheet, Appendix D
		41.8933	rad/s	ω (rpm) * 2π/60	
Power consumption (operational)	P_c	1.2902	kW	$Pc = 1.222 + 0.0011\ L\ r_o^2\ \omega^2$	
Motor efficiency	η_{motor}	0.8			Assumed value of motor efficiency
Purchased power	P_p	***1.6128***	***kW***	P_c / η_{motor}	
Section - Stripping					
Liquid mass flow-rate	L	0.2927	kg/s	-	ChemCad simulation output, Appendix A
Outer radius of packing	r_o	56.01	in	-	Higee Stripping Design Spreadsheet, Appendix D
		1.422654	m	r_o (in)*0.0254	
Angular velocity	ω	255	rpm		Higee Stripping Design Spreadsheet, Appendix D
		26.7070	rad/s	ω (rpm) * 2π/60	
Power consumption (operational)	P_c	1.6868	kW	$Pc = 1.222 + 0.0011\ L\ r_o^2\ \omega^2$	
Motor efficiency	η_{motor}	0.8			Assumed value of motor efficency.
Purchased power	P_p	***2.1085***	***kW***	P_c / η_{motor}	

APPENDIX F

DATA FOR SELECTION PLOTS ($\Delta K_L a_e/\Delta a_c$ vs. a_c)

Rectification Section

Acceleration at eye	**Overall mass transfer Coefficient**	**Incremental increase in Overall Mass transfer Coefficient**	**Incremental Increase in acceleration at the eye**	**Rate of incremental in Overall mass transfer coefficient with incremental increase in acceleration at eye**	**Power consumed**
a_c (g's)	$K_l a_e \times 10^2$ (s^{-1})	$\Delta K_l a_e \times 10^2$ (s^{-1})	Δa_c (g's)	$\Delta K_l a_e \times 10^2/\Delta a_c$ (s^{-1}/g's)	P_c (kW)
1	0.0558	-	-	-	-
10	0.1302	0.0744	9	0.00827	1.2350
20	0.1689	0.0387	10	0.00387	1.2487
30	0.1969	0.028	10	0.0028	1.2627
40	0.2196	0.0227	10	0.00227	1.2764
50	0.2391	0.0195	10	0.00195	1.2902
60	0.2563	0.0172	10	0.00172	1.3056
70	0.2718	0.0155	10	0.00155	1.3231
80	0.2860	0.0142	10	0.00142	1.3364
90	0.2992	0.0132	10	0.00132	1.3514
100	0.3115	0.0123	10	0.00123	1.3672
110	0.3231	0.0116	10	0.00116	1.3814
120	0.3341	0.011	10	0.0011	1.3988
130	0.3445	0.0104	10	0.00104	1.4144
140	0.3544	0.0099	10	0.00099	1.4308

Stripping Section

Acceleration at eye	**Overall mass transfer Coefficient**	**Incremental increase in Overall Mass transfer Coefficient**	**Incremental Increase in acceleration at the eye**	**Rate of incremental in Overall mass transfer coefficient with incremental increase in acceleration at eye**	**Power consumed**
a_c (g's)	$K_l a_e \times 10^2$ (s^{-1})	$\Delta K_l a_e \times 10^2$ (s^{-1})	Δa_c (g's)	$\Delta K_l a_e \times 10^2 / \Delta a_c$ (s^{-1}/g's)	P_c (kW)
1	0.0262	-	-	-	-
10	0.0597	0.0335	9	0.00372	1.6445
20	0.0769	0.0172	10	0.00172	1.7578
30	0.0893	0.0124	10	0.00124	1.8692
40	0.0994	0.0101	10	0.00101	2.0021
50	0.1080	0.0086	10	0.00086	2.1085
60	0.1156	0.0076	10	0.00076	2.2260
70	0.1224	0.0068	10	0.00068	2.3543
80	0.1287	0.0063	10	0.00063	2.4927
90	0.1345	0.0058	10	0.00058	2.6116
100	0.1399	0.0054	10	0.00054	2.7379
110	0.145	0.0051	10	0.00051	2.8704
120	0.1499	0.0049	10	0.00049	2.9764
130	0.1545	0.0046	10	0.00046	3.1211
140	0.1588	0.0043	10	0.00043	3.2367

APPENDIX G

PRESSURE DROP CALCULATION SPREADSHEETS

Rectification Section

Pressure drop calculation in Higee rotor
-Yash T.

Inputs
Output

Pressure drop calculations are based on "Kelleher, T. (1993). Mass Transfer and Hydraulic
Operating Characteristics of a Pilot-Plant Scale High Gravity Contacting Unit. Austin, The University of Texas. M.S.Equation 4.6, Pg 34

$\Delta P = \{\rho_g \omega^2 (r_o^2 - r_i^2)/2 + \{(5B'/22)(\varepsilon G/[\pi h \rho g])^2 ([1/r_i^{1.1}] - [1/r_o^{1.1}])\}$

where,

$B' = (a_p \rho_g/\varepsilon^3)(G/[2\pi rh\, a_p \mu_g])^{0.1} r^{0.1}$

ΔP - pressure drop, Pa	r_o - outer radius, m	G -gas rate, kg/s	
ρ_g - gas density, kg/m^3	r_i - inner radius, m	μ_g - gas viscosity, kg/m-s	
ω - radial velocity, rad/s	r - mean radius, m	ε - void fraction	
a_p - sp surface of packing, m^2/m^3	h - axial height, m		

Rectification Section

Process parameters from ChemCad simulation				
Vapor mass flow rate	G	0.0528	kg/s	
Vapor bulk density	ρ_g	1.386	kg/m^3	
Gas viscosity	μ_g	0.00001	kg/ (m -s)	
Packing properties				
Porosity	ε	0.92		
Specific surface area of packing	a_p	2500	m^2/m^3	
Higee configuration				
Outer radius	r_o	30.47	in	
		0.7739	m	
Inner radius	r_i	11.01	in	
		0.2797	m	
Mean radius	r	22.91	in	
		0.5819	m	
Radial distance	Δr	19.46	in	$r_o - r_i$
		0.4943	m	
Axial height	h	0.2797	m	
Radial velocity	ω	400	rpm	
		41.8933	rad/s	
Calculations				
Constant	A	4449.7925	kg/m^4	$(a_p * \rho_g)/\varepsilon^3$
	C	1.0450	-	$\{(G)/(2\pi rh a_p \mu_g)\}^{0.1}$
	B'	4404.9068	kg/m^4	$A * C * r^{0.1}$
Pressure Drop	ΔP	637.7493	Pa	$\{\rho_g \omega^2 (r_o^2 - r_i^2)/2 + \{(5B'/22) * (\varepsilon L/(\pi h \rho_g))^2 * (1/r_i^{1.1} - 1/r_o^{1.1})\}$
		65.0326	kg/m^2	ΔP (Pa) *0.101972
		0.0064	atm	ΔP (Pa) *0.00001
		0.0925	psi	ΔP (Pa) /6894.8
Pressure Drop per inch of packing	$\Delta P/\Delta r$	0.0048	psi/in	ΔP (psi) / Δr (in)
Pressure Drop per theoretical stage	$\Delta P/N_{theo}$	0.0071	psi/theoretical stage	ΔP (psi) / N_{theo} , N_{theo} = 13

Stripping Section

Pressure drop calculation in Higee rotor
-Yash T.

Inputs
Output

Pressure drop calculations are based on "Kelleher, T. (1993). Mass Transfer and Hydraulic Operating Characteristics of a Pilot-Plant Scale High Gravity Contacting Unit. Austin, The University of Texas. M.S.Equation 4.6, Pg 34

$\Delta P = \{\rho_g \omega^2 (r_o^2 - r_i^2)/2\} + \{(5B'/22)(\varepsilon G/[\pi h \rho g])^2 ([1/r_i^{1.1}] - [1/r_o^{1.1}])\}$

where,

$B' = (a_p \rho_g/\varepsilon^3)(G/[2\pi r h a_p \mu_g])^{0.1} r^{0.1}$

ΔP - pressure drop, Pa	r_o - outer radius, m	G -gas rate, kg/s
ρ_g - gas density, kg/m^3	r_i - inner radius, m	μ_g - gas viscosity, kg/m-s
ω - radial velocity, rad/s	r - mean radius, m	ε - void fraction
a_p - sp surface of packing, m^2/m^3	h - axial height, m	

Stripping Section

Process parameters from ChemCad simulation			
Vapor mass flow rate	G	0.0484	kg/s
Vapor bulk density	ρ_g	0.8067	kg/m^3
Gas viscosity	μ_g	0.00001	kg/ (m -s)
Packing properties			
Porosity	ε	0.92	
Specific surface area of packing	a_p	2500	m^2/m^3
Higee configuration			
Outer radius	r_o	56.01	in
		1.4227	m
Inner radius	r_i	27.19	in
		0.6906	m
Mean radius	r	44.03	in
		1.1182	m
Radial distance	Δr	28.82	in
		0.7320	m
Axial height	h	0.6906	m
Radial velocity	ω	255	rpm
		26.7070	rad/s

Calculations				
Constant	A	2589.9333	kg/m^4	$(a_p * \rho_g)/\varepsilon^3$
	C	0.8905	-	$\{(G)/(2\pi r h a_p \mu_g)\}^{0.1}$
	B'	2332.2477	kg/m^4	$A*C*r^{0.1}$
Pressure Drop	ΔP	445.3410	Pa	$\{\rho_g \omega^2 (r_o^2 - r_i^2)/2\} + \{(5B'/22)*(\varepsilon L/(\pi h \rho_g))^2 * (1/r_i^{1.1} - 1/r_o^{1.1})\}$
		45.4123	kg/m^2	ΔP (Pa) *0.101972
		0.0045	atm	ΔP (Pa) *0.00001
		0.0646	psi	ΔP (Pa) /6894.8
Pressure Drop per inch of packing	$\Delta P/\Delta r$	0.0022	psi/in	ΔP (psi) / Δr (in)
Pressure Drop per theoretical stage	$\Delta P/N_{theo}$	0.0050	psi/theoretical stage	ΔP (psi) / N_{theo} , N_{theo} = 13

APPENDIX H

DATA FOR SENSITIVITY PLOTS

Rectification section

Radial velocity	**Overall Volumetric mass transfer coefficients**	**Power consumption**	**Pressure drop per theoretical stage**
ω	$K_L a_e \times 10^2$	P_c	$\Delta P/N_{theo}$
(rpm)	(s-1)	(kW)	(psi/stage)
400	0.2391	1.2902	0.0071
500	0.2771	1.3286	0.0111
600	0.3125	1.3755	0.0159
700	0.3460	1.4309	0.0217
800	0.3779	1.4949	0.0283
900	0.4084	1.5674	0.0358
1000	0.4378	1.6484	0.0442
1100	0.4661	1.7380	0.0535
1200	0.4936	1.8360	0.0636
1300	0.5203	1.9426	0.0747
1400	0.5463	2.0578	0.0866
1500	0.5717	2.1814	0.0994
1600	0.5965	2.3136	0.1131

Stripping section

Radial velocity	**Overall Volumetric mass transfer coefficients**	**Power consumption**	**Pressure drop per theoretical stage**
ω	$K_L a_e \times 10^2$	P_c	$\Delta P/N_{theo}$
(rpm)	(s-1)	(kW)	(psi/stage)
255	0.1081	1.6868	0.0050
300	0.1204	1.8653	0.0069
400	0.1457	2.3657	0.0122
500	0.1688	3.0090	0.0191
600	0.1904	3.7953	0.0275
700	0.2109	4.7245	0.0374
800	0.2303	5.7967	0.0489
900	0.2489	7.0119	0.0619
1000	0.2669	8.3700	0.0764
1100	0.2842	9.8711	0.0924
1200	0.3010	11.5151	0.1100
1300	0.3172	13.3021	0.1291
1400	0.3331	15.2321	0.1497
1500	0.3486	17.3050	0.1718
1600	0.3638	19.5209	0.1955

VITA

YASH TAMHANKAR

Candidate for the Degree of

Master of Science/Arts

Thesis: DESIGN OF A HIGH GRAVITY DISTILLATION UNIT FOR ON FARM ETHANOL DEWATERING

Major Field: Chemical Engineering

Biographical:

Personal Data:
Born in Pune, India to Sharadchandra Tamhankar and Ketaki Tamhankar on August 7, 1984

Education:
Completed the requirements for the Master of Science in Chemical Engineering at Oklahoma State University, Stillwater, Oklahoma in December, 2010.

Completed the requirements for the Bachelor of Engineering in Chemical Engineering at University of Pune, Pune, Maharashtra, India in 2006.

Experience:
Teaching Assistant, August 2008 – Present, School of Chemical Engineering, Oklahoma State University, Multiple courses.

Commissioning Engineer, November 2006 – April 2008, Praj Industries Ltd., Pune, India, Equipment design, Plant Start up & optimization, Training of plant operators.

Professional Memberships:
American Institute of Chemical Engineers (AIChE), Omega Chi Epsilon Honor Society.

Name: Yash Tamhankar Date of Degree: December, 2010

Institution: Oklahoma State University Location: Stillwater, Oklahoma

Title of Study: DESIGN OF A HIGH GRAVITY DISTILLATION UNIT FOR ON FARM ETHANOL DEWATERING

Pages in Study: 119 Candidate for the Degree of Master of Science

Major Field: Chemical Engineering

Scope and Method of Study:

High gravity (Higee) distillation refers to separation of components in a rotating packed bed type contacting device. Rotating packed beds utilize centrifugal force to create artificial gravity up to 200 times greater in magnitude than earth's gravity. The increased acceleration results in smaller liquid films and smaller bubble sizes. Consequently, higher mass transfer fluxes and throughputs can be obtained in a small size, low weight unit. Height Equivalent to Theoretical Plate (HETP) reduction from 1.5-3 feet for conventional columns to 1-3 inches in Hi-Gee units has been reported. The reduced weight and size, low residence time and possibility of setting up mobile units, makes Hi-Gee attractive for on-site distillation of heat sensitive and fouling fermented juice. Previous study by the Department of Bio-Systems and Agriculture Engineering at Oklahoma State University (OSU) has established the need to distill 250 GPH of fermented juice with 6-10 vol % ethanol to produce 15 GPH of 190 proof ethanol, on farm. The aim of this study is to size the Higee rotors for processing 250 gallons per hour of fermented juice.

Findings and Conclusions:

Concepts employed in design of packed columns can be utilized with appropriate modifications. The designed rotor configurations are; 30.47 in x 11.01 in x 11.01in for the Rectification Higee and 56.01 in x 27.19 in x 27.19 in for the Stripping Higee. A trade- off between the increase in overall mass transfer coefficient and the power consumed was utilized for selecting the above mentioned configurations of Higee, respectively. The footprint of both the designed rotors is relatively small. A small 3 HP (brake) motor is adequate to drive the two rotors. An indirect material balance control strategy has been established for Higee. This study presents the first documented design of a Higee unit to meet pre-specified production rate and purity targets.

ADVISER'S APPROVAL: Dr. James R. Whiteley